Non-peer reviewed preprint submitted to EarthArXiv

Environmental and ecological changes across the Permian–Triassic transition in Türkiye: integrating virtual outcrop models and new fieldwork data

Baran Karapunar[1,*], Xia Wang[2,*], Anja B. Frank[3], Müjde Gürsoy[4], Stella Z. Buchwald[3], Mónica Alejandra Gómez Correa[3], Zhipeng Liu[5], Xuanni Xu[2], Lingzan Meng[2], Damla Demir[6], Erdal Koşun[7], William J. Foster[3]

[1] School of Earth and Environment, University of Leeds, LS2 9JT Leeds, United Kingdom.

[2] Key Laboratory of Deep-time Geography and Environment Reconstruction and Application of Ministry of Natural Resources, Institute of Sedimentary Geology, Chengdu University of Technology, 610059 Chengdu, China.

[3] Institute for Geology, Department of Earth System Sciences, University of Hamburg, 20146 Hamburg, Germany.

[4] Natural History Museum, MTA General Directorate of Mineral Research and Exploration, 06530 Çankaya, Ankara, Türkiye.
[5] College of Geophysics, Chengdu University of Technology, 610059 Chengdu, China.

[6] Department of Geological Engineering, Kütahya Dumlupınar University, Kütahya, Türkiye.
[7] Department of Geological Engineering, Akdeniz University, 07058 Antalya, Türkiye.

*Corresponding authors: b.karapunar@leeds.ac.uk; xiawang@cdut.edu.cn

Abstract: The Permian–Triassic transition is characterized by major environmental changes (e.g., hyperthermals, perturbations in carbon cycle) and the largest known mass extinction event in the Phanerozoic. However, successions with a relatively complete sedimentological and paleontological record across the Permian–Triassic are limited to a few well-known sections in Europe and South China. Here, we synthesize sedimentological, geochemical and paleontological data from the Permian–Triassic succession of southwestern Türkiye, putting it into a consistent stratigraphic framework and incorporate 3D open-access virtual outcrop models with a virtual field guide to improve the accessibility, reproducibility and sustainability of fieldwork findings. The fossiliferous Upper Permian to Lower Triassic successions in the studied locations reach over a kilometer thickness. In addition, due to the contemporaneous opening of the Neotethys Ocean the sedimentary units from the Antalya Nappe (Çürük Dağ, Kemer; Öznurtepe, Gazipaşa, Demirtaş) were deposited on a carbonate platform in the Neotethys ocean, while successions from the Aladağ Nappe (Taşkent) were deposited on the northern side of the carbonate platform towards the subducting Palaeotethys Ocean. In all sections, the Changhsingian (uppermost Permian) is represented by highly fossiliferous platform carbonates. The Changhsingian successions terminate

with a thin oolitic grainstones ("transitional oolites"), which is quantitatively identified as the Permian–Triassic mass extinction interval and corresponds with a negative carbon isotope excursion. The limited availability of geochemical proxies, however, hinders our understanding of the drivers of the extinctions. The transitional oolites are overlain by a microbialite-dominated carbonates deposited in the Griesbachian, and then oolites. This carbonate-rich deposition was replaced with a mixed carbonate-siliciclastic dominated succession later in the Early Triassic (Dienerian–Spathian), where marine ecosystems slowly recover. These environmental and biotic changes are similar to the known record from the tropical paleolatitudes in the western (Italy, Hungary) and eastern Palaeotethys (Iran, China).

Keywords: Permian, Triassic, mass extinction, FAIR principles, virtual outcrop models, digital field guide

Introduction

The Permian–Triassic transition records the largest known mass extinction event in Earth's history. Extreme environmental changes, such as climate warming at a rapid pace and high magnitude, induced by the emplacement of the Siberian Traps Large Igneous Province (Burgess et al. 2017; Dal Corso et al. 2022; Wignall & Bond 2024), rendering it important for understanding the co-evolution of life and the planet in extreme conditions, whilst also potentially offering insights into projected environmental and ecological perturbations. What is known about the Permian–Triassic transition is, however, heavily biased by well-studied sections in South China, because those sections have a well-constrained stratigraphic framework allowing for high resolution investigations (Shen et al. 2011; Burgess et al. 2014). There are also other well-studied regions around the world that are key for understanding this event, such as central Europe, but the amount of available data from different disciplines from the same regions and sites is not as extensive as many expect. For example, central Europe has an extensive history of paleontological and sedimentological research (e.g., Broglio-Loriga et al. 1988, 1990; Posenato et al. 2019), but a high-resolution stratigraphic scheme or extensive geochemical investigations are currently lacking. Therefore, to improve our understanding of the Permian–Triassic transition, more interdisciplinary studies are required from different regions and sections.

The Permian–Triassic successions in Türkiye have been important for characterizing the Permian–Triassic transition, as they largely represent Neotethys oceanic basins, different from the Palaeotethys successions in South China and central Europe, and they show a different evolutionary trajectory across the Permian/Triassic boundary. Furthermore, the successions in Türkiye are sedimentologically unique with an extensive anachronistic carbonate response (e.g., Baud et al. 2005; Heindel et al. 2018), and some fossil groups not known from age-equivalent rocks globally (e.g., hexactinellid sponge spicules, Kozur et al. 1996). Despite being important in developing our understanding of the Permian–Triassic transition, the successions in Türkiye have not received the same amount of extensive attention as other regions, like Svalbard (e.g., Smyrak-

Sikora et al. 2025) and are still understudied. Moreover, the key successions in Türkiye are often in remote areas, which are difficult to relocate from previous studies. In addition to this, the original outcrops of these sections have been destroyed in rural areas over the last few decades. For example, the roads that expose the Taşkent Yolu and Taşkent Şam Deresi sections are being significantly altered due to reconstruction, and the previously reported outcrops at Demirtaş were quarried for Lower Triassic oolitic limestones. Together, this demonstrates the importance of characterizing the Permian–Triassic transition in Türkiye, before key sections are lost by human-induced destruction.

Fieldwork is a fundamental element of geological research, but locating sections and the locations of previous samples is often difficult, which makes reproducing fieldwork challenging. This is partly because of inadequate documentation due to a lack of existing technology in the past and partly because the sections change over time (e.g., changes due to weathering or human influence). Assigning different formation names for the same deposits or confusion of lithostratigraphic units can also lead to several disparities between studies (e.g., Posenato 2008) and hinder synthesizing data between studies into a consistent stratigraphic framework. There are exceptions, such the Permian/Triassic boundary GSSP in China (Yin et al. 2001) and the candidate GSSP sections in Hungary (Haas et al. 2006) and Italy (Brandner et al. 2009), where each individual bed has been numbered for decades allowing studies to correlate data collected by different authors (e.g., Farabegoli & Perri 2012; Foster et al. 2024), but sections like these are exceptions to how fieldwork data is generally shared. Furthermore, fossils and sedimentary structures are often documented in the field but cannot be sampled. This further poses a risk that unsampled fossils and sedimentary structures are lost over time, and subsequent studies cannot reproduce the data. The issues with fieldwork make it difficult for earth scientists to stick to the FAIR data principles (Findable, Accessible, Interoperable, and Reusable), which are supported by the EU Commission (Wilkinson et al. 2016). The digitization of outcrops and creation of virtual models, however, allows geoscientists to both document and record fieldwork and sample locations in greater detail, offering great potential in making fieldwork, and *in situ* field data (such as fossil counts and identifications from bedding planes) consistent with the FAIR principles. The invention of affordable unmanned aerial verhicles (UAVs), high-resolution camaras with in-built Lidar, GPS, and 3D modelling software, combined with the development of online platforms, therefore, not only improves accessibility, but also the reproducibility of field work. To go even further, geological fieldwork is not accessible to everyone, due to challenges with the terrain and, therefore, by creating virtual models of outcrops and field data, field sites can be explored without visiting the localities directly (e.g., Senger et al. 2022).

Here, we document the Permian–Triassic transition in the Antalya and Aladağ Nappes in Türkiye. We demonstrate how UAVs can be used to create virtual models that can be utilized to generate accessible, publicly available virtual field trips and to document fieldwork-related data collection. In addition, we also synthesize pre-existing data for the sections between different studies to provide a high-resolution overview of the ecological and environmental changes during the

Permian–Triassic transition. The Antalya and Aladağ Nappes in Türkiye is an ideal region to create virtual field guides as these Nappes hold records of the major ecological and environmental changes associated with the Permian–Triassic transition. This new synthesis also allows for making pre-existing data consistent with FAIR principles, as previously provided GPS coordinates and section names were checked for their accuracy and replaced by a single GPS coordinate and unique name for each section, removing duplicate naming and inaccurate location information. Furthermore, we combine data from different studies into a consistent stratigraphic framework to explore the timing and nature of the Permian–Triassic mass extinction.

1. Geological Setting

We have digitized and sampled sections in four different areas (Çürük Dağ, Öznurtepe, Demirtaş, and Taşkent; Figure 1). The sedimentary successions in these places belong to two allochthonous tectono-stratigraphic units of the Tauride Block, namely the Antalya Nappe (Çürük Dağ, Öznurtepe, Demirtaş) and the Aladağ Nappe (Taşkent) (Özgül 1984, 1997; Altıner et al. 2000, 2021). Starting around the Permian–Triassic transition, the tectonic units of Türkiye became tectonically active and were transformed as it marked the junction between the opening of the Neotethys ocean and the subduction of the Palaeotethys Ocean (Şengör & Yılmaz 1981). During the Permian, the tectonic units of Türkiye are regarded to represent deposition along the northern margin of Gondwana facing the Palaeotethys Ocean. The Palaeotethys Ocean was also being actively subducted to the north, and it is suggested that the studied sedimentary successions were part of a large carbonate platform (Robertson et al. 2012). The Upper Permian platform carbonates of the studied localities are attributed to the Southern Biofacies Belt, which is confined by the foraminifera genera *Paradagmarita* and *Shanita* and extends from Türkiye to Iran, Saudi Arabia, Oman, western Yunnan, Myanmar, and western Thailand (Altıner et al. 2000). During the Triassic, this carbonate platform is interpreted to have ruptured to produce extensional basins, with the Antalya Nappe becoming isolated on the northern margin of the southern Neotethys, whilst the Aladağ Nappe was part of the Tauride-Anatolide carbonate platform facing the southern side of the Inner Tauride Ocean by the Late Triassic (Robertson et al. 2004, 2012). Rifting of the Antalya Nappe is considered to have started around the Anisian-Ladinian transition (Şengör & Yılmaz 1981). Hence, the sedimentary successions during the Permian–Triassic transition were affected by the tectonic evolution of the Tethyan ocean basins.

At all four localities, the Permian–Triassic boundary is placed at the contact between Changhsingian oolite and Griesbachian stromatolite beds (Grooves et al. 2005; Angiolini et al. 2007; Payne et al. 2007; Varol et al. 2011). A gradual decline in $\delta^{13}C$ from 4‰ to 0–2‰ near the formation boundaries at the studied sections at Çürük Dağ, Demirtaş, Taşkent and Öznurtepe (Richoz 2006; Payne et al. 2007; Frank et al. in review) is further consistent with the global carbon cycle perturbation observed across the Permian–Triassic transition (Korte & Kozur 2010) and

indicates an uppermost Changhsingian age for the oolite deposit. The presence of Griesbachian conodonts, including *Hindeodus parvus* (Kozur & Pjatakova, 1976), at Çürük Dağ confirms the earliest Griesbachian age for the overlying stromatolite beds (Crasquin-Soleau 2002; Richoz 2006).

The deposits across the Permian–Triassic transition in the studied localities are almost uninterrupted except of few hiatuses at some horizons. A depositional gap and pressure dissolution (stylolitic contact) have been interpreted at the Permian/Triassic boundary based on the truncation on top of the oolite bed at Taşkent (Ünal et al. 2003; Payne et al. 2007). Baud et al. (2005) reported pressure dissolution at the contact of the uppermost Changhsingian oolite bed and the overlying Griesbachian stromatolite at Taşkent. Kershaw et al. (2011) identified an erosion surface between the Changhsingian algal wackestone/packstone and the Changhsingian oolite at Çürük Dağ.

Çürük Dağ

The Middle–Late Permian at Çürük Dağ is represented by the Pamucak Formation (Figure 2; Lys & Marcoux 1978) which consists of ca. 600 meters thick carbonate succession and yields abundant fossils including brachiopods, calcareous algae, bryozoans, foraminifera, gastropods, ostracods, and echinoderms (Brachiopoda: Angiolini et al. 2007, Verna et al. 2011; Trilobita: Lerosey-Aubril & Angiolini 2009; Ostracoda: Crasquin-Soleau et al. 2004). The Pamucak Formation contains deposits of ca. 12 meters thick Changhsingian (Richoz 2006), as indicated by the foraminifera *Paradagmarita monodi* Lys in Lys & Marcoux 1978, a low diversity brachiopod assemblage dominated by *Spinomarginifera* and *Orthothetina*, and *Hindeodus* cf. *praeparvus* Kozur, 1996 (Angiolini et al. 2007). The nodular limestone of the Permian Pamucak Formation is overlain by a 30 cm oolite bed and the stromatolites of the Lower Triassic Kokarkuyu Formation (Altıner & Zaninetti 1981) at Çürük Dağ (Marcoux & Baud 1988; Baud et al. 2005). The earliest Triassic has been assigned to the lowermost microbialites based on the presence of the conodonts *Hindeodus parvus* (Kozur & Pjatakova, 1976) and *Isarcicella isarcica staeschei* (Dai & Zhang, 1989) (Crasquin-Soleau 2002; Richoz 2006).

Demirtaş and Öznurtepe

The Upper Permian deposits at Demirtaş and Öznurtepe belong to Yüğlük Tepe Limestone (Figure 2; Özgül 1985), which yields the uppermost Changhsingian inferred by *Paradagmarita monodi* Lys in Lys & Marcoux 1978 (Özgül 1985; Groves et al. 2005). The Yüğlük Tepe Limestone is overlain by the Sapadere Formation (Özgül 1985). The lower members of the Sapadere Formation, the Beslengiler Limestone Member and Taşlıca Member, were assigned to the Scythian (= Early Triassic) based on the presence of the foraminifera *Postcladella kalhori* (Brönniman, Zaninetti & Bozorgnia, 1972), and the molluscs *Unionites fassaensis* (Wismann in Münster, 1841), *Claraia* sp., and *Ladinaticella costata* (Münster, 1841) (Özgül 1985; Groves et al. 2005). The Beslengiler Limestone Member starts with a thin oolite bed and consists of stromatolites and oolite successions (Özgül 1985). The Taşlıca Member comprises yellow coloured mudstone marl alternations.

Taşkent

At Taşkent, the Late Permian is represented by the Çekiç Dağı Formation (Figure 2), which yields algal and foraminiferal limestone deposits overlain by an oolite bed (Özgül 1997). The Yellice Member of the Çekiç Dağı Formation represents the upper Permian in Taşkent (Özgül 1997). The Changhsingian age is assigned based on the foraminifera *Paradagmarita monodi* Lys in Lys & Marcoux 1978 (Groves et al. 2005; Payne et al. 2007). The Changhsingian sequence in Taşkent reaches up to ca. 50 meters in thickness (Altıner et al. 2021). The Çekiç Dağı Formation is overlain by the Triassic Gevne Formation (Özgül 1997). The lowermost İspatlı Member of the Gevne Formation consists of stromatolites and oolites in the lower part, and mudstone-limestone alternations above them. This member is considered Lower Triassic due to the presence of taxa such as the foraminifera *Postcladella kalhori* (Brönniman, Zaninetti & Bozorgnia, 1972), and molluscs *Unionites fassaensis* (Wismann in Münster, 1841), *Claraia clarae* (Emmrich, 1844), and *Ladinaticella costata* (Münster, 1841) (Özgül 1997; Ünal et al. 2003). The thickness of the Lower Triassic rock succession reaches 600 meters in Taşkent (Groves et al. 2005), and up to 715 meters in its type section (Özgül 1997).

Table 1. The GPS points of the logged and modelled sections.

Section	Latitude	Longitude	Altitude (m)
Çürük Dağ Crest	N36°41.543	E030°27.681	1429
Çürük Dağ Cliff	N36°41.537	E030°27.556	1409
Çürük Dağ Valley	N36°41.568	E030°27.460	1406
Öznurtepe Road	N36°19.972	E032°21.602	126
Öznurtepe Creek	N36°19.890	E032°21.474	65
Demirtaş	N36°28.821	E032°15.038	409
Taşkent Şam Deresi	N36°47.994	E032°33.461	1642
Taşkent Şam Deresi hill	N36°48.335	E032°33.258	1841
Taşkent Yolu	N36°50.615	E032°30.023	1902

2. Methods

A commercial unmanned aerial vehicle (UAV, DJI Mini4pro with an 1/1.3-inch CMOS, effective pixels: 48 MP, weight<250g) were used for the photo acquisition during a fieldtrip during 26th September to 2nd October 2024. Using manual terrain-following flight method, aerial photos were taken with forward and lateral overlap rates both >70%. During the data preprocessing and verification phase, images exhibiting focus blur, abnormal exposure, or invalid regions were

filtered out to ensure data quality. To enhance modeling accuracy and efficiency, a multi-phased, cross-software processing method is adopted:

Agisoft Metashape pro is first employed with the alignment accuracy set to high, reference preselection set to "source" or "estimated," and a key point limit of 40,000 to perform aerial triangulation. For the Taşkent Yolu model, 1,784 out of 2,750 photos were aligned, generating 743,648 tie points. For the Demirtaş model, 1,468 out of 1,487 photos were aligned, generating 849,843 tie points. For the Öznurtepe Creek model, 2,194 out of 2,804 photos were aligned, generating 1,184,433 tie points. For the Öznurtepe Road model, 365 out of 1,228 photos were aligned, generating 142,265 tie points. The Çürük Dağ Crest, Cliff and Valley model (6,072 photos) and Taşkent Şam Deresi model (8,651 photos) achieved full alignment using the estimation algorithm, generating 1,905,737 (Çürük Dağ Crest, Cliff and Valley model) and 4,465,031(Taşkent Şam Deresi model) tie points. After the aerial triangulation of each dataset, an XML file containing camera parameters and image control points data is exported for subsequent modeling in iTwin Capture. Aerial triangulation reports are also generated for detailed inspections. This dual-software workflow effectively improved model warping and stratification problems.

In the multi-view bundle adjustment phase, image indexing is achieved through a hierarchical pyramid matching algorithm based on GNSS/IMU orientation systems combined with multi-view geometry principles. Perspective distortions inherent in oblique imagery are corrected using control-point-constrained error equations. Dense matching utilizes multi-primitive algorithms and high-occlusion detection techniques to improve homologous point matching in complex terrains or objects. Subsequently, irregular triangular meshes are built using octree subdivision or region-growing methods, with dynamic adjustment of triangle density to generate high-precision digital surface models. Finally, texture mapping is performed through coordinate transformation and color matching to accurately project 2D image color onto the 3D mesh, yielding both realistic untextured (white) and textured models.

The final model outputs are: Taşkent Yolu model (4.46 GB, 16 tiles), Demirtaş model (5.71 GB, 14 tiles), Öznurtepe Creek model (4.05 GB, 18 tiles), Öznurtepe Road model (863 MB, 1 tiles), Çürük Dağ Crest, Cliff and Valley model (12.9 GB, 44 tiles), and Taşkent Şam Deresi model (31.8 GB, 89 tiles). The datasets of outcrop models have been uploaded to Zenodo (doi:xxx) for download and can be visualized in software such as DasViewer. All models have been visualized on Outcrop3D, a non-commercial web-based digital outcrop platform (Wang et al. 2024). The links to models are: Çürük Dağ Crest, Cliff and Valley (https://outcrop3d.deep-time.org/?model=a52519f2-ff78-ea42-6403-42f5022c8e31); Demirtaş (https://outcrop3d.deep-time.org/?model=ec2a8188-27b3-1da2-47b1-302f67660205); Öznurtepe Creek (https://outcrop3d.deep-time.org/?model=9cc59e1d-fcb6-b6ce-1912-bd017d00749e); Öznurtepe Road (https://outcrop3d.deep-time.org/?model=fd1234a8-a099-6f92-61a9-ab64c907ed4d); Taskent Yolu (https://outcrop3d.deep-time.org/?model=16ad6c91-681e-d0a8-2afd-55d57ebf489f); Taşkent Şam Deresi (https://outcrop3d.deep-time.org/?model=05b1d3a7-7d7e-684b-8005-8b774090b52e).

To understand the nature and timing of the extinction event we used the extinction pulse algorithm of Wang & Zhong (2018), utilizing the parallel functions incorporated into the algorithm to speed-up the analysis by Foster et al. (2024), to quantify the timing of extinction with pre-existing data from three investigated sections: Demirtaş, Çürük Dağ and Taşkent (Crasquin-Soleau et al. 2004; Groves et al. 2005; Jenny in Richoz 2006; Angiolini et al. 2007; Forel 2015; Altıner et al. 2021, 2025), and synthesized the log heights from each section into a consistent framework. Richoz (2006) did not report the log heights for the paleontological data, but the log heights were reported for carbon isotopes from the same samples. There is also data from other studies that could not be incorporated into the analysis, because exact information for the sample location within the succession was missing (i.e., Lys in Marcoux et al. 1986) or because the data appeared to be duplicated between studies (e.g., Jenny in Marcoux et al. 1986; Jenny in Richoz 2006). The extinction pulse algorithm cannot process negative log heights, and therefore the sections start with 0 meters based on the lowermost sample. The number of extinction pulses recognized by the algorithm is also affected by the number of pulses the algorithm is told to investigate and, therefore, the maximum number of pulses was set to six to avoid underrepresenting the true number of extinction pulses.

In the studied locations, we measured sections across the Permian/Triassic boundary for stratigraphic logging and took rock samples for organic and inorganic geochemical analyses. The detailed results of the geochemical analyses will be published in separate articles (Frank et al. in review; Buchwald et al. in review). We further compiled available geochemical data from previous publications (Demirtaş 2018; Lau et al. 2016; Loope et al. 2013; Riccardi 2007; Richoz, 2006; Silva-Tamayo et al. 2018) with the newly collected data to present an overall picture of geochemical proxies. More geochemical data is available but was not included either due to a lack of log heights, no data in tabular form or a focus on a very small interval, which did not capture the Permian–Triassic transition (e.g., Baud et al. 1989; Varol et al. 2011; Collin et al. 2015). To combine the selected studies, the original log heights were scaled with the formation boundary set to 0 m.

Additionally, we collected fossil samples. The taxonomic descriptions of all fossil groups will be published in a separate publication, but some characteristic fossils are presented here. We further prepared thin sections and polished sections across the Upper Permian–Lower Triassic beds from each locality. All fossil samples and rock samples figured herein are housed at the Natural History Museum, Ankara under the collection name BK-2024. The thin sections are currently stored at the University of Hamburg and will be transferred to the NHM, Ankara.

3. Results

Çürük Dağ

The Çürük Dağ section corresponds to a mountain situated at the head of the Göynük Valley, near Üçoluk village and approximately 15 km NW of Kemer. The Permian–Triassic transition is exposed on the southern flank of Çürük Dağ. The model includes the three outcrops described in this study: the crest (N36°41.543, E030°27.681), the cliff (N36°41.537, E030°27.556), and the valley (N36°41.568, E030°27.460) (Figures 3–4).

The Permian succession in Çürük Dağ is represented by the Pamucak Formation (Figure 5; Lys & Marcoux 1978). The upper part of the Pamucak Formation comprises dark-grey, fossil-rich carbonates which can be classified as wackestones and packstones (according to Dunham's classification, e.g., Flügel 2009) and hosts abundant fossils, including brachiopods, calcareous algae, bryozoans, foraminifera, gastropods, ostracods, and echinoderms (Brachiopoda: Angiolini et al. 2007, Verna et al. 2011; Trilobita: Lerosey-Aubril & Angiolini 2009; Ostracoda: Crasquin-Soleau et al. 2002, 2004). As we follow the succession further up, the limestone becomes nodular (Figure 6; Appendix 1-Figure 37). The limestones bear bellerophontids, the brachiopods *Spinomarginifera* and *Orthothetina* and large calcareous algae (Figure 8). The scree deposits, originating from the Permian Pamucak Formation in the valley section, are dominated mainly by the two brachiopod genera, bellerophontids, and burrow fragments up to 2 cm in diameter. The scree material contain few infaunal bivalves including *Edmondia* and the pseudorthoceratid *Lopingoceras lopingense*. In the scree, it is also possible to find gypsum crystals (daisy rosettes).

Above the nodular limestones, the lithofacies abruptly changes into oolitic grainstones (Figure 8G; App. 1-Figure 40). The top of the Pamucak Formation is defined by the lower surface of the transitional oolitic beds, which is overlain by the stromatolites of the Lower Triassic Kokarkuyu Formation (Marcoux & Baud 1988; Baud et al. 2005). We have marked the base of the oolites as the formation boundary following Marcoux & Baud (1988) as it represents an abrupt facies change. The transitional oolite was deposited on an erosional surface and within the transitional oolite bed, flat pebbles composed of oolitic grainstone were observed (App. 1-Figure 38). The oolite bed is overlain by microbialites and stromatolites (Kershaw et al. 2011, 2012), but in the crest section there is a thin carbonate mudstone layer (10 cm thick) between the oolite bed and the stromatolites (Figure 6), which is probably the discontinuous bed identified as thrombolites by Kershaw et al. (2012). The Griesbachian age has been assigned to the microbialites based on the presence of the conodonts *Hindeodus parvus* (Kozur & Pjatakova, 1976) and *Isarcicella isarcica staeschei* (Dai & Zhang, 1989) (Crasquin-Soleau 2002; Richoz 2006). At the Çürük Dağ crest outcrop, where the microbialites of the Kokarkuyu Formation are more thoroughly exposed, the first 16 meters of the formation are characterized by thromobolites and domal stromatolites (Kershaw et al. 2012; App. 1-Fig. 34). Lipid biomarker data suggests that the layered microbial mats forming these microbialites were likely cyanobacteria-dominated, with anoxygenic photoautrophic bacteria and sulfate-reducing bacteria inhabiting anoxic zones within the microbial mat (Heindel et al. 2018).

Microbialites are overlain by oolitic grainstones with sparse fossil content (Fig. 8F). Further up in the section, light-yellow mudstones yield a low diversity mollusc dominated fauna including *Claraia clarae* (Emmrich, 1844) and *Eumorphotis* (App. 1-Figs 16–17). The Lower Triassic yellow mudstones of the Kokarkuyu Formation are freshly exposed in the valley section, while they are only exposed as small pieces of scree on the crest. These mudstones contain cosmopolitan mollusc genera, i.e., *Neoschizodus*, *Claraia, Eumorphotis* (Figure 8), and a new myophoricardiid bivalve genus that resembles *Unionites* in external shell morphology. The yellow mudstones also include pyrite deposits (Figure 8E). Similar to the ripple marks preserved in the yellow mudstones of the Öznurtepe Road section, the transition from microbialites and dolomitized limestone layers to silty mudstones is also characterized by asymmetrical ripple-marks (App. 1-Fig. 19). Going up sequence, the succession comprises shell beds, gutter casts infilled with shells (App. 1-Figs 20–21). In the scree from this outcrop, some rocks contain bivalve external moulds, infilled with sediments in different color (App. 1-Figs 22–23). Further up in the lower Triassic mudstone succession in the valley, there is a grading upward succession starting with microgastropod and bivalve dominated shell beds, continuing with laminated mudstones, and terminating with cross-bedding (App. 1-Figs 24–27). As following up the creek towards the dirt road, so higher up in the succession, the creek contains rocks with flat pebbles (App. 1-Fig. 29).

Demirtaş

The Demirtaş exposures are ~25 km southeast of Alanya, ~20 km north of Gazipaşa, and 10 km northeast of Demirtaş on the Sapadere Creek (Figure 11). The Permian–Triassic transition in this area was first described in detail by Özgül (1985) who named the Yüğlük Tepe and Sapadere Formation for the Upper Permian and Lower Triassic, respectively. Here, the measured sections are located in the type region of these formations and near the section named as Demirtaş-Kuşdavut by Richoz (2006), and ca. 1 km southwest of the Tırlar section measured by Şahin & Altıner (2019). The studied Permian–Triassic transition is located slightly north of a small limestone quarry, which is next to the road that diverged from Kaşlıoğlu Street and leads to the Yaylakonak Neighborhood. The Permian/Triassic boundary is well-exposed in the woods at N36°28.821, E032°15.038 (Figure 9) as well as in the small quarry (Crasquin et al. 2009), but because of the freshly cut surfaces it is difficult to discern sedimentological features in the quarry. A further exposure (N36°28.7447 E032°14.7688) is located on the southern side of the road, between the small northern quarry and a larger southern quarry (App. 2-Fig. 14), but the formation contact and Permian part of the succession is not as well-exposed.

Generating the models for Demirtaş was cumbersome, because of the dense woodland, making it difficult to fly the UAV and for the images from the UAV to be stitched when generating the model (Figure 10). In addition, flying the UAV above the canopy hinders clear sight of the outcrops. Despite the dense vegetation, the Yüğlük Tepe Formation is well exposed with dark grey packstones and wackestones filled with a diversity of fossils including crinoids, large

bellerophontid gastropods, brachiopods, calcareous algae, and foraminifera (Figure 14L; App. 2-Figure 16). The transitional oolite at the base of the Sapadere Formation (Figure 14J–K) is poorly exposed. The overlying thick stromatolitic beds of the Sapadere Formation are well exposed, forming a small cliff (App. 2-Figure 6–7). In the basal stromatolites, thin horizons of microgastropods and shelly debris can be observed.

Previous logs of the Demirtaş section give different thicknesses for the "microbialite unit", i.e., ~27.5 m in Groves et al. (2005), 20 m in Riccardi (2007) and ~18.5 m in Richoz (2006). We only measured ~9 m of microbialites (stromatolites and thrombolites) followed by 9.5 m of dominantly oolitic beds that also occasionally contain cross bedding (Figure 12). The differences between Groves et al. (2005) and our study could be because the sections were measured at different locations, but the exact location was not given in Groves et al. (2005). The thickness of the microbialite unit was measured 8–10 meters in the type section of the Sapadere Formation, which is located ca. 2 km northeast of the studied section (Özgül 1985). The oolitic grainstones are, however, heavily recrystallized and it is difficult to discern sedimentological features in the field. The oolitic grainstones are capped by microbialite beds. The succession then transitions to laminated, yellow-weathered micritic beds of the Taşlıca Member with bedding planes exposing abundant, typical Lower Triassic bivalves, such as *Claraia clarae* (Emmrich, 1844), and *Neoschizodus* (Figs 14B–E). The subsequent succession is poorly exposed as small outcrops within the woods.

Öznurtepe Road and Creek

The Öznurtepe Road section (Figs 15A–B) is a road cut along the Küçüklü Köyü Yolu ~10 km northeast of Gazipaşa (Fig. 11). The Permian–Triassic transition at the Öznurtepe sections was first reported by Crasquin et al. (2009). When looking down into the valley of Sinad Creek from the Öznurtepe Road section, the Öznurtepe Creek section is visible on the western shore of the creek, where the weathering resisting Upper Permian limestones and Early Triassic microbialites form a distinct cliff. It is also clear that the succession repeats itself, and the creek and road section do not connect along the strike of the beds. The Öznurtepe Creek section can be accessed by following an unpaved road into the creek valley, that branches off Küçüklü Köyü Yolu ~2 km in direction of Gazipaşa. The creek must be crossed to reach the western shore of Sinad Creek (Figure 15C), where the Permian–Triassic transition is exposed at least twice due to faulting. 3D outcrop models were created from the Öznurtepe Road section (N36°19.972, E032°21.602; Figure 16) and the southern outcrop of the Öznurtepe Creek section (N36°19.890, E032°21.474; Figure 17). While generating a digital 3D outcrop model from the road cut at Öznurtepe Road is rather straightforward, the vegetation at the Öznurtepe Creek affected the quality of the model by covering some parts of the section, but nevertheless the formation boundary is visible in the model.

At the Öznurtepe Road and Creek sections (Figure 18), the Upper Permian Yüğlük Tepe Formation is composed of fossiliferous wackestone, which yield abundant fossils, e.g., bellerophontids, crinoids, and calcareous algae (Figure 19B–C; App. 3-Figs 5–6, 21, 25). At the Öznurtepe Road section, the Upper Permian Yüğlük Tepe Formation can be followed from lower to upper beds along the road, because the beds are highly tilted and almost vertical. At Öznurtepe Creek, the limestones of the Yüğlük Tepe Formation are overlain by a relatively thin (<10 cm thick) oolitic grainstone bed with similar characteristics (e.g., size, grade of recrystallization) as other Permian–Triassic sections in the Taurides and other Tethyan deposits (Li et al. 2015). It is overlain by the Griesbachian stromatolitic and thrombolitic beds of the Beslengiler Member of the Sapadere Formation. The contact between the oolitic grainstone and the first microbialite bed is hummocky (Crasquin et al. 2009, fig. 42) At Öznurtepe Road, the Yüğlük Tepe/Sapadere formation boundary is obscured by calcite crystals that have formed in a zone of severe tectonic deformation and folding (Figure 15A). When following the road towards Gazipaşa (southwards), the thick microbialitic beds of the Beslengiler Member of the Sapadere Formation are also exposed at Öznurtepe Road above the syncline hinge zone (Fi. 15B). In contrast to Çürük Dağ where several thrombolitic beds and domal stromatolites can be observed, only one < 50 cm thick domal stromatolite bed was identified at Öznurtepe by Kershaw et al. (2012), and the microbialites mainly consist of planar stromatolites. In the microbialites, microfossils (foraminifera, ostracods, gastropods) have been found in low abundances and diversity (Foster et al. 2019 supporting information; and new samples). Above the microbialites, thick oolitic beds are formed in the Early Triassic, with ooids with a diameter up to 1 mm (App. 3-Fig. 31). They are overlain by thinly bedded yellow weathered mudstones/siltstones of the Taşlıca Member, that exposes beds with ripple marks (App. 3-Figure 17). In addition, the Taşlıca Member hosts the first Triassic macrofossils including the cosmopolitan bivalves *Claraia, Unionites*? and *Neoschizodus* (App. 3-Figs 13–16). In the Öznurtepe Creek section, the yellow weathering mudstones of the Taşlıca Member were metamorphosed into slates with crenulation folds (App. 3-Figure 32; Bozkaya & Yalçın 2005).

Taşkent

Taşkent Yolu

This section is exposed along Taşkent Yolu (Road) at N36°50.615, E032°30.023, approximately 9 km south of the Taşkent district, Konya (Figure 22). The exposure described here is on the northern side of the road and was excavated to widen the road during our last visit in 2024 (Fig. 20), when the pictures were taken for the outcrop models (Fig. 21). The studied section is ca. 0.6 km south of the GPS coordinates given for the Permian–Triassic section previously measured by Baud et al. (2005). Starting from the measured section previously reported by Baud et al. (2005), the Çekiç Dağı Formation yields limestone facies with large calcareous algae (1 cm in diameter) *Permocalculus anatoliensis* (Güvenç, 1966) (App. 4-Fig. 1) and large gastropods (App. 4-Fig. 2–

4). The skeletal carbonates of the Çekiç Dağı Formation are overlain by oolitic grainstones, and microbialites of the İspatlı Member of the Gevne Formation. The yellow mudstones of the İspatlı Member of the Gevne Formation at this locality yields an undescribed myophoricardiid bivalve genus and the cosmopolitan bivalves *Neoschizodus* and *Eumorphotis* (Figs 23G–H). The yellow mudstone outcrop also bears an unidentified ammonoid in a gastropod oolite (Fig. 23I). Different from the sections in Antalya, large oncolites (Fig. 23F; App. 4–Figs 7–8) and oolites with microgastropods are deposited on top of the yellow siliciclastics after the microbialites. Towards younger layers on the southern side of the road, oolitic grainstone deposits composed of microgastropods and oolitic rip-up clasts are cropping out (App. 4–Figs 11–15). These are overlain by green-grey siliciclastics with abundant microgastropods. On top of that are reddish siliciclastics with ripple marks, gutter casts and rip-up clasts (App. 4–Figs 16–18). The reddish silicilastics also have Kinneyia (Fig. 23E), a sedimentary structure that has been interpreted as microbial mat (e.g., Pruss et al. 2004), but might also be formed by physical processes, such as earthquakes (Herminghaus et al. 2016; Pratt 2021). These siliciclastics are overlain by light gray limestone, having a vermiform appearance (App. 4-Figs 19, 20, 24). Thin section revealed that the vermiform appearance is a result of micro pressure dissolution (Fig. 23D). These gray limestones intercalate with the green to reddish mudstones and in the upper part of the succession (App. 4-Fig. 21). The gray limestones with micro pressure dissolution structures cropping out ca. 1.4 km southwest of the Permian/Triassic boundary, and yield *Tirolites cassianus* (Quenstedt, 1849) (Fig. 23C), indicating the Spathian substage (e.g., Broglio Loriga et al. 1990). Around this outcrop, it is also possible to find yellow mudstones with *Ladinaticella costata* (Münster, 1841) and *Rhizocorallium* isp. and the gastropod oolite bed, characterized by dominant and moderately diverse gastropod fauna (Fig. 23A–B; App. 4-Fig. 25).

Taşkent Şam Deresi

The Taşkent Şam Deresi section (N36°47.994, E032°33.461; Figs 24A–B, 25) is located along the road parallel to Şam Deresi Creek and is ca. 700 meters south of the measured section called DT (N36°48.335, E032°33.258) by Altıner et al. (2021). Below the oolitic grainstones marking the formation boundary, 50 meters of the Changhsingian was measured by Altıner et al. (2021). The Permian limestone-mudstone alternation continues and reaches up to couple of hundred meters, but the position of the Wuchiapingian/Changhsingian stage boundary is uncertain in the section. The Upper Permian Çekiç Dağı Formation yields large gastropods, algae, crinoids, echinoids, bryozoans and brachiopods including *Comelicania*, *Orthothetina* and *Spinomarginifera* (Fig. 29, App. 4-Figure 35–36). As in the Taşkent Yolu section, the skeletal carbonates are overlain first by oolitic grainstones and microbialites, then by large oncolites (Fig. 26). Higher in the section, the carbonate succession terminates with an oolitic grainstone bed showing dark stripes (App. 4-Figs 41–43). The dark stripes appear to originate from intercalation of aragonitic ooids and calcitic grains (Figs 28A–B). These oolitic grainstones also yield medium sized bivalves, possibly myophorids. The yellow mudstones are not well exposed in the section, and, due to many faults, the succession appears to be repeated making it difficult to measure, but the subsequent unit of

poorly cemented, green and reddish silicilastics are well exposed. There are abundant *Neoschizodus* and *Eumorphotis* on the bedding surfaces of the siltstones in this unit (Fig. 30D). They also yield a horizon with tubular structures composed of mudstone (Fig. 30D, App. 4-Figs 45–47), which are either rip-up clasts or possibly redeposited burrow molds. Further along the section, the reddish mudstones are overlain by yellow mudstone deposits with large burrows (*Rhizocorallium* isp. App. 4-Fig. 48). The gastropod *Ladinaticella costata* (Münster, 1841), and large *Bakevellia* sp. reaching up to 4 cm (Fig. 30A, App. 4-Figs 49–50). Large *Bakevellia* species and *Ladinaticella costata* are also characteristic to the Spathian of Italy (Neri & Posenato 1985).

In all studied sections the Permian–Triassic transitional deposits start with the carbonate beds classified as wackestones/packstones and continue with oolite, microbialite, stromatolites, then with yellow colored Dienerian mudstones. Although some greenish mudstones, possibly from the Smithian, were found in Çürük Dağ, the reddish silicilastics of the Olenekian are only exposed in Taşkent, which are overlain and intercalated with *Tirolites* bearing fray colored mudstones, indicating Smithian/Spathian boundary (Fig. 27). Hence, environmental and community evolution can be tracked for a much longer interval in Taşkent.

Geochemical record

Geochemical investigations at the studied locations most commonly determine carbon and, less commonly, oxygen and sulfur cycle perturbations (Baud et al. 1989; Demirtaş 2018; Frank et al. in review; Riccardi 2007; Richoz 2006). Multiple studies have also focused on identifying changes in the environmental conditions across the Permian/Triassic boundary with a dominant focus on reconstructing paleoredox conditions (Collin et al. 2015; Frank et al. in review; Lau et al. 2016; Loope et al. 2013; Riccardi 2007; Varol et al. 2011), while only one study investigated pH changes (Silva-Tamayo et al. 2018). Other environmental changes commonly associated with the Permian–Triassic mass extinction, such as increased sea surface temperatures or changes in nutrient availability, have not yet been investigated at the discussed sections.

Reported $\delta^{13}C_{carb}$ isotope data reveal a decrease from approximately 4 ‰ in the Late Permian to 0–2 ‰ in the Early Triassic at Çürük Dağ (Demirtaş 2018; Richoz 2006; Figure 7), Demirtaş (Riccardi 2007; Richoz 2006; Figure 13), Öznurtepe (Demirtaş 2018; Frank et al. in review) and Taşkent (Lau et al. 2017; Richoz 2006; Silva-Tamayo et al. 2018; Fig. 28) (Appendix 5). The $\delta^{18}O$ trends from Çürük Dağ (Demirtaş 2018; Richoz 2006), Demirtaş (Riccardi 2007; Richoz 2006), and Taşkent (Lau et al. 2017; Richoz 2006; Silva-Tamayo et al. 2018) also reveal a shift towards heavier values across the Permian–Triassic transition with a drop from approximately -4–5‰ to -8‰. From Öznurtepe, $\delta^{18}O$ data only exists from the Early Triassic, which reveals a $\delta^{18}O$ value around -8‰ for the Beslengiler Limestone Member, which agrees with the other locations, while the Taşlıca Member records a wide range in values (Demirtaş 2018).

A variety of proxies have been applied to reconstruct redox changes at the investigated locations (see Appendix 5 for detailed discussions). Local redox changes were studied at Çürük Dağ and Öznurtepe using redox sensitive metal trends and Ce anomalies, with the latter also being applied

to Demirtaş (Collin et al. 2015; Frank et al. in review; Loope et al. 2013). Overall, these proxies support prevalent oxic conditions in the Early Triassic, while the redox interpretations for the Late Permian were more ambiguous, suggesting the potential development of anoxic episodes. Sulfur isotope data from Demirtaş was even interpreted to indicate the appearance of euxinic events. A global spread of seafloor anoxia concurrent with the Permian–Triassic transition is further supported by the decreasing trend in $\delta^{238}U$ reported at Taşkent (Lau et al. 2016), however, as U isotopes are a global redox poxy, no information on the local redox conditions at Taşkent during this period are currently available.

While the complete Ca isotope record reported for Taşkent reveals a negative excursion suggesting acidification, the interval 25 m below and above the formation boundary does not show a discernable trend (Silva-Tamayo et al. 2018) (Appendix 5, Fig. 28). At the other three localities no geochemical pH proxies have been reported thus far, thus few constraints exist to determine whether pH changes occurred concurrent to the Permian–Triassic mass extinction.

Overall, geochemical data from the investigated localities are still scarce, with multiple environmental changes important for biodiversity changes unconstraint, revealing the need for future work at the studied locations to better understand the mechanisms driving the Permian–Triassic mass extinction at these key sections representing the southern Palaeotethys and Neotethys.

Timing of extinction

At Çürük Dağ, when all the stratigraphic ranges of the different fossil groups are investigated together, 34 extinction pulses can be quantitatively identified with 70% confidence (Fig. 7). When 3 or 4 pulses were identified, the extinction pulse that is not a consequence of edge effects is identified at 0.43 m, which is within the thin transitional oolite beds. The diverse Early Triassic ostracod record is unique to Çürük Dağ (Forel 2015) but is problematic. There are too many species within the same genus (up to 23 species in *Bairdia*), which is unusual both during the Permian and in the Triassic. The high ostracod diversity in the Early Triassic might be partially because of higher sample size from the Triassic than the Permian, as the diversity is correlated with the sample size (Crasquin et al. 2009, figure 4) but seems to be caused by oversplitting. When ostracods are removed from the analysis, the main extinction pulse is still identified at 0.43 m (Fig. 7). At Demirtaş and Taşkent, two significant extinction pulses are identified (Appendix 6 and 7), one being the consequence of edge effects, and the main extinction pulse at 0.26 m and 1.67 m, respectively, at the top of the transitional oolite bed (Figs 13, 28).

4. Discussion

We have documented the Permian–Triassic transition in southwestern Türkiye in detail using 3D outcrop modelling, stratigraphic logging, photography, geochemical and paleontological analyses.

These new data and analyses have implications on our understanding ecosystem change at the studied localities, including the change in environmental settings through time and the timing of extinction. Based on the new findings and challenges encountered while integrating them with existing knowledge, we recommend standardizing formation boundaries and names across all localities and adhering to the FAIR principles for data sharing.

4.1 The Formation Names

The preferred formation names differ between publications even at the same location. The studied sections are located in the Antalya and Aladağ Nappes and considered to be deposited at distant paleogeographic locations/basins. Hence, it is uncertain whether the Permian and Early Triassic sections within the Antalya Nappe (Çürük Dağ, Demirtaş and Öznurtepe) and the Aladağ Nappe (Taşkent) can be considered to belong to the same stratigraphic formations.

Çürük Dağ

Şenel (1997) assigned the late Permian deposits around Çürük Dağ to the Dinek Formation (Dinek Limestones: Kalafatçıoğlu, 1973), which has a type section in Sivridağ located northwest of Çürük Dağ. According to Kalafatçıoğlu, the Dinek Limestones attain 200 m thickness in their type locality but reaches over 1,000 meters in thickness. The Dinek Limestones are overlain by Permian Fesliğen Dolomites, which are underlying the Triassic sandstones. The information on the faunal content of the Dinek Formation and the stratigraphic succession in its type locality is limited and needs to be updated to assess its relationship to the Pamucak Formation (Lys & Marcoux, 1978). The present information is not adequate to clarify whether they represent two distinct formations or whether they are two different names used for the laterally continued same deposits (synonyms). If so, the Dinek Formation has the priority for usage, as it was defined prior to the Pamucak Formation. Şenel (1997) used the name Kesmeköprü Formation for the Lower Triassic deposits at Çürük Dağ, but this name cannot be traced in the literature, even in the references that were provided by Şenel (1997), therefore considered a nomen nudum.

Öznurtepe and Demirtaş

Lower Triassic successions at Öznurtepe and Demirtaş were assigned to the Kokarkuyu Formation (Altıner 1981, Altıner et al. 2021) and partly to the Akıncıbeli Formation at Demirtaş (Şahin & Altıner 2019). The Akıncıbeli Formation was used in an unpublished report (Demirtaşlı 1987) and later than the description of the Sapadere Formation (Özgül 1985), hence, it needs to be abandoned. A revision of regional stratigraphy is needed to assess if the Beslengiler Limestone Member and Taşlıca Member are junior synonyms of the Kokarkuyu Formation. It should also be considered that the original description of the Kokarkuyu Formation only encompasses the Griesbachian microbialites and oolites, as well as the yellow Dienerian mudstones, but not the Olenekian green to red siliciclastics and yellow mudstones with *Ladinaticella costata* (Münster, 1841).

The Lower Triassic rocks were assigned in some publications to the Katarası Formation (e.g., Şenel et al. 2016), which was later regarded as a group by Altıner et al. (2025). The Katarası

Formation was named in an unpublished MTA report by Demirtaşlı (1967), hence, it is not a formally established name (Özgül et al. 1973) and should be abandoned.

Although we decreased the number of formation names covering the Permian–Triassic transition in the studied sections down to six, the names can be further decreased into four by revising the existing formation names in Antalya Nappe. As the general lithological change is the same in all localities, the names might be potentially decreased into two. In all sections, the lithology starts with well-bedded Upper Permian limestone-mudstone alternation and the overlying oolitic bed and continues with the Griesbachian stromatolite and Lower Triassic mudstones (Figs 6, 12, 18, 26). Such revision should consider that successions in the sections in Antalya (Çürük Dağ, Öznurtepe, Demirtaş) are part of the Antalya Nappe and considered to be deposited in the Neotethys Basin, whereas the Taşkent successions are part of the Aladağ Nappe and generally reconstructed in the Palaeotethys Basin. Although there are minor differences in the faunal composition, there are many common taxa at the studied localities. Overall, the lithology and the fossil record do not suggest these successions are part of disconnected basins. There is a clear need for detailed study of the successions for revision of the formation names mentioned above and a standardization of the formation names in the studied localities.

4.2 Position of the Permian–Triassic boundary and formation boundaries

The Permian–Triassic boundary was constrained only in the Çürük Dağ section. The transitional oolite records the uppermost Changhsingian conodont *Hindoedus* cf. *praeparvus* Kozur, 1996 (Angiolini et al. 2007) and the subsequent lowermost microbialite bed records the index fossil conodont *Hindeodus parvus* (Kozur & Pjatakova, 1976) (Crasquin-Soleau et al. 2002). The Permian/Triassic boundary in all other sections is placed based on lithological correlations and overall fossil content (e.g., Changhsingian marker *Paradagmarita monodi* Lys in Lys & Marcoux 1978; Early Triassic marker *Postcladella kalhori* (Brönniman, Zaninetti & Bozorgnia, 1972)) and the negative carbon isotope excursion reported in the transitional oolites in all sections (e.g., Richoz 2006, Figs 7, 13, 28). There is a need for further studies involving conodont biostratigraphy and geochronology to corroborate the position of the Permian/Triassic boundary. Studies are also needed for locating the Wuchiapingian/Changhsingian boundary and Early Triassic stage boundaries.

One of the confusions in the published literature is the position of formation boundaries. Nearly all studies place formation boundaries above the transitional oolites in the studied formations (Groves et al. 2005; Baud et al. 2005; Richoz 2006; Payne et al. 2007; Crasquin et al. 2009; Altıner et al. 2021, 2025). However, in the original description, the Sapadere Formation starts with a thin oolitic bed in its type section (Özgül 1985), so in Demirtaş and in Öznurtepe, the transitional oolites by definition mark the base of the Sapadere Formation. In Taşkent, Özgül (1997) included the oolite bed in the lower formation, the Yellice Limestone Member of the Çekiç Dağı Formation, hence, in Taşkent, the transiotional oolites, by definition, belong to the uppermost part of the Çekiç

Dağı Formation. The transitional oolites was neither described in the Upper Permian Pamucak Formation by Lys & Marcoux (1978) nor in the Lower Triassic Kokarkuyu Formation by Altıner & Zaninetti (1981). Subsequently, it was included in Kokarkuyu Formation by Marcoux & Baud (1988), but then in Pamucak Formation (Baud et al. 2005; Richoz 2006; Crasquin et al. 2009; Altıner et al. 2021, 2025).

The oolitic beds mark an abrupt change in the environment and the onset of a significant decline in biodiversity, so the facies change from skeletal carbonates (packstones/wackestone) to poorly fossiliferous oolites and microbialites. Although an oolitic facies alone cannot be attributed to a mass extinction event, together with an abrupt decline in diversity, it indicates a high carbonate saturation in the absence of calcifying organisms (Groves & Calner 2004; Grooves et al. 2005; Kershaw et al. 2011). Furthermore, the preservation and size of the ooids within the oolitic transitional bed is consistent with the oolitic beds of the Kokarkuyu and Gevne formations. For that reason, we herein included the first oolite bed in the younger formations under an informal name "transitional oolite" as it represents the transition from the Permian to the Triassic and marks the onset of the extinction event, which represents transition from the Paleozoic Evolutionary Fauna dominance to Modern Evolutionary fauna dominance (Sepkoski 1981).

4.3 Extinction horizon (the onset of extinction interval)

Although there is a consensus that the microbialites (i.e., stromatolites and thrombolites) in the studied sections are interpreted as post extinction deposits (e.g., Groves et al. 2005; Crasquin et al. 2009; Kershaw et al. 2011), the extinction horizon has been placed at different horizons along the succession: the top of the Changhsingian transitional oolites, the bottom of the transitional oolites, further below within nodular limestones. Grooves et al. (2005) reported an unconformity above the transitional oolite in Taşkent and placed the extinction boundary on top of the transitional oolites. This is based on the disappearance of taxa prior to and during deposition of the transitional oolites being attributed to the Signor-Lipps effect and facies shift into a high energy oolitic deposit. The transitional oolites were also referred to as "disaster deposits" by Grooves et al. (2005). Whether or not the transitional oolites mark the extinction event or post-extinction deposits was also repeatedly discussed (Baud et al. 2005; Crasquin et al. 2009; Kershaw et al. 2011). Angiolini et al. (2007) considered the brachiopods in the Changhsingian nodular limestones as a post-extinction "survival fauna", implying a much lower stratigraphic position for the extinction in the stratigraphic section.

The quantitative evaluation of recognizing extinction pulses using the extinction pulse algorithm (developed by Wang & Zhong 2018) gives consistent results between the three investigated sections (Figs 7, 13, 28). It is, however, important to note that the extinction pulse algorithm is heavily affected by edge effects, meaning it will recognize an artificial extinction pulse associated with the final fossil occurrences within a dataset. At all three sections, it can also be observed that the stratigraphic ranges of algae and brachiopods do not extend into the oolitic bed. In addition, it can also be observed from the stratigraphic logs and field work that large gastropods and crinoids,

which have not been taxonomically described, and are not included in the analysis, also do not extend into the oolitic beds except for bellerophontids and coelostylinid gastropods. The recognition that the main extinction pulse occurs within the transitional oolite is, therefore, a consequence of the stratigraphic ranges of foraminifera, and ostracods at Çürük Dağ, that dominate the diversity of pre-extinction fossils. Foraminifera also show a gradual disappearance prior to the extinction pulse identified by the algorithm, which can be attributed to the Signor-Lipps effect. In addition, the lack of high-resolution sampling of fossil groups beyond foraminifera and algae across the Permian–Triassic transition means that the timing of extinction is best inferred from the foraminifera and algal fossil records. Therefore, the disappearance of algae at the base of the transitional oolite beds, and the identified extinction pulse driven by the foraminifera fossil record, suggest the mass extinction is best defined as an extinction interval starting at the base of the transitional ooids until its upperpart with the extinction pulse associated with foraminifera (Figs 7, 13, 28). This extinction interval coincides with the occurrence of the upper Changhsingian *Hindeodus* cf. *praeparvus* Kozur, 1996 and prior to the first occurrence of Triassic conodonts, suggesting the extinction occurred in the latest Permian, prior to the Permian/Triassic boundary.

4.4 Environmental evolution across the Permian–Triassic in the Antalya and Aladağ Nappes and their correlation with other sections

The lithofacies of the Permian Pamucak (Çürük Dağ), Yüğlük Tepe (Demirtaş, Öznurtepe), and Çekiç Dağı (Taşkent) formations are similar to shallow marine, pre-extinction, carbonate platforms successions known from across the Palaeo- and Neotethys oceans (e.g., Great Bank of Guizhou: Lehrmann et al. 2003, and Transcaucasian–NW Iranian region: Gliwa et al. 2020), in that they are skeletal limestones dominated by calcareous algae, fusulinid foraminifera, large gastropods, crinoids, rugose corals, bryozoans and brachiopods (Altıner 2000; Ünal et al. 2003; Figs 8, 14L, 19, 29). In addition, the stromatolite, thrombolite and oolitic lithofacies at the base of the post-extinction (mostly Griesbachian) Kokarkuyu (Çürük Dağ), Sapadere (Demirtaş, Öznurtepe), and Gevne (Taşkent) formations are also consistent with shallow, post-extinction, carbonate platform successions from across the Palaeo- and Neotethys oceans. A major sedimentological shift occurs, however, in the late Griesbachian–Dienerian, where the carbonate succession shifts to a mixed siliciclastic-carbonate succession characteristic of the homoclinal carbonate ramps from central Europe during the Early Triassic (e.g., Werfen Formation, Italy: Broglio Loriga et al. 1983; Servino Formation, Italy: Foster et al. 2018; or Aggtelek Karst: Hips 1998).

The pre-extinction Permian formations in the Antalya and Aladağ nappes contain calcareous algae including the red algae *Gymnocodium* and *Permocalculus* at Demirtaş, Öznurtepe and Çürük Dağ, indicating a shallow water environment on the shelf in the photic zone (ca. 0–200 meters depth) (Flügel 2009). At Çürük Dağ, the Permian Pamucak Formation terminates with nodular limestones,

before the transitional oolites of the Kokarkuyu Formation. It is unsure whether the nodular limestones and intercalated thin layers of mudstones were formed as a result of post-depositional processes (such as pressure dissolution), or reflect the synsedimentary depositional regime shifts from carbonate dominance to siliciclastic dominance (due to variations in carbonate to clay input), or might be formed as a result of heavy bioturbation (e.g., Kahsnitz & Willems 2019). Following the depositional model that Ünal et al. (2003) suggested for the Permian–Triassic transition in the Aladağ Nappe in the Central Taurides, a shallowing upward trend can be interpreted until the transitional oolites in all sections. There were oscillations in water depth, first by slight deepening indicated by slightly offshore microbialites (recorded as being formed by layered cyanobacterial, benthic mats; Heindel et al. 2018) and then shallowing indicated by near shore oolites and clastic deposits with ripple marks, the latter suggesting deposition in a setting above wave base. The dominance of anachronistic lithofacies (oolite deposits, microbialites and calcite crystal fans) reflect deposition when seawater was likely super-saturated with respect to calcium carbonate, which characterizes the immediate aftermath of the end-Permian mass extinction (Kershaw et al. 2011; Foster et al. 2019) as a consequence of a large carbon injection into the ocean-atmosphere system (Cui et al. 2021) and a disruption of the carbon cycle as a result of extinction or decline of biomass of organisms with skeletal carbonate (Grooves et al. 2005). Oolite deposition has been observed in many other sections across the Permian–Triassic transition in Tethys (e.g., Haas et al. 2007; Li et al. 2015). The switch from carbonate platform facies to a mixed siliciclastic-carbonate homoclinal ramp facies (Figure 31) indicates an increase in sediment supply, which might be associated with increased physical weathering rates due to increased temperatures or declined plant biomass (Algeo & Twitchett 2010; Xu et al. 2025), and rifting during the opening of the Neotethys (Şahin & Altıner 2019). From the Dienerian onwards, storm-induced rip-up clasts, flat pebbles and tempestites in Çürük Dağ, Öznurtepe, Demirtaş and Taşkent indicate deposition above storm-weather wave base (e.g., Hips 1998; Török 1998; Wignall and Twitchett 1999). Some rocks contain bivalve external moulds, infilled with differently colored sediments, indicating subaqueous shell dissolution and a depositional hiatus.

Following the environmental model of Ünal et al. (2003) suggesting lateral facies change from near shore to offshore as oolite-stromatolite-shallow water carbonates, one may interpret the thicker oolitic and thinner stromatolitic deposits in Taşkent, Öznurtepe and Demirtaş, compared to Çürük Dağ, to reflect a shallowing trend in west to east direction. However, it should be noted that Taşkent sections yield thicker successions compared to more condensed successions at Çürük Dağ, Demirtaş and Öznurtepe, and the thickness of each unit is influenced by the sediment input and deposition.

It is also noteworthy that the timing of the carbon isotope excursion is different between the three sections, where at Taşkent the isotope excursion onset is 40 cm below the transitional oolites (onset of extinction), at Demirtaş ~ 250 cm below the transitional oolites, and at Çürük Dağ, at the base of the transitional oolites (Richoz 2006; Riccardi 2007). A similar diachronous pattern in the carbon isotope excursion has also been observed for the lowermost oolitic beds of the Tesero

Member in the Dolomites, Italy (Kraus et al. 2009). This suggests that the transitional oolitic beds are diachronous, and the transitional oolitic bed at Demirtaş (Sapadere Formation) is stratigraphically younger than the Taşkent (Gevne Formation) and Çürük Dağ sections (Kokarkuyu Formation). The relative position differences in sediment accumulation rates. Nevertheless, the timing of extinction in the Demirtaş and Taşkent sections appear to be at the top of transitional oolite, while the peak is found within the transitional oolites in Çürük Dağ. In addition, considering the high similarity of carbon isotope profiles between the Antalya and Aladağ Nappes (Richoz 2006) and the Dolomites in Italy (Korte & Kozur 2005; Richoz 2006; Kraus et al. 2009), such as the preservation of double negative carbon isotope excursion, we do not agree that the erosional surface between the oolitic and stromatolite lithofacies represents a large unconformity, as previously suggested (see Crasquin et al. 2009, and Ünal et al. 2003).

The pattern of extinction at Çürük Dağ, Demirtaş and Taşkent is also very similar to shallow water sections from the Dolomites in Italy, where the pre-extinction Permian carbonates are separated from post-extinction carbonates by a transitional oolitic bed with a mixture of reworked and autochthonous Permian holdover fossils (Farabegoli et al. 2007; Brandner et al. 2009; Farabegoli & Perri 2012). Similarly, the transitional oolitic bed at Çürük Dağ, Demirtaş and Taşkent in Türkiye consists of autochthonous Permian holdover fossils (Marcoux et al. 1986; Grooves et al. 2005). Similarities in facies change between the Antalya Nappes (Türkiye) and the Dolomites (Italy) was also recognized by Ünal et al. (2003).

The faunal content and lithology of the studied sections correlate well with the Upper Permian Bellerophon Formation and the Lower Triassic Werfen Formation. Similar to the Bellerophon Formation in Italy, which was named after the abundant bellerophontid gastropods, the bellerophontids also represent one of the most abundant taxa in Çürük Dağ, Demirtaş and Öznurtepe, and the successions consist of light and dark wackestone-mudstone alternations. In northern Italy, Austria, Croatia, and both the Aggtelek Karst and Balaton Highlands in Hungary, the mixed carbonate-siliciclastic successions are represented by reddish siltstones and sandstones interpreted to represent a "terrigenous event" during the Smithian, often referred to as the Campil Event (Broglio Loriga et al. 1990; Aljinović 1995; Twitchett & Wignall 1996; Hips 1998; Posenato 2008; Hofmann et al. 2015; Foster et al. 2018). Part of the İspatlı Member of the Gevne Formation at the Taşkent sections is also a red colored terrigenous unit and it contains *Eumorphotis reticulata* (Richthofen, 1860) and *Costatoria subrotunda* (Bittner, 1901), that are characteristic to Smithian beds of the Werfen Formation (Broglio Loriga & Posenato 1986; Broglio Loriga & Mirabella 1986). This suggests that the Campil Event was also occurred in Türkiye and that the Taşkent successions can be correlated to successions in Italy (Werfen Formation: Broglio Loriga et al. 1990; Servino Formation: Foster et al. 2018) and in Hungary (Bódvaszilas Sandstone Formation, Szin Marl Formation: Hips 1998). In addition, the overlying limestones and marls are lithologically equivalent to the lower Spathian Val Badia Member of the Werfen Formation in Italy (Broglio Loriga et al. 1983) and equivalent units across central Europe (e.g., Szin Marl Formation in Hungary: Hips 1998; Foster et al. 2015; Servino Formation, Italy: Foster et al. 2018) both in terms

of lithology and fossil content, i.e., the diagnostic *Tirolites cassianus* (Quenstedt, 1849) and *Ladinaticella costata* (Münster, 1841). These similarities suggest that the environmental changes across the Smithian–Spathian transition can be directly correlated between central European sections and sections in Türkiye.

4.5 Adhering to FAIR principles

Whilst reviewing the pre-existing data from the Permian–Triassic successions of Türkiye, it became clear that an improvement in technology is not the only way that earth scientists can better adhere to the FAIR principles. In some publications the data is only described, but the original raw data is not made publicly available. In such case, the original data does not become available for use of subsequent researchers. Keeping the raw data confidential prevents comparing the results with replicated data (in the case of geochemical data), or testability (for instance identification of fossil specimens) and might result in subsequent loss of the original data. Keeping data not publicly available is not regarded as good scientific practice and can be considered scientific misconduct under certain circumstances (e.g., Deutsche Forschungs-gemeinschaft 2025, All European Academies 2025). There are also examples, where the raw data is shown in a figure (such as a range chart; Marcoux & Baud 1988 or stratigraphic column: Varol et al. 2011; Altıner et al. 2021), but the data is not in an accessible format (such as a data table or comma separated values file with exact measurements), meaning the data could not be integrated into a new analysis without error when extracting from the figure into data points. This emphasizes the need for a change in scientific data sharing practices amongst researchers to make their data adhere to the FAIR principles. It is also important for the authors here to highlight that this also includes improving our own personal practices, and here we are only showing some examples we came across from the Permian–Triassic transition in Türkiye.

In the case of paleontological studies, previous studies provided range charts showing range of microfossils (e.g., Jenny in Marcoux et al. 1986; Jenny in Richoz 2006), but taxonomic names differ among publications even in the publications written by the same author published in different years, likely a result of taxonomic revisions. In the absence of figures and plates of identified specimens, such datasets become problematic as the identifications cannot be verified, and in the long term, the different names used for the same taxon creates an artificial inflation of diversity. Sometimes, authors mention key index fossils that are also not figured, such as *Claraia* (e.g., Özgül 1985; Crasquin et al. 2009). To our knowledge, we provide the first image of *Claraia* from the studied sections (Fig. xx). We recommend that authors provide images of the fossils, even in the case of poor preservation. This will help to better assess the original community composition, infer changes in biodiversity, and identify the patterns of extinction more accurately. A good example from Türkiye is Angiolini et al. (2007), who despite focusing on brachiopods showed images of foraminifera, algae and conodonts mentioned in the text. Providing images is important not only for the verification of taxonomic identifications and preventing over- or underestimations

of diversity, but also for recording additional data (e.g., body size) of fossils to assess an ecological response.

The lack of raw data sharing made it difficult to integrate key geochemical studies into this review. For instance, sulfur isotope data from Demirtaş produced by Riccardi (2007) was not included in a tabular form but nevertheless it could be accessed after contacting one of the advisers on the PhD thesis of Riccardi (2007). Another issue arises when geochemical data is included only as calculated ratios or proxies, such as Mg/Ca or Ce anomalies, rather than the original elemental concentrations, as methods can evolve inhibiting the comparison of modern studies with the published record. For example, Loope et al. (2013) used La concentrations to calculate Ce anomalies in Demirtaş based on the methods of Bau & Dulski (1996), even though the authors pointed out the concern that La behaves anomalously in seawater. A revised method of calculating Ce anomalies avoiding the use of La concentrations was introduced by Lawrence et al. (2006), which was used by a more recent study (Frank et al. in review). Hence, Ce anomalies reported by Frank et al. and Loope et al. are not directly comparable. However, as both studies included their raw data, we were able to recalculate the Ce anomaly data from Loope et al. (2013) with the newer method, enabling a comparison of the Ce anomaly work from Demirtaş with the newer data from Çürük Dağ and Öznurtepe by Frank et al. (in review). This example emphasizes the advantage of including a complete data set including the raw data used for calculating proxies, as it enables reproducibility as well as a continued use of the study, even if methods evolve. Hence, we recommend providing the complete geochemical data set used in a study in a tabular form.

5. Acknowledgments

We would like to thank Saliha Dündar (TPAO) and Jörn Peckmann (University of Hamburg) for assisting us with fieldwork and Aymon Baud (Lausanne University) and John Payne (Stanford University) for assisting us remotely with fieldwork and sharing their wealth of information on the sections they have visited. Martin Nose (SNSB-BSPG) and Birgit Leipner-Mata (FAU Erlangen-Nürnberg) are acknowledged for helping prepare thin sections and Lee Kump for providing the geochemical data from Riccardi (2007). Crispin Little and Paul Wignall (University of Leeds) are acknowledged for the discussion on the tubular structures found in the lower Triassic at Taşkent. Bingqian Wang, Xin Chen, Jianhua Chen and Hanting Zhong are thanked for their help in review and upload the 3D models. BK, SB, AF, MAGC, and WJF were funded by Deutsche Forschungsgemeinschaft (project no. FO1297/1-1). BK further received funding from NERC (NE/X012859/1; NE/X015025/1) for some of the field trips. MG funded by MTA (Project no 2024-08-16-02-1).

6. References

All European Academies (2023) *The European code of conduct for research integrity - Revised dition 2023*. ALLEA, Berlin, 20 pp.

Algeo, T.J. and Twitchett, R.J. (2010) Anomalous Early Triassic sediment fluxes due to elevated weathering rates and their biological consequences. *Geology*, **38,** 1023–1026.

Aljinović, D. (1995) Storm influenced shelf sedimentation-an example from the Lower Triassic (Scythian) siliciclastic and carbonate succession near Knin (Southern Croatia and Western Bosnia and Herzegovina). *Geologia Croatica*, **48,** 17–32.

Altıner, D. (1981) *Recherches stratigraphiques et micropaléontologiques dans le Taurus Oriental au NW de Pinarbasi (Turquie)*, Faculté des sciences de l'Université de Genève, 1–450 pp.

Altıner, D., Özkan-Altıner, S., Atasoy, S.G. and Şahin, N. (2021) *Paynita permotaurica* n. gen., n. sp., and the other dagmaritin foraminifera from the Changhsingian (Permian) of southern Turkey: review of dagmaritin phylogeny. *Journal of Foraminiferal Research*, **51,** 14–31.

Altıner, D., Özkan-Altıner, S. and Koçyiğit, A. (2000) Late Permian Foraminiferal Biofacies Belts in Turkey: Palaeogeographic and Tectonic Implications. *Geological Society, London, Special Publications*, **173,** 83–96.

Altıner, D., Payne, J.L., Lehrmann, D.J., Atasoy, S.G. and Özkan-Altıner, S. (2024) New foraminifera from the Changhsingian (Upper Permian) of the Taurides (southern Turkey) with remarks on their evolutionary origins. *Journal of Paleontology*, **98,** 745–772.

Altıner, D. and Zaninetti, L. (1981) Le Trias dans la région de Pinarbasi, Taurus oriental, Turquie: Unités lithologiques, micropaléontologie, milieux de dépôt. *Rivista Italiana di Paleontología*, **86,** 705–760.

Angiolini, L., Carabelli, L., Nicora, A., Crasquin-Soleau, S., Marcoux, J. and Rettori, R. (2007) Brachiopods and other fossils from the Permo–Triassic boundary beds of the Antalya Nappes (SW Taurus, Turkey). *Geobios*, **40,** 715–729.

Bau, M. and Dulski, P. (1996) Distribution of yttrium and rare-earth elements in the Penge and Kuruman iron-formations, Transvaal Supergroup, South Africa. *Precambrian Research*, **79,** 37–55.

Baud, A., Magaritz, M. and Holser, W.T. (1989) Permian-Triassic of the Tethys: Carbon isotope studies. *Geologische Rundschau*, **78,** 649–677.

Baud, A., Richoz, S. and Marcoux, J. (2005) Calcimicrobial cap rocks from the basal Triassic units: western Taurus occurrences (SW Turkey). *Comptes Rendus Palevol*, **4,** 569–582.

Bittner, A. (1901) Lamellibranchiaten aus der Trias des Bakonyer Waldes. *Resultate der wissenschaftlichen Erforschung des Balatonsees*, **2,** 1–107.

Bozkaya, Ö. and Yalçın, H. (2005) Diagenesis and very low-grade metamorphism of the Antalya Unit: mineralogical evidence of Triassic rifting, Alanya-Gazipaşa, Central Taurus Belt, Turkey. *Journal of Asian Earth Sciences*, **25,** 109–119.

Brandner, R., Horacek, M., Keim, L. and Scholger, R. (2009) The Pufels/Bulla road section: deciphering environmental changes across the Permian-Triassic boundary to the Olenekian by integrated litho-, magneto-and isotope stratigraphy. A field trip guide. *Geo. Alp*, **6,** 116–132.

Broglio Loriga, C., Góczán, F., Haas, J., Lenner, K., Neri, C., Oravecz Sheffer, A., Posenato, R., Szabo, I. and Toth Makk, A. (1990) The Lower Triassic sequences of the Dolomites (Italy) and Transdanubian mid-mountains (Hungary) and their correlation. *Memorie di Scienze Geologiche, già Memorie degli Istituti di Geologia e Mineralogia dell'Università di Padova*, **42,** 41–103.

Broglio Loriga, C., Masetti, D. and Neri, C. (1983) La Formazione di Werfen (Scitico) delle Dolomiti occidentali: sedimentologia e biostratigrafia. *Rivista Italiana di Paleontología*, **88,** 501–598.

Broglio Loriga, C. and Mirabella, S. (1986) Il genere *Eumorphotis* Bittner 1901 nella biostratigrafia dello Scitico, Formazione di Werfen (Dolomiti). *Memorie di Scienze Geologiche, già Memorie degli Istituti di Geologia e Mineralogia dell'Università di Padova*, **38,** 245–281.

Broglio Loriga, C., Neri, C., Pasini, M. and Posenato, R. (1988) Marine fossil assemblages from Upper Permian to lowermost Triassic in the western Dolomites (Italy). *Memorie della Società geologica Italiana*, **34,** 5–44.

BROGLIO LORIGA, C. and Posenato, R. (1986) *Costatoria* (*Costatoria*?) *subrotunda* (Bittner, 1901). A Smithian (Lower Triassic) marker from Tethys. *Rivista Italiana di Paleontologia e Stratigrafia*, **92,** 189–200.

Brönnimann, P., Zaninetti, L. and Bozorgnia, F. (1972) Triassic (Skythian) smaller foraminifera from the Elika Formation of the central Alborz, northern Iran, and from the Siusi Formation of the Dolomites, northern Italy. *Mitteilung Gesellschaft der Geologie-und Bergsbaustudenten, Innsbruck*, **21,** 861–884.

Buchwald, S.Z., Birgel, D., Senger, K., Mosociova, T., Pei, Y., Frank, A.B., Galasso, F., Gómez Correa, M.A., Koşun, E., Karapunar, B., Wang, X., Kustatscher, E., Prinoth, H., Steinkrauss, R., Peckmann, J. and Foster, W.J. (in review) Primary productivity blooms on the Barents Shelf, Svalbard, associated with the 1 Permian Triassic mass extinction. *AGU Advances*, 1–24.

Burgess, S.D., Bowring, S. and Shen, S.-z. (2014) High-precision timeline for Earth's most severe extinction. *Proceedings of the National Academy of Sciences*, **111,** 3316–3321.

Burgess, S.D., Muirhead, J.D. and Bowring, S.A. (2017) Initial pulse of Siberian Traps sills as the trigger of the end-Permian mass extinction. *Nature Communications*, **8(**164), 1-6.

Collin, P.-Y., Kershaw, S., Tribovillard, N., Forel, M.-B. and Crasquin, S. (2015) Geochemistry of post-extinction microbialites as a powerful tool to assess the oxygenation of shallow marine water in the immediate aftermath of the end-Permian mass extinction. *International Journal of Earth Sciences*, **104,** 1025–1037.

Crasquin-Soleau, S., Marcoux, J., Angiolini, L., Richoz, S., Nicora, A., Baud, A. and Bertho, Y. (2004) A new ostracode fauna from the Permian-Triassic boundary in Turkey (Taurus, Antalya Nappes). *Micropaleontology*, **50,** 281–295.

Crasquin-Soleau, S., Richoz, S., Marcoux, J., Angiolini, L., Nicora, A. and Baud, A. (2002) Les événements de la limite Permien–Trias: derniers survivants et/ou premiers re-colonisateurs parmi les ostracodes du Taurus (Sud-Ouest de la Turquie). *Comptes Rendus Géoscience*, **334,** 489–495.

Crasquin, S., Baud, A., Kershaw, S., Richoz, S., Kosun, E. and Forel, M. (2009) The Permian-Triassic transition in the Southwestern Taurus Mountains (South Turkey). In: *IGCP 572 annual Meeting & Field Workshop in southern Turkey, Antalya, Sept. 2-6, 2009*.

Cui, Y., Li, M., Van Soelen, E.E., Peterse, F. and Kürschner, W.M. (2021) Massive and rapid predominantly volcanic CO2 emission during the end-Permian mass extinction. *Proceedings of the National Academy of Sciences*, **118,** e2014701118.

Dai, J. and Zhang, J. (1989) Conodonts. In: *Study of the Permo-Triassic Biostratigraphy and Event Stratigraphy of northern Sichuan and southern Shaanxi, Geological Memoir* (Ed F. Li), **2 (9)**, pp. 428–135, Beijing.

Dal Corso, J., Song, H., Callegaro, S., Chu, D., Sun, Y., Hilton, J., Grasby, S.E., Joachimski, M.M. and Wignall, P.B. (2022) Environmental crises at the Permian–Triassic mass extinction. *Nature Reviews Earth & Environment***,** 1–18.

Demirtaş, F. (2018) *Investigation of Permian-Triassic boundary around Antalya in terms of sedimentology, petrography and geochemistry*, Akdeniz University, Antalya, Turkey, 111 pp.

Demirtaşlı, E. 1967. Lithostratigraphic units and petroleum prospects of the area between Pınarbaşı-Sarız-Mağara districts, MTA Report No: 3489. Ankara.

Emmrich, H. (1844) Über die Schichtenfolge der Flötz-Gebirge des Gader-Thales, der Seisser-Alpe und insbesondere bei St. Cassian. *Neues Jahrbuch für Mineralogie, Geologie und Paläontologie*, **1844,** 791–803.

Farabegoli, E. and Perri, M.C. (2012) Millennial physical events and the end-Permian mass mortality in the western Palaeotethys: Timing and primary causes. In: *Earth and Life: Global Biodiversity, Extinction Intervals and Biogeographic Perturbations Through Time*, pp. 719–758. Springer.

Forel, M.-B. (2015) Heterochronic growth of ostracods (Crustacea) from microbial deposits in the aftermath of the end-Permian extinction. *Journal of Systematic Palaeontology*, **13,** 315–349.

Deutsche Forschungsgemeinschaft (2025) *Guidelines for safeguarding good research practice: Code of conduct*. Deutsche Forschungsgemeinschaft, 25 pp.

Foster, W.J., Danise, S., Price, G.D. and Twitchett, R.J. (2018) Paleoecological analysis of benthic recovery after the late Permian mass extinction event in eastern Lombardy, Italy. *Palaios*, **33,** 266–281.

Foster, W.J., Danise, S., Sedlacek, A., Price, G.D., Hips, K. and Twitchett, R.J. (2015) Environmental controls on the post-Permian recovery of benthic, tropical marine ecosystems in western Palaeotethys (Aggtelek Karst, Hungary). *Palaeogeography, Palaeoclimatology, Palaeoecology*, **440,** 374–394.

Foster, W.J., Frank, A.B., Li, Q., Danise, S., Wang, X. and Peckmann, J. (2024) Thermal and nutrient stress drove Permian-Triassic shallow marine extinctions. *Cambridge Prisms – Extinction, **2**,* 1–9.

Foster, W.J., Lehrmann, D.J., Yu, M. and Martindale, R.C. (2019) Facies selectivity of benthic invertebrates in a Permian/Triassic boundary microbialite succession: implications for the "microbialite refuge" hypothesis. *Geobiology*, **17,** 523–535.

Frank, A.B., Karapunar, B., Grasby, S.E., Koşun, E., Lahajnar, N., Gómez Correa, M.A., Buchwald, S.Z., Metzke, M. and Foster, W.J. (in review) Assessing the role of anoxia as a potential extinction driver in the shallow marine Neotethys during the Permian–Triassic mass extinction. *Chemical Geology*.

Flügel, E., & Munnecke, A. (2010). *Microfacies of carbonate rocks: analysis, interpretation and application*. Berlin: Springer, pp. 984.

Gliwa, J., Ghaderi, A., Leda, L., Schobben, M., Tomás, S., Foster, W.J., Forel, M.-B., Ghanizadeh Tabrizi, N., Grasby, S.E. and Struck, U. (2020) Aras Valley (northwest Iran): high-resolution stratigraphy of a continuous central Tethyan Permian–Triassic boundary section. *Fossil Record*, **23,** 33–69.

Groves, J.R. and Altıner, D. (2005) Survival and recovery of calcareous foraminifera pursuant to the end-Permian mass extinction. *C. R. Palevol*, **4,** 487–500.

Groves, J.R., Altıner, D. and Rettori, R. (2005) Extinction, survival, and recovery of lagenide foraminifers in the Permian–Triassic boundary interval, central Taurides, Turkey. *Journal of Paleontology*, **79,** 1–38.

Groves, J.R. and Calner, M. (2004) Lower Triassic oolites in Tethys: a sedimentologic response to the end-Permian mass extinction. In: *Geological Society of America Abstracts with Programs*, **36**, pp. 336.

Güvenç, T. (1966). Description de quelques espèces d'algues calcaires (Gymnocodiacées et Dasycladacées) du Carbonifère et du Permien des Taurus Occidentaux. *Revue de Micropaléontologie*, ***9*(2)**, 94–103.

Haas, J., Demény, A., Hips, K., Zajzon, N., Weiszburg, T.G., Sudar, M. and Pálfy, J. (2007) Biotic and environmental changes in the Permian–Triassic boundary interval recorded on a western Tethyan ramp in the Bükk Mountains, Hungary. *Global and Planetary Change*, **55,** 136–154.

Heindel, K., Foster, W.J., Richoz, S., Birgel, D., Roden, V.J., Baud, A., Brandner, R., Krystyn, L., Mohtat, T. and Koşun, E. (2018) The formation of microbial-metazoan bioherms and biostromes following the latest Permian mass extinction. *Gondwana Research*, **61,** 187–202.

Herminghaus, S., Thomas, K.R., Aliaskarisohi, S., Porada, H. and Goehring, L. (2016) Kinneyia: a flow-induced anisotropic fossil pattern from ancient microbial mats. *Frontiers in Materials*, **3,** 30.

Hips, K. (1998) Lower Triassic storm-dominated ramp sequence in northern Hungary: an example of evolution from homoclinal through distally steepened ramp to Middle Triassic flat-topped platform. *Geological Society, London, Special Publications*, **149,** 315–338.

Hofmann, R., Hautmann, M. and Bucher, H. (2015) Recovery dynamics of benthic marine communities from the Lower Triassic Werfen Formation, northern Italy. *Lethaia*, **48,** 474–496.
Kahsnitz, M.M. and Willems, H. (2019) Genesis of Paleocene and Lower Eocene shallow-water nodular limestone of South Tibet (China). *Carbonates and Evaporites*, **34,** 199–218.
Kalafatçıoğlu, A. (1973) Geology of the western part of Antalya Bay. *Bulletin of the Mineral Research and Exploration*, **81,** 31–84.
Kershaw, S., Crasquin, S., FOREL, M.B., Randon, C., COLLIN, P.Y., Kosun, E., Richoz, S. and Baud, A. (2011) Earliest Triassic microbialites in Çürük Dag, southern Turkey: composition, sequences and controls on formation. *Sedimentology*, **58,** 739–755.
Kershaw, S., Crasquin, S., Li, Y., Collin, P.Y., Forel, M.B., Mu, X., Baud, A., Wang, Y., Xie, S. and Maurer, F. (2012) Microbialites and global environmental change across the Permian–Triassic boundary: a synthesis. *Geobiology*, **10,** 25–47.
Korte, C. and Kozur, H.W. (2005) Carbon isotope stratigraphy across the Permian/Triassic boundary at Jolfa (NW-Iran), Peitlerkofel (Sas de Pütia, Sass de Putia), Pufels (Bula, Bulla), Tesero (all three Southern Alps, Italy) and Gerennavár (Bükk Mts., Hungary). *Jounal of Alpine Geology*, **47,** 119–135.

Korte, C. and Kozur, H.W. (2010) Carbon-isotope stratigraphy across the Permian–Triassic boundary: a review. *Journal of Asian Earth Sciences*, **39,** 215–235.
Kozur, H. and Pjatakova, M. (1976) Die Conodontenart *Anchignathodus parvus* n. sp., eine wichtige Leitform der basalen Trias von Nord- und Zentral-Iran. *Koninklijke Nederlandse Akademie Van Wetenschappen-Amsterdam, Reprinted from Proceedings, Series B*, **79,** 123–128.

Kozur, H.W. (1996) The conodonts *Hindeodus*, *Isarcicella* and *Sweetohindeodus* in the uppermost Permian and lowermost Triassic. *Geologia Croatica*, **49,** 81–115.
Kozur, H.W., Kaya, O. and Mostler, H. (1996) First evidence of Lower to middle Scythian (Dienerian-lower Olenekian) radiolarians from the Karakaya Zone of northwestern Turkey. *Geologisch-Palaontologische Mitteilungen Innsbruck, Sonderband*, **4,** 271–285.
Kraus, S.H., Siegert, S., Mette, W., Struck, U. and Korte, C. (2009) Stratigraphic significance of carbon isotope variations in the shallow-marine Seis/Siusi Permian–Triassic boundary section (Southern Alps, Italy). *Fossil Record*, **12,** 197–205.
Lau, K.V., Maher, K., Altıner, D., Kelley, B.M., Kump, L.R., Lehrmann, D.J., Silva-Tamayo, J.C., Weaver, K.L., Yu, M. and Payne, J.L. (2016) Marine anoxia and delayed Earth system recovery after the end-Permian extinction. *PNAS*, **9**, 2360–2365.
Lawrence, M.G., Greig, A., Collerson, K.D. and Kamber, B.S. (2006) Rare earth element and yttrium variability in South East Queensland waterways. *Aquatic Geochemistry*, **12,** 39–72.
Lehrmann, D.J., Payne, J.L., Felix, S.V., Dillett, P.M., Wang, H., Yu, Y. and Wei, J. (2003) Permian–Triassic boundary sections from shallow-marine carbonate platforms of the Nanpanjiang Basin, South China: implications for oceanic conditions associated with the end-Permian extinction and its aftermath. *Palaios*, **18,** 138–152.

Lerosey-Aubril, R. and Angiolini, L. (2009) Permian trilobites from Antalya Province, Turkey, and enrollment in Late Palaeozoic trilobites. *Turkish Journal of Earth Sciences*, **18,** 427–448.

Li, F., Yan, J., Chen, Z.-Q., Ogg, J.G., Tian, L., Korngreen, D., Liu, K., Ma, Z. and Woods, A.D. (2015) Global oolite deposits across the Permian–Triassic boundary: a synthesis and implications for palaeoceanography immediately after the end-Permian biocrisis. *Earth-Science Reviews*, **149,** 163–180.

Loope, G.R., Kump, L.R. and Arthur, M.A. (2013) Shallow water redox conditions from the Permian–Triassic boundary microbialite: The rare earth element and iodine geochemistry of carbonates from Turkey and South China. *Chemical Geology*, **351,** 195–208.

Lys, M. and Marcoux, J. (1978) Les niveaux du Permien supérieur des Nappes d'Antalya (Taurides occidentales, Turquie). *Compte Rendu Hebdomadaire des Séances de l'Académie des Sciences, Paris, ser. D.*, **286,** 1417–1420.

Marcoux, J. and Baud, A. (1988) The Permo-Triassic boundary in the Antalya Nappes (Western Taurides-Turkey). *Mem. Soc. geol. Italia, IGCP Project 203 Spec. Volume*, **34,** 243–252.

Marcoux, J., Baud, A., Krystyn, L. and Monod, O. (1986) Guide book part 2, Western Taurides, Antalya – Seydisehir – Isparta – Antalya. In: *Late Permian and Triassic in Western Turkey, Field Workshop 1986* (Ed J. Marcoux), **2**, pp. 1–64.

Münster, G.z. (1841) Beschreibung und Abbildung der in den Kalkmergelschichten von St. Cassian gefundenen Versteinerungen. In: *Beiträge zur Geologie und Petrefacten-Kunde des südöstlichen Tirol's vorzüglich der Schichten von St. Cassian* (Eds H.L. Wissmann, G.z. Münster and K.F. Braun), pp. 25–152. Buchner, Bayreuth.

Neri, C. and Posenato, R. (1985) New biostratigraphical data on uppermost Werfen Formation of western Dolomites (Trento Italy). *Geologisch-Palaontologische Mitteilungen Innsbruck*, **14,** 87–107.

Özgül, N. (1984) Stratigraphy and tectonic evolution of the Central Taurides. In: *Geology of the Taurus Belt. International Symposium*, pp. 77–90.

Özgül, N. (1985) Alanya Tectonic window and geology of its western part. In: *Ketin Symposium*, pp. 97–120. Türkiye Jeoloji Kurumu, Ankara.

Özgül, N. (1997) Stratigraphy of the tectonostratigraphic units around Bozkır-Hadim-Taşkent region (northern part of the Central Taurides). *Bulletin of the Mineral Research and Exploration*, **119,** 113–174.

Özgül, N., Metin, S., Göğer, E., Bingöl, İ., Baydar, O. and Erdoğan, B. (1973) Tufanbeyli dolayının (Doğu Toroslar, Adana) Kambriyen-Tersiyer kayaları. *Türkiye Jeoloji Kurumu Bülteni*, **16,** 82–100.

Payne, J.L., Lehrmann, D.J., Follett, D., Seibel, M., Kump, L.R., Riccardi, A., Altıner, D., Sano, H. and Wei, J. (2007) Erosional truncation of uppermost Permian shallow-marine carbonates and implications for Permian-Triassic boundary events. *Geol Soc Am Bull*, **119,** 771–784.

Posenato, R. (2008) Global correlations of mid Early Triassic events: the Induan/Olenekian boundary in the Dolomites (Italy). *Earth-Science Reviews*, **91,** 93–105.

Posenato, R. (2019) The end-Permian mass extinction (EPME) and the Early Triassic biotic recovery in the western Dolomites (Italy): state of the art. *Bollettino della Società Paleontologica Italiana*, **58,** 11–34.

Pratt, B.R. (2021) Kinneyia-type wrinkle structures on sandstone beds: not microbially induced but deformation features caused by synsedimentary earthquakes. *Palaios*, **36,** 313–325.

Pruss, S., Fraiser, M. and Bottjer, D.J. (2004) Proliferation of Early Triassic wrinkle structures: implications for environmental stress following the end-Permian mass extinction. *Geology*, **32,** 461–464.

Quenstedt, F.A. (1849) *Petrefactenkunde Deutschlands, Cephalopoden*. LF Fues, Tübingen, 580 pp.

Riccardi, A. (2007) *Carbonate-Associated Sulfate: Assessment of and Use as an Isotopic Proxy for Global Sulfur Cycling During End-Permian Mass Extinction*, The Pennsylvania State University, 127 pp.

Richoz, S. (2006) Stratigraphie et variations isotopiques du carbone dans le Permien supérieur et le Trias inférieur de quelques localités de la Néotéthys (Turquie, Oman et Iran). *Mémoires de Géologie (Lausanne)*, **46,** 1–251.

Robertson, A.H., Parlak, O. and Ustaömer, T. (2012) Overview of the Palaeozoic–Neogene evolution of neotethys in the Eastern Mediterranean region (southern turkey, cyprus, Syria). *Petroleum Geoscience*, **18,** 381–404.

Robertson, A.H., Ustaömer, T., Pickett, E.A., Collins, A.S., Andrew, T. and Dixon, J.E. (2004) Testing models of Late Palaeozoic–Early Mesozoic orogeny in Western Turkey: support for an evolving open-Tethys model. *Journal of the Geological Society*, **161,** 501–511.

Şahin, N. and Altıner, D. (2019) Testing of Permian–Lower Triassic stratigraphic data in a half-graben/tilt-block system: evidence for the initial rifting phase in Antalya Nappes. *Canadian Journal of Earth Sciences*, **56,** 1262–1283.

Şenel, M. (1997) *1:100,000 scale Türkiye Geological Maps, No. 7, Antalya O24 Sheet*. MTA General Directorate Geological Surveys Department, Ankara.

Şenel, M., Bedi, M. and Çörekcioğlu, E. (2016) *1:100,000 scale Türkiye Geological Maps, No. 7, Antalya O24 Sheet*. MTA General Directorate Geological Surveys Department, Ankara.

Senger, K., Betlem, P., Birchall, T., Gonzaga Jr, L., Grundvåg, S.-A., Horota, R.K., Laake, A., Kuckero, L., Mørk, A. and Planke, S. (2022) Digitising Svalbard's geology: the Festningen digital outcrop model. *First Break*, **40,** 47–55.

Şengör, A.M.C. and Yılmaz, Y. (1981) Tethyan evolution of Turkey: a plate tectonic approach. *Tectonophysics*, **75,** 181–241.

Sepkoski, J.J. (1981) A factor analytic description of the Phanerozoic marine fossil record. *Paleobiology, 7*, 36–53.

Shen, J., Schoepfer, S.D., Feng, Q., Zhou, L., Yu, J., Song, H., Wei, H. and Algeo, T.J. (2015) Marine productivity changes during the end-Permian crisis and Early Triassic recovery. *Earth Science Reviews*, **149,** 136–162.

Shen, S.-z., Crowley, J.L., Wang, Y., Bowring, S.A., Erwin, D.H., Sadler, P.M., Cao, C.-q., Rothman, D.H., Henderson, C.M. and Ramezani, J. (2011) Calibrating the end-Permian mass extinction. *science*, **334,** 1367–1372.

Silva-Tamayo, J.C., Lau, K.V., Jost, A.B., Payne, J.L., Wignall, P.B., Newton, R.J., Eisenhauer, A., Depaolo, D.J., Brown, S. and Maher, K. (2018) Global perturbation of the marine calcium cycle during the Permian-Triassic transition. *Bulletin*, **130,** 1323–1338.

Smyrak-Sikora, A., Betlem, P., Engelschiøn, V.S., Foster, W.J., Grundvåg, S.-A., Jelby, M.E., Jones, M.T., Shephard, G.E., Śliwińska, K.K. and Vickers, M.L. (2025) Phanerozoic paleoenvironmental and paleoclimatic evolution in Svalbard. *EGUsphere*, **2025,** 1–112.

Stampfli, G., Marcoux, J. and Baud, A. (1991) Tethyan margins in space and time. *Palaeogeography, Palaeoclimatology, Palaeoecology*, **87,** 373–409.

Török, Á. (1998) Controls on development of Mid-Triassic ramps: examples from southern Hungary. *Geological Society, London, Special Publications*, **149,** 339–367.

Twitchett, R.J. and Wignall, P.B. (1996) Trace fossils and the aftermath of the Permo-Triassic mass extinction: evidence from northern Italy. *Palaeogeography, Palaeoclimatology, Palaeoecology*, **124,** 137–151.

Ünal, E., Altıner, D., Yılmaz, I.Ö. and Özkan-Altıner, S. (2003) Cyclic sedimentation across the Permian–Triassic boundary (central Taurides, Turkey). *Rivista italiana di Paleontologia e Stratigrafia*, **109,** 359–376.

Varol, B., Koşun, E., Pinar, N.Ü. and Ayranci, K. (2011) Pyritized mudstone and associated facies in the Permian–Triassic boundary of the Çürük Dağ section, Southern Turkey. *Journal of Asian Earth Sciences*, **40,** 1068–1078.

Verna, V., Angiolini, L., Crasquin, S. and Nicora, A. (2011) Guadalupian brachiopods from western Taurus, Turkey. *Rivista Italiana di Paleontologia e Stratigrafia*, **117,** 51–104.

von Richthofen, F.F. (1860) *Geognostische Beschreibung der Umgegend von Predazzo, Sanct Cassian und der Seisser Alpe in Süd-Tyrol.* Justus Perthes, Gotha, 327 pp.

Wang, S.C. and Zhong, L. (2018) Estimating the number of pulses in a mass extinction. *Paleobiology*, **44,** 199–218.

Wang, X., Zhong, H., Chen, J., Lin, Z., Wang, B., Hou, M., Li, Y., and Wang, C. (2024) DDE-Outcrop3D: A new pathway to the Deep-time Earth, EGU General Assembly 2024, Vienna, Austria, 14–19 Apr 2024, EGU24-16328, https://doi.org/10.5194/egusphere-egu24-16328.

Wignall, P.B. and Bond, D.P. (2024) The great catastrophe: causes of the Permo-Triassic marine mass extinction. *National Science Review*, **11,** nwad273 (1–14).

Wilkinson, M.D., Dumontier, M., Aalbersberg, I.J., Appleton, G., Axton, M., Baak, A., Blomberg, N., Boiten, J.-W., da Silva Santos, L.B. and Bourne, P.E. (2016) The FAIR Guiding Principles for scientific data management and stewardship. *Scientific data*, **3,** 1–9.

Xu, Z., Yu, J., Yin, H., Merdith, A.S., Hilton, J., Allen, B.J., Gurung, K., Wignall, P.B., Dunhill, A.M. and Shen, J. (2025) Early Triassic super-greenhouse climate driven by vegetation collapse. *Nature Communications*, **16,** 5400.

Yin, H.-F., Zhang, K., Tong, J., Yang, Z. and Wu, S. (2001) The global stratotype section and Point (GSSP) of the Permian-Triassic boundary. *Episodes*, **24,** 102–114.

Figure Captions

Figure 1. A) Topographic map of Türkiye, the black box indicates the studied region. **B)** The studied sections at five localities.

Figure 2. Formations at the studied localities, and their stratigraphic ages.

Figure 3. A) Panaromic aerial photography of Çürük Dağ, the white boxes indicates the studied sections. **B)** Çürük Dağ valley section. **C)** Çürük Dağ cliff section, the head of the hammer is at the last nodular limestone bed just below the transitional oolites. **D)** Çürük Dağ crest section.

Figure 4. Image processing workflow to create the virtual outcrop model of Çürük Dağ sections.

Figure 5. Geological map of the region around the study area in Çürük Dağ (modified after MTA 1:25.000 scale maps). Coordinates are given in Universal Transverse Mercator (Zone 36S) and in World Geodetic System (WGS1984).

Figure 6: Detailed log of the Çürük Dağ sections showing palaeontological and lithological observations made in the field (modified after Frank et al. in review). The colour represents the rock colours and the red dashed line indicates the formation boundary.

Figure 7. A composite plot showing the lithological transition, changes in geochemical proxies and the nature of the extinction event at the Çürük Dağ sections. The quantified extinction pulse is shown as a dashed horizontal red line at 0.43 m, where 0 m marks the formation boundary at the base of the "transitional ooids". Fossil data after Jenny in Richoz (2006), Crasquin et al. (2004), Altıner et al. (2024), Altıner et al. (2021), Angiolini et al. (2007), Heindel et al. (2018) and Forel et al. (2015). Geochemistry data after Richoz (2006), Demirtaş (2018) and Frank et al. (in review). Stratigraphic log after this study, m = mudstone, w = wackestone, p = packestone, g = grainstone, b = bindstone.

Figure 8. Sedimentary structures, fossils and facies at Çürük Dağ. **A)** Polished section of flat pebbles containing yellow mudstone rip-up clasts, Dienerian, Kokarkuyu Formation, BK-2024/667a. **B)** Flat pebbles containing yellow mudstone rip-up clasts, Dienerian, Kokarkuyu Formation, BK-2024/667b. **C)** *Neoschizodus ovatus* (Goldfuss, 1837), Dienerian, Kokarkuyu Formation, BK-2024/534. **D)** *Eumorphotis inaequicostata* (Benecke, 1876) in yellow mudstone beds,with two encrusting microconchids, Dienerian, Kokarkuyu Formation, BK-2024/47. **E)** Tempestite in yellow mudstone beds, includes thin shelled bivalves, gastropods and pyrite crystals (appear in dark), Dienerian, Kokarkuyu Formation, TSCV_1. **F)** Oolite bed with *Neoschizodus* shells, which underlies the yellow mudstone layer, Griesbachian, Kokarkuyu Formation, TSCCr_1. **G)** Oolite bed with *Coelostylina* sp., which underlies the yellow mudstone layer, Griesbachian, Kokarkuyu Formation, TSCCr_1. **H)** *Spinomarginifera* sp. Changhsingian, Pamucak Formation, BK-2024/31. **I)** *Orhothetina ladina* (Stache, 1878), Changhsingian, Pamucak Formation, BK-2024/58a. **J)** Bellerophontida indet. sp., Changhsingian, Pamucak Formation, BK-2024/64. **K)** Packstone with *Gymnocodium* sp. just below the transitional oolite, Changhsingian, Pamucak Formation, TSCV_7. **L)** Wackestone with bellerophontid gastropods,

trilobite, *Gymnocodium* sp., foraminifera, Changhsingian, Pamucak Formation, TSCCl_2. **M)** Bryozoa, Changhsingian, Pamucak Formation, BK-2024/662.

Figure 9. A) Aerial view of the Permian–Triassic outcrop at Demirtaş, retriewed from the virtual model. **B)** Formation boundary at Demirtaş, the head of the hammer stands between the Changhsingian wackestone of the Yüğlük Tepe Limestone and transitional oolites of the Sapadere Formation.

Figure 10. Image processing workflow to create the virtual outcrop model of the Demirtaş section.

Figure 11. Geological map of the region around the study area in Demirtaş and Öznurtepe (modified after MTA 1:100.000 scale maps). Coordinates are given in Universal Transverse Mercator (Zone 36S) and in World Geodetic System (WGS1984).

Figure 12. Detailed log of the Demirtaş section showing palaeontological and lithological observations made in the field. The colour represents the rock colours and the red dashed line the formation boundary.

Figure 13. A composite plot showing the lithological transition, changes in geochemical proxies and the nature of the extinction event at the Demirtaş section. The quantified extinction pulse is shown as a dashed horizontal red line at 0.26 m, where 0 m marks the formation boundary at the base of the "transitional ooids". Fossil data after Jenny in Richoz (2006), Altıner et al. (2024), Altıner et al. (2021), and Groves et al. (2005). Geochemistry data after Richoz (2006), Riccardi (2007), and Frank et al. (in review). Stratigraphic log after this study, m = mudstone, w = wackestone, p = packestone, g = grainstone, b = bindstone.

Figure 14. Sedimentary structures, fossils and facies at Demirtaş. **A)** Rip-up clasts with carbonate cement just above yellow mudstones, Dienerian, Sapadere Formation, Taşlıca Member, TSD_7. **B)** *Claraia clarae* (Emmrich, 1844) in yellow mudstones, Dienerian, Sapadere Formation, Taşlıca Member, BK-2024/89a. **C)** *Claraia clarae* (Emmrich, 1844) in yellow mudstones, Dienerian, Sapadere Formation, Taşlıca Member, BK-2024/89e. **D–E)** *Claraia aurita* (Hauer, 1850) and Kinneyia (wrinkle structures) in yellow mudstones, Dienerian, Sapadere Formation, Taşlıca Member, BK-2024/639. **F)** Ooolitic grainstones with dolomite nucleus, which underlies the yellow mudstones, Griesbachian, Sapadere Formation, Beslengiler Limestone Member, TSD_1. **G)** Laminar microbialites which overlies transitional oolites, Griesbachian, Sapadere Formation, Beslengiler Limestone Member, TSD_5. **H)** *Earlandia* sp. in laminar microbialites which overlies transitional oolites, Griesbachian, Sapadere Formation, Beslengiler Limestone Member, TSD_5. **I)** *Postcladella kalhori* (Brönnimann, Zaninetti & Bozorgnia, 1972) in laminar microbialites Griesbachian, Sapadere Formation, Beslengiler Limestone Member, TSD_5. **J)** Transitional oolites, Changhsingian, Sapadere Formation, Beslengiler Limestone Member, TSD_4. **K)** A microgastropod in transitional oolites, Sapadere Formation, Beslengiler Limestone Member, TSD_4. **L)** Packstone with *Gymnocodium* sp., bryozoa and bellerophontid gastropod, Changhsingian, Yüğlük Tepe Limestone.

Figure 15. The Permian–Triassic outcrop at the Öznurtepe Road section, retriewed from the models. **A)** Dark Upper Permian limestones of the Yüğlük Tepe Limestone (on the left), the formation boundary is obscured by heavy deformation (syncline and faults), white arrow indicates the uppermost bed that could be observed at the outcrop. The layers on the right side is

the Griesbachian microbialites. **B)** Continuation of the section, transition from the Griesbachian microbialites to yellow mudtone layers. **C)** Overview of the Öznurtepe Creek section, where the Early Triassic microbialites form a cliff. **D)** Formation boundary between Yüğlük Tepe Limestone and Sapadere Formation, the hammer stands on the first transitional oolite bed of the Sapadere Formation.

Figure 16. Image processing workflow to create the virtual outcrop model of the Öznurtepe Road section.

Figure 17. Image processing workflow to create the virtual outcrop model of the Öznurtepe Creek section.

Figure 18. Detailed log of the Öznurtepe sections showing palaeontological and lithological observations made in the field (modified after Frank et al. in review). The colour represents the rock colours and the red dashed line the formation boundary.

Figure 19. Sedimentary structures, fossils and facies at Öznurtepe. **A)** Microbialite layer with stylolites (dark bands), Griesbachian, Sapadere Formation, Beslengiler Limestone Member, TSO_4. **B)** Transitional oolite with a bellerophontid gastropod, Changhsingian, Sapadere Formation, Beslengiler Limestone Member, TSO_3. **C)** *Permocalculus* sp. and foraminifera, Changhsingian, Yüğlük Tepe Limestone, TSO_1.

Figure 20. Overview of the Taşkent Yolu section. **A)** Permian–Triassic transition before the road construction, line indicates the formation boundary between the Çekiç Dağı Formation and the Gevne Formation. **B)** Permian–Triassic transition after the road construction.

Figure 21. Image processing workflow to create the virtual outcrop model of the Taşkent Yolu section.

Figure 22. Geological map of the region around the study area in Taşkent (modified after MTA 1:25.000 scale maps). Coordinates are given in Universal Transverse Mercator (Zone 36S) and in World Geodetic System (WGS1984).

Figure 23. Sedimentary structures, fossils and facies at Taşkent Yolu. **A)** Gastropod oolite, Spathian, Gevne Formation, TSTBAm_1. **B)** *Omphaloptychia* sp., within the gastropod oolite, Spathian, Gevne Formation, BK-2024/170b. **C)** *Tirolites cassianus* (Quenstedt, 1849), Spathian, Gevne Formation, BK-2024/174. **D)** Pressure dissolution (dark lines) thin section of gray limestone with *Tirolites cassianus*, pressure dissolution, Spathian, Gevne Formation, TSTBAm_2. **E)** Kinneyia (wrinkle structures) on reddish siliciclastics, Smithian, Gevne Formation, BK-2024/163. **F)** Thin section of oncolites, Dienerian, Gevne Formation, TSTB_2. **G)** *Eumorphotis multiformis* (Bittner, 1899), Dienerian, Gevne Formation, BK-2024/159. **H)** *Neoschizodus praeorbicularis* (Bittner, 1901), Dienerian, Gevne Formation, BK-2024/625. **I)** Thin section of ammonoid bearing gastropod oolite found in the yellow siliciclastics, Dienerian, Gevne Formation, TSTB_1.

Figure 24. A) Overview Taşkent Şam Deresi section, where Upper Permian limestones of the Çekiç Dağı Formation are overlain by lower Triassic Gevne Formation. **B)** Formation boundary

between the Çekiç Dağı Formation and the Triassic Gevne Formation, pointed by a person. **C)** Taşkent Şam Deresi hill section, the hammer stands at the formation boundary.

Figure 25. Image processing workflow to create the virtual outcrop model of the Taşkent Şam Deresi section.

Figure 26. Detailed log of the Taşkent Şam Deresi sections showing palaeontological and lithological observations made in the field. The colour represents the rock colours and the red dashed line the formation boundary.

Figure 27. Generalized stratigraphic profile from the Changhsingian to the Spathian in Taşkent. The log height is not scaled to bed thicknesses. The layers are colored to their appearance in the field.

Figure 28. A composite plot showing the litholgoical transition, changes in geochemical proxies and the nature of the extinction event at the Taşkent Şam Deresi section. The quantified extinction pulse is shown as a dashed horizontal red line at 1.67 m, where 0 m marks the formation boundary at the base of the "transitional ooids". Fossil data after Jenny in Richoz (2006), Altıner et al. (2024), Altıner et al. (2021), and Groves et al. (2005). Geochemistry data after Richoz (2006), Lau et al. (2016), Silva-Tamayo et al. (2018), and Frank et al. (in review). Stratigraphic log after this study, m = mudstone, w = wackestone, p = packestone, g = grainstone, b = bindstone.

Figure 29. Sedimentary structures, fossils and facies at Taşkent Şam Deresi. **A)** Thin section of oolitic grainstone with dark stripes, Dienerian, Gevne Formation, TSTDT_5. **B)** Close up of oolitic grainstone with dark stripes, Dienerian, Gevne Formation, TSTDT_5. **C)** *Coelostylina* sp. in domal thrombolites above the laminar microbialite layer, Griesbachian, Gevne Formation, TSTDT_3. **D)** Microgastropods, *Earlandia* sp. and *Postcladella kalhori* (Brönnimann, Zaninetti & Bozorgnia, 1972) in laminar microbialites just above the thrombolite layer, Griesbachian, Gevne Formation, TSTDT_2. **E)** Thrombolite just above the transitional oolite, Griesbachian, Gevne Formation, TSTDT_1. **F)** Transitional oolite, with juvenile bellerophontid and *Coelostylina* sp., uppermost Changhsingian, Gevne Formation, TSTDT_0. **G)** Crinoid columnal, Changhsingian, Çekiç Dağı Formation, BK-2024/117. **H)** *Comelicania haueri* (Stache, 1878), Changhsingian, Çekiç Dağı Formation, BK-2024/116. **I)** Packstone with *Permocalculus* sp., gastropods and bivalves, Changhsingian, Çekiç Dağı Formation, TSTDT_8. **J)** Bryozoans, Changhsingian, Çekiç Dağı Formation, BK-2024/711.

Figure 30. Sedimentary structures, fossils and facies at Taşkent Şam Deresi. **A)** *Ladinaticella costata* (Münster, 1841) in yellow mudstones, Spathian, Gevne Formation, BK-2024/676. **B)** Ripple marks in reddish siliciclastics, Smithian, Gevne Formation, BK-2024/709. **C)** Flat pebbles in reddish siliciclastics, Smithian, Gevne Formation, BK-2024/722. **D)** Tubular structures (rip-up clasts or redeposited burrow molds) and *Eumorphotis* sp. in greenish mudstone, Smithian, Gevne Formation, BK-2024/138. **E)** *Postcladella kalhori* (Brönnimann, Zaninetti & Bozorgnia, 1972) in carbonate mudstones, below greenish siliciclastic mudstones, Dienerian, Gevne Formation, TSTDT_4. **F)** Microgastropod in carbonate mudstones, below greenish siliciclastic mudstones, Dienerian, Gevne Formation, TSTDT_4.

Figure 31. Depositional model for the Permian-Triassic transition for the Antalya and Aladağ Nappes. The depositional environment is interpreted as switching from a carbonate platform to a homoclinal mixed carbonate-siliciclastic ramp in the Dienerian. Whilst major changes are recorded during the extinction event, i.e., the expansion of oolitic shoals and microbialites, the depositional environment remained consistent. Likewise, the Smithian "Campil Event" records the replacement of carbonate with siliciclastic lithologies, but the depositional environment remained consistent. Griesbachian microbialites are interpreted as developing in deep subtidal platform environments, but may have also developed in shallow subtidal settings too.

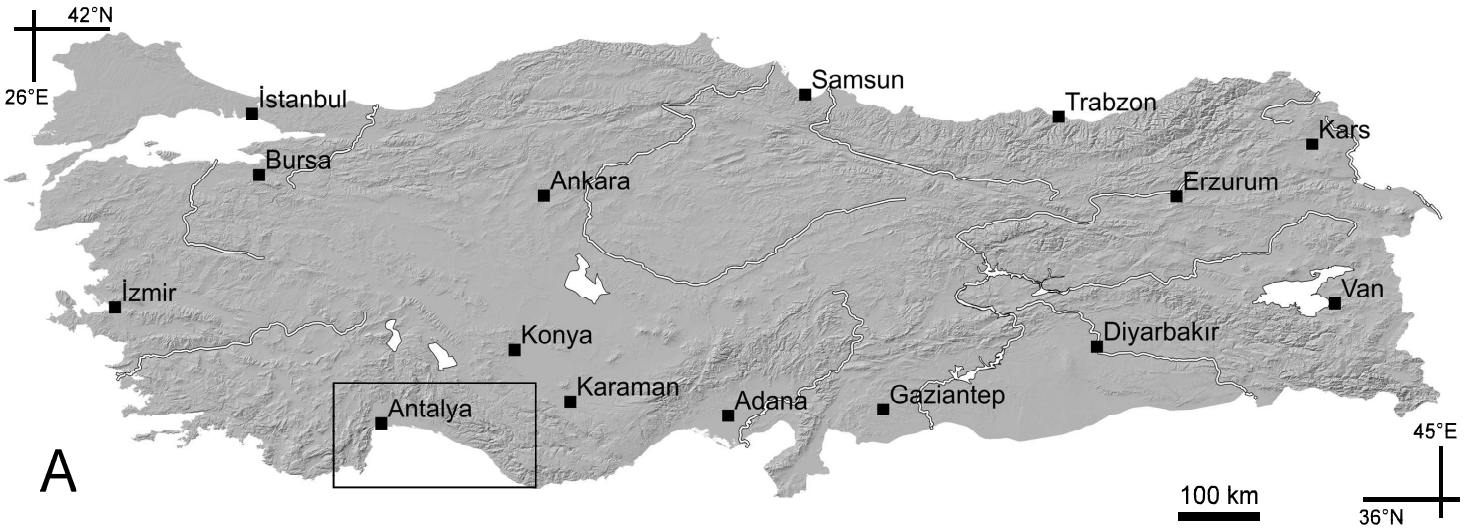

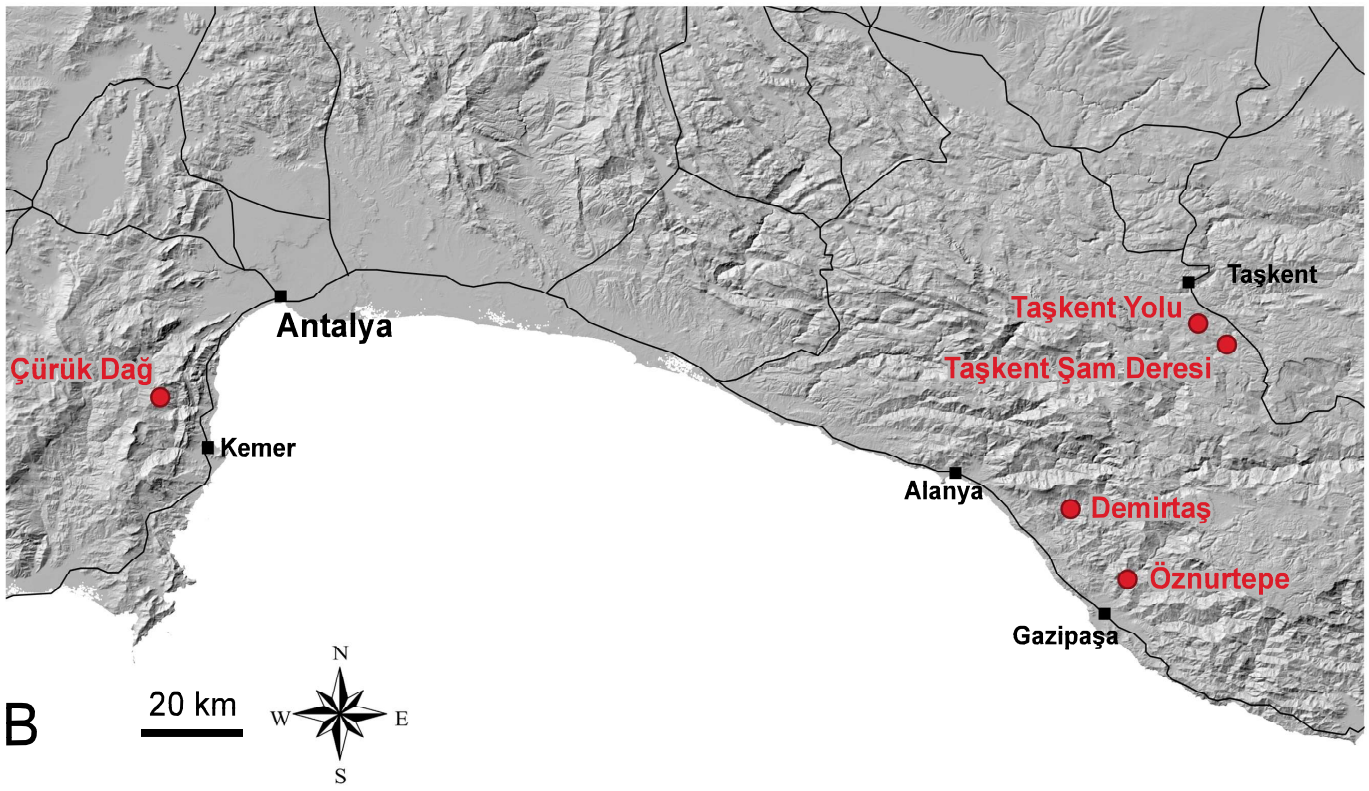

Figure_1_Türkiye

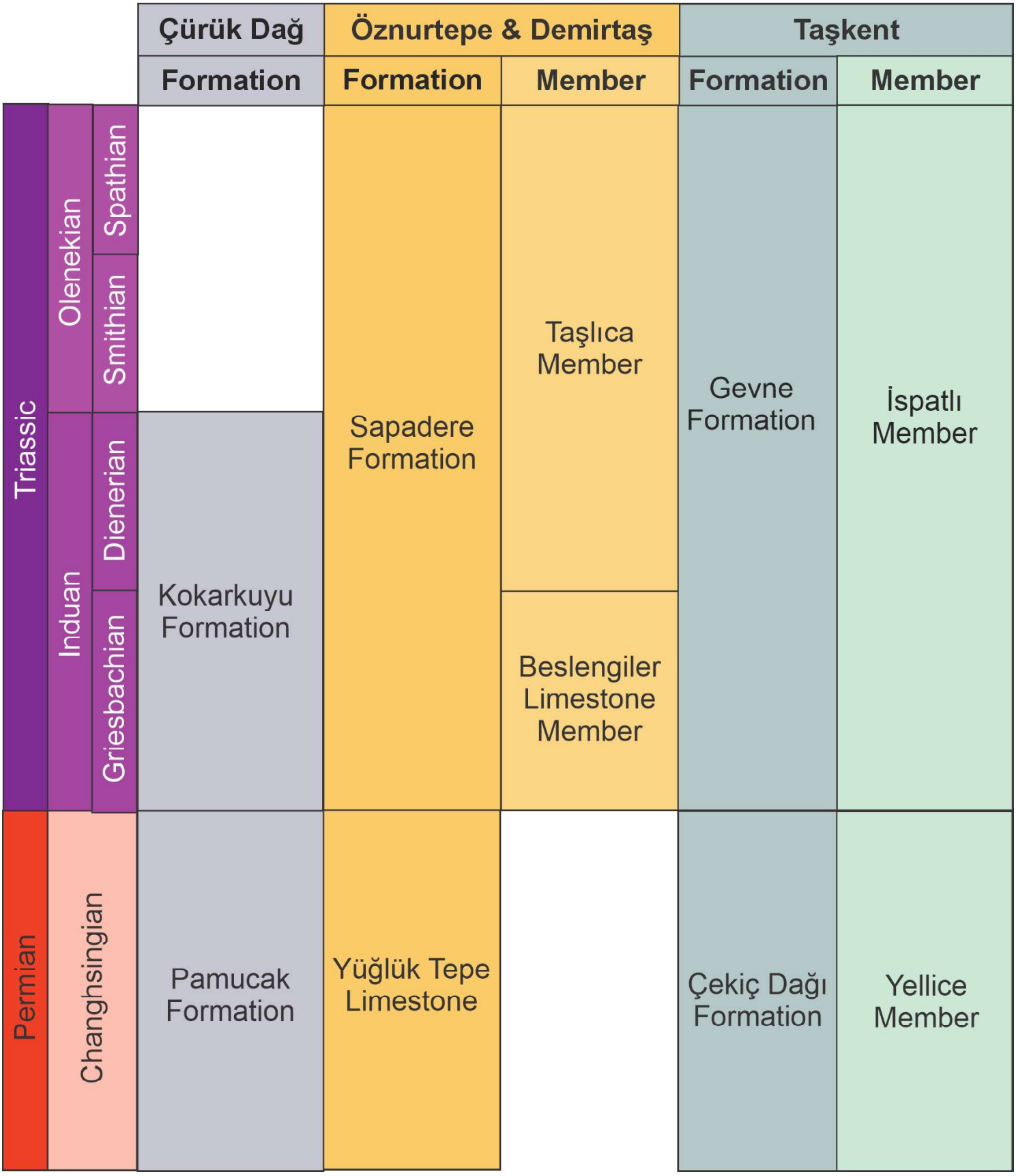

Figure_2_Stratigraphy

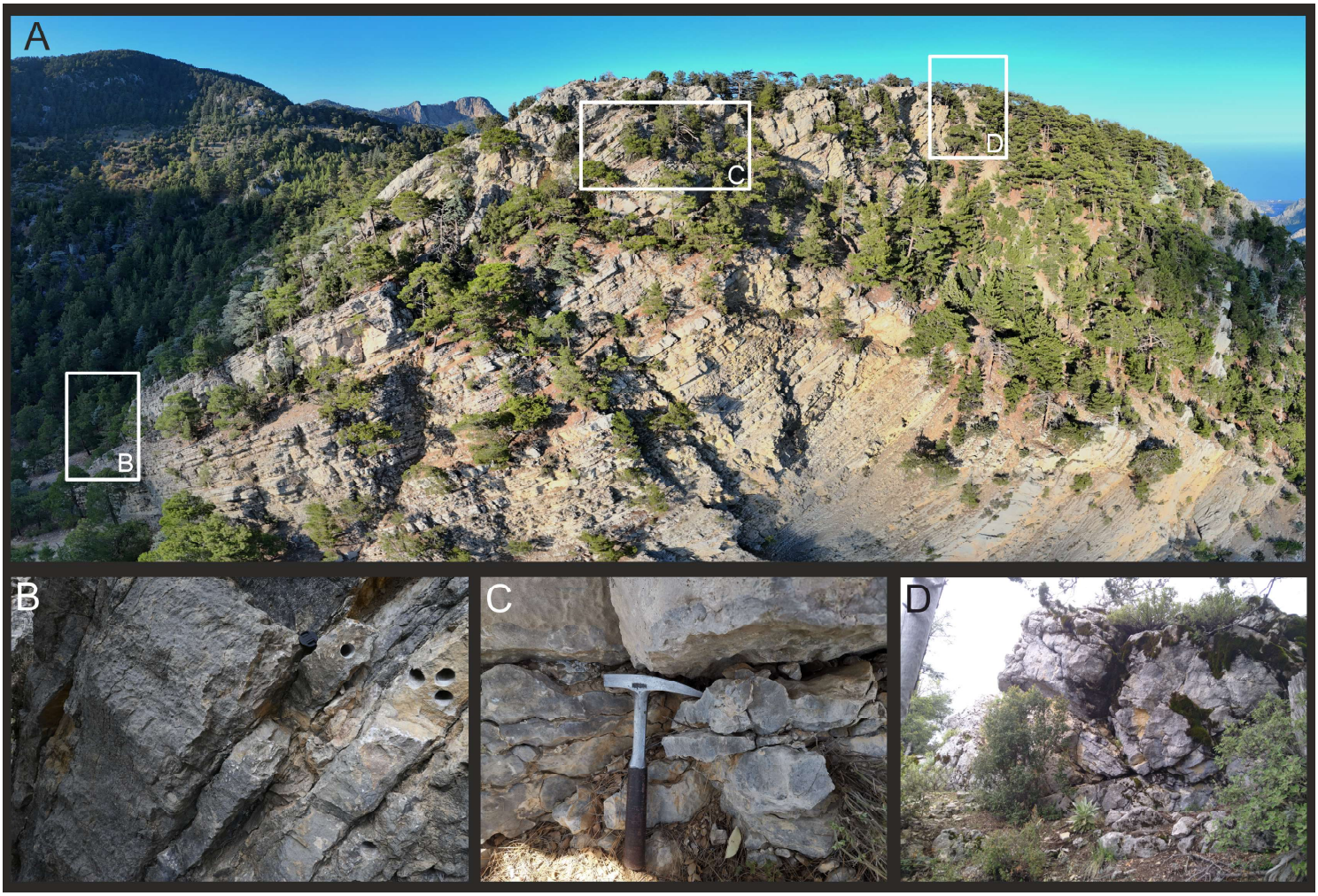

Figure_3_Curukdag

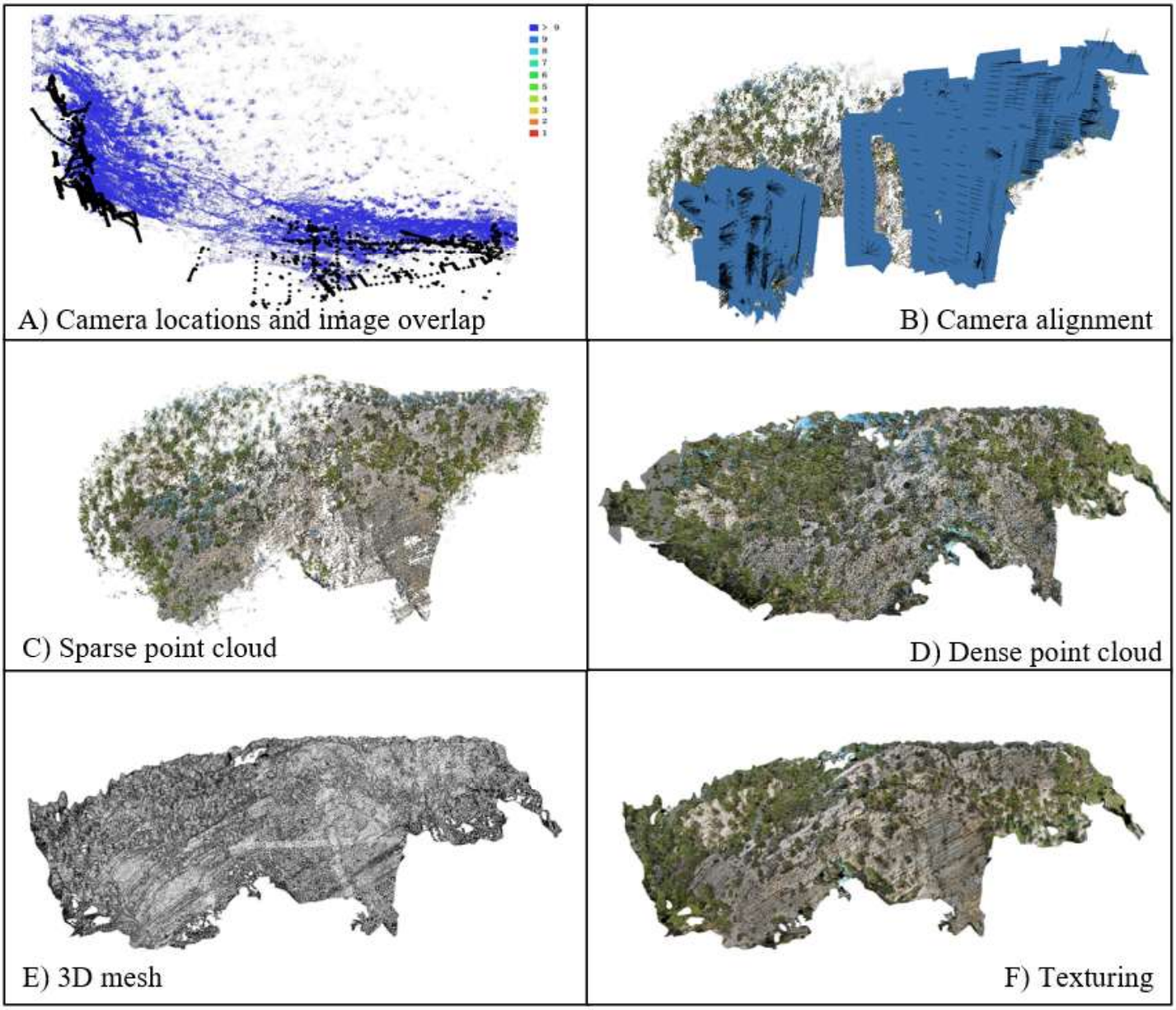

Figure_4_Curuk_dag_model

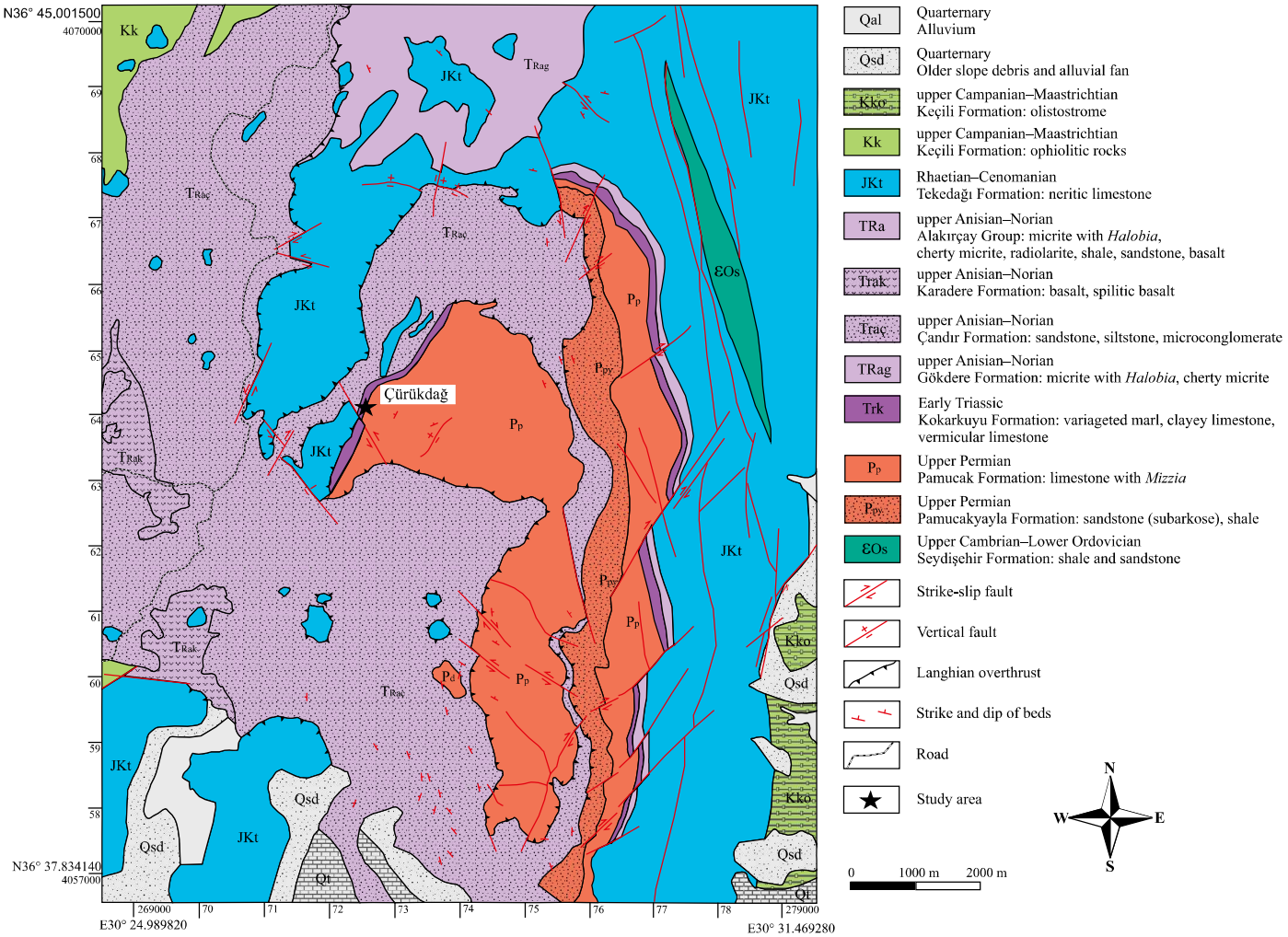

Figure_5_Cürükdag_O24c2_O25d1

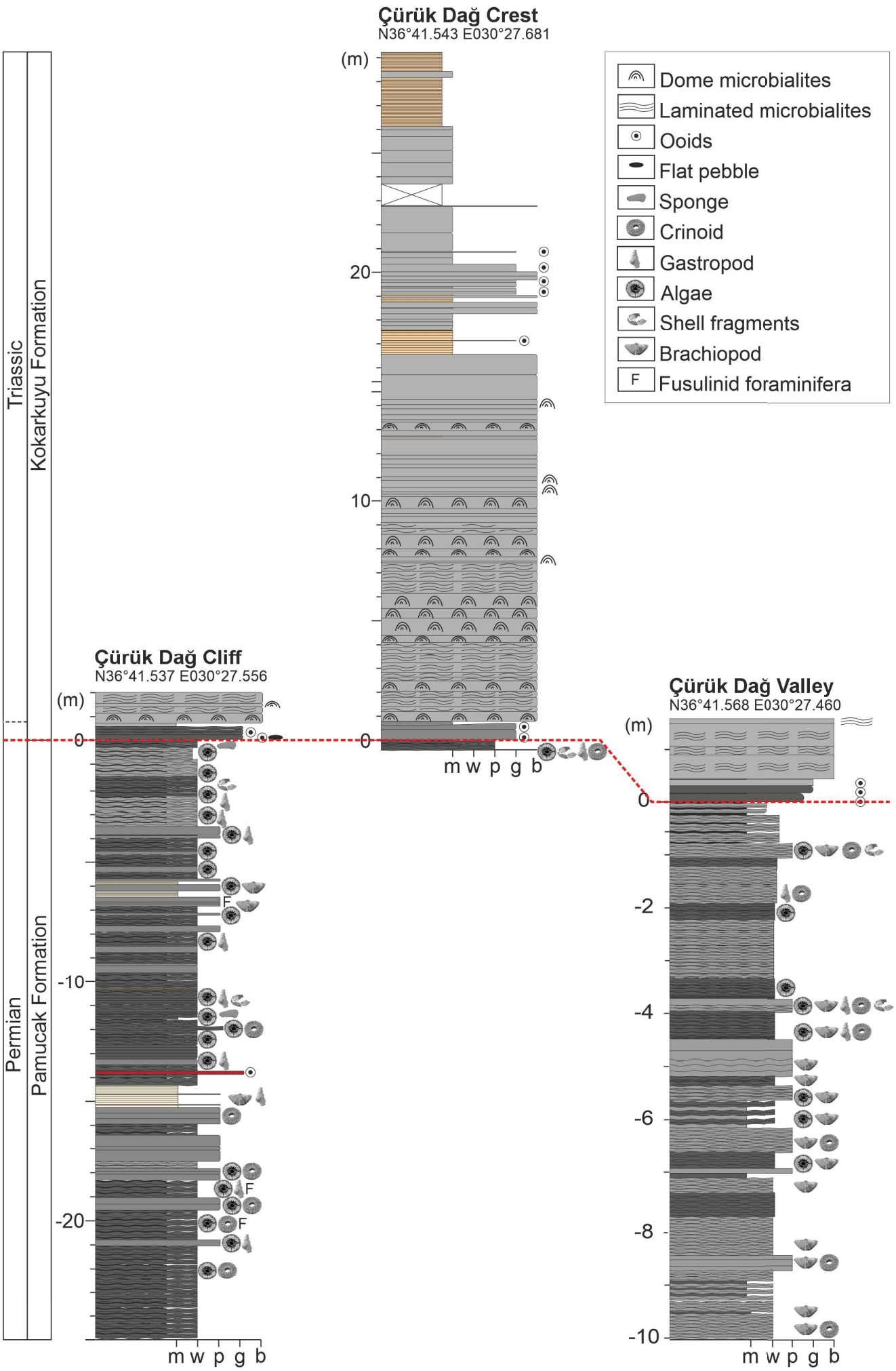

Figure_6_Curuk_Dag_log

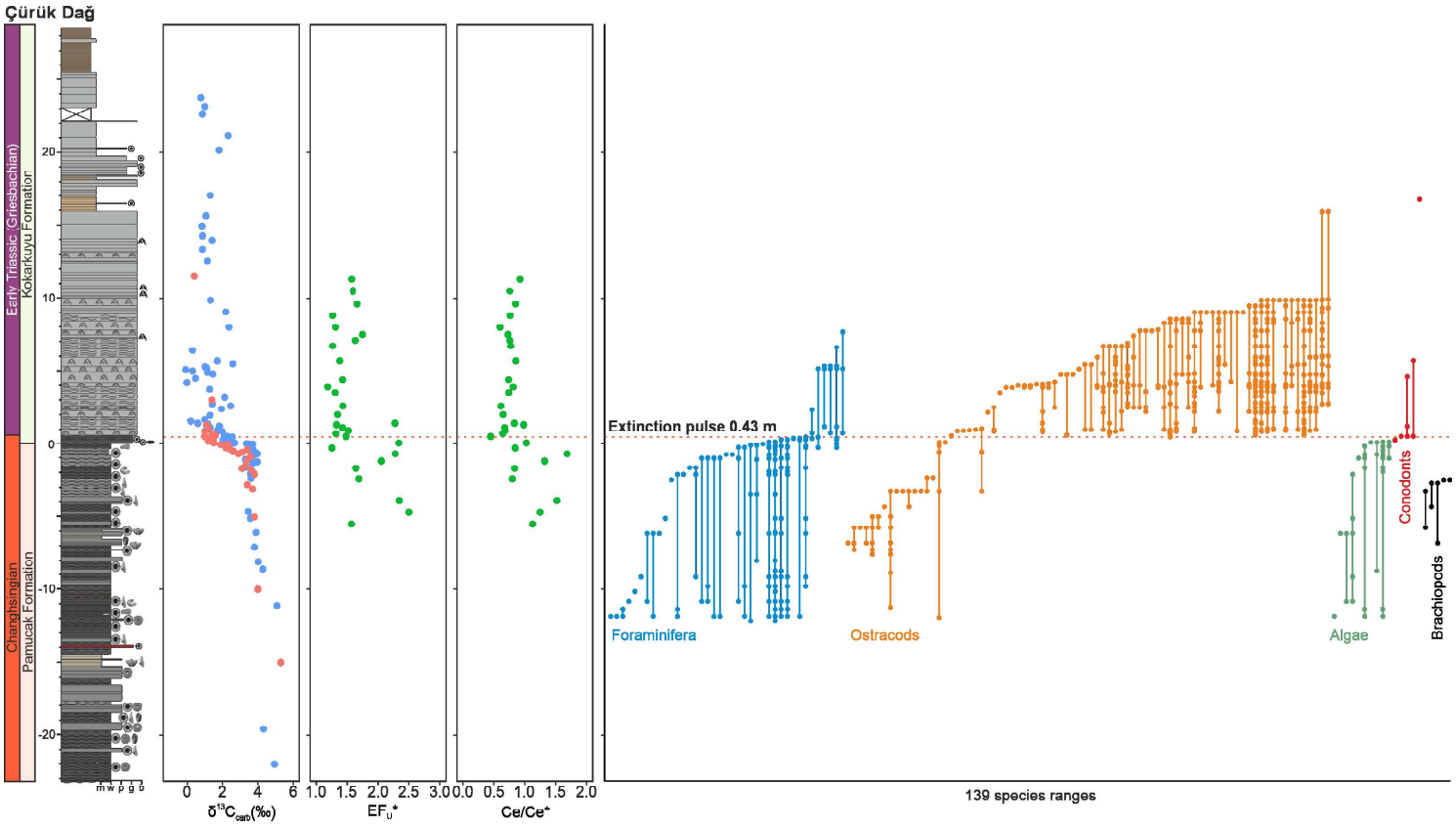

Figure_7_Cürükdag_extinction_pulse

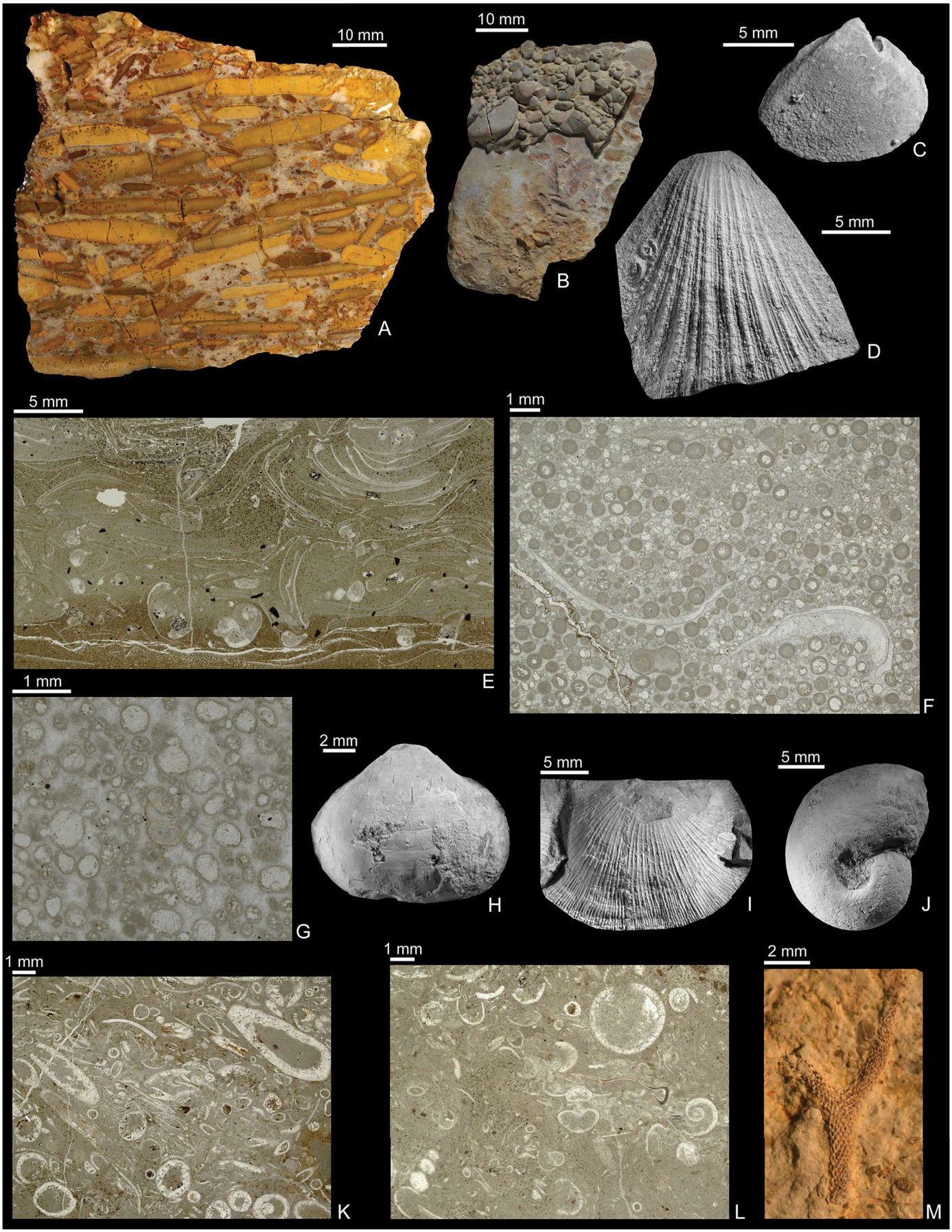

Curukdag.tif

Figure_8_Cürükdag

Figure_9_Demirtas

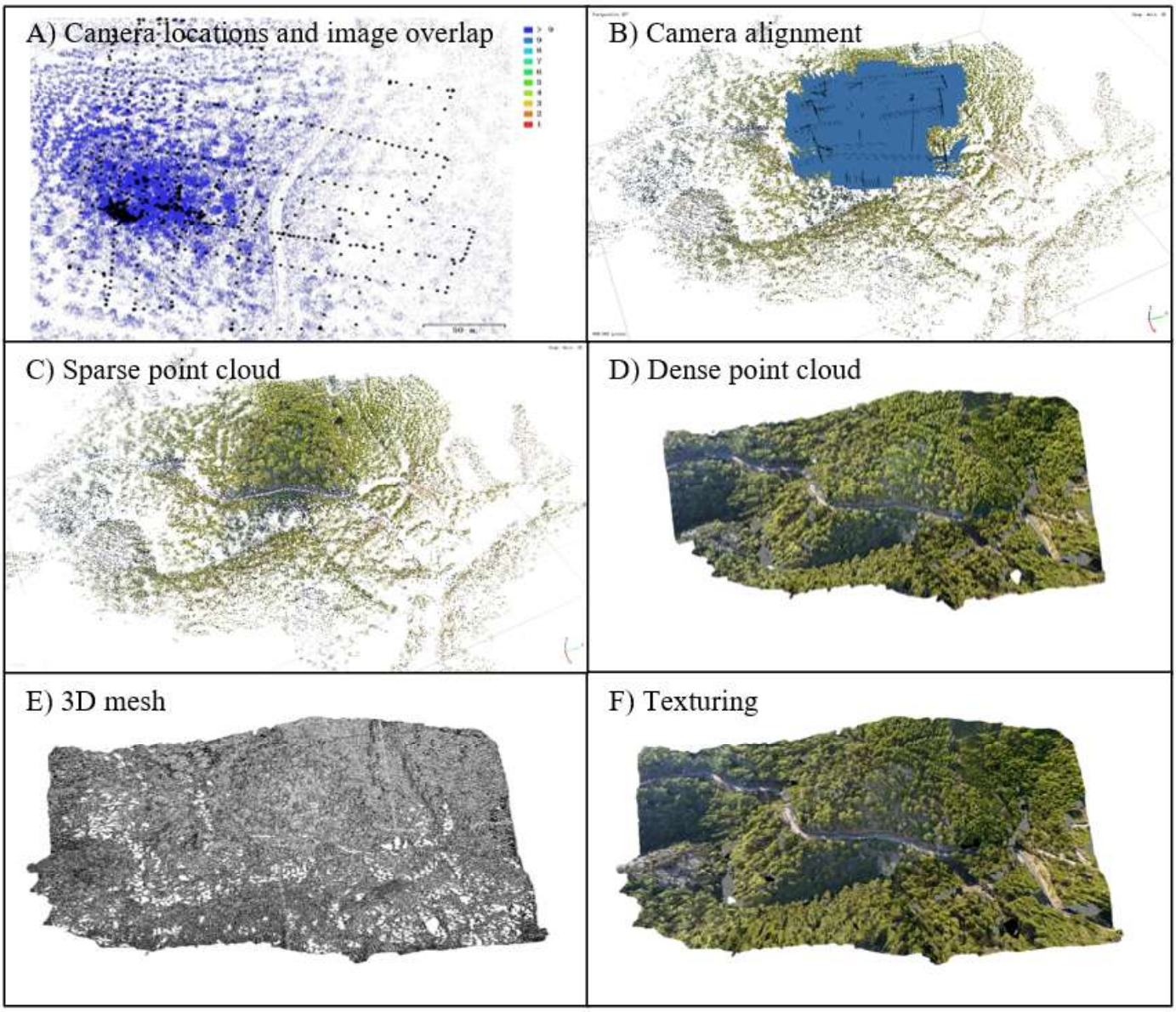

Figure_10_Demirtas

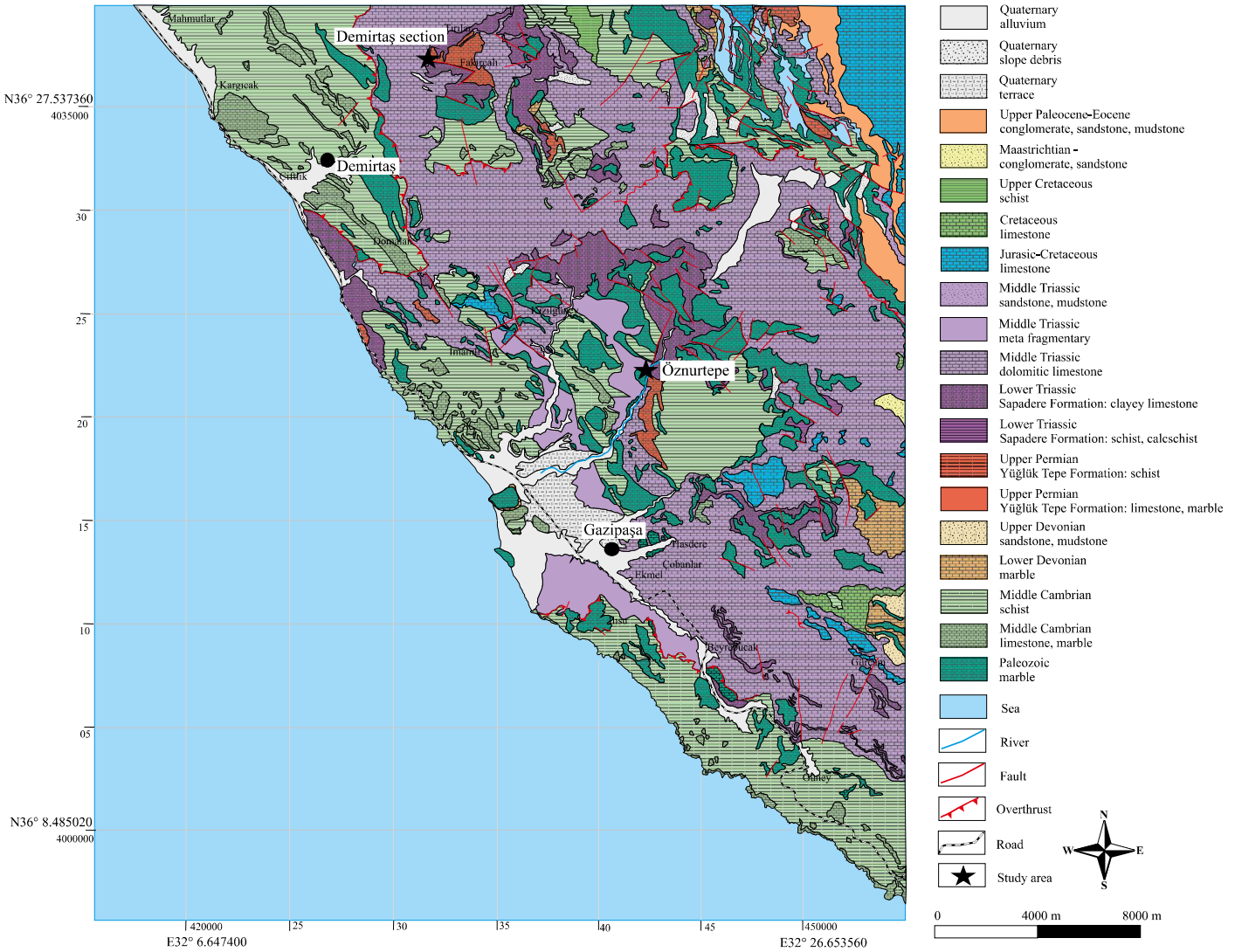

Figure_11_Demirtas_Oznurtepe_P 28

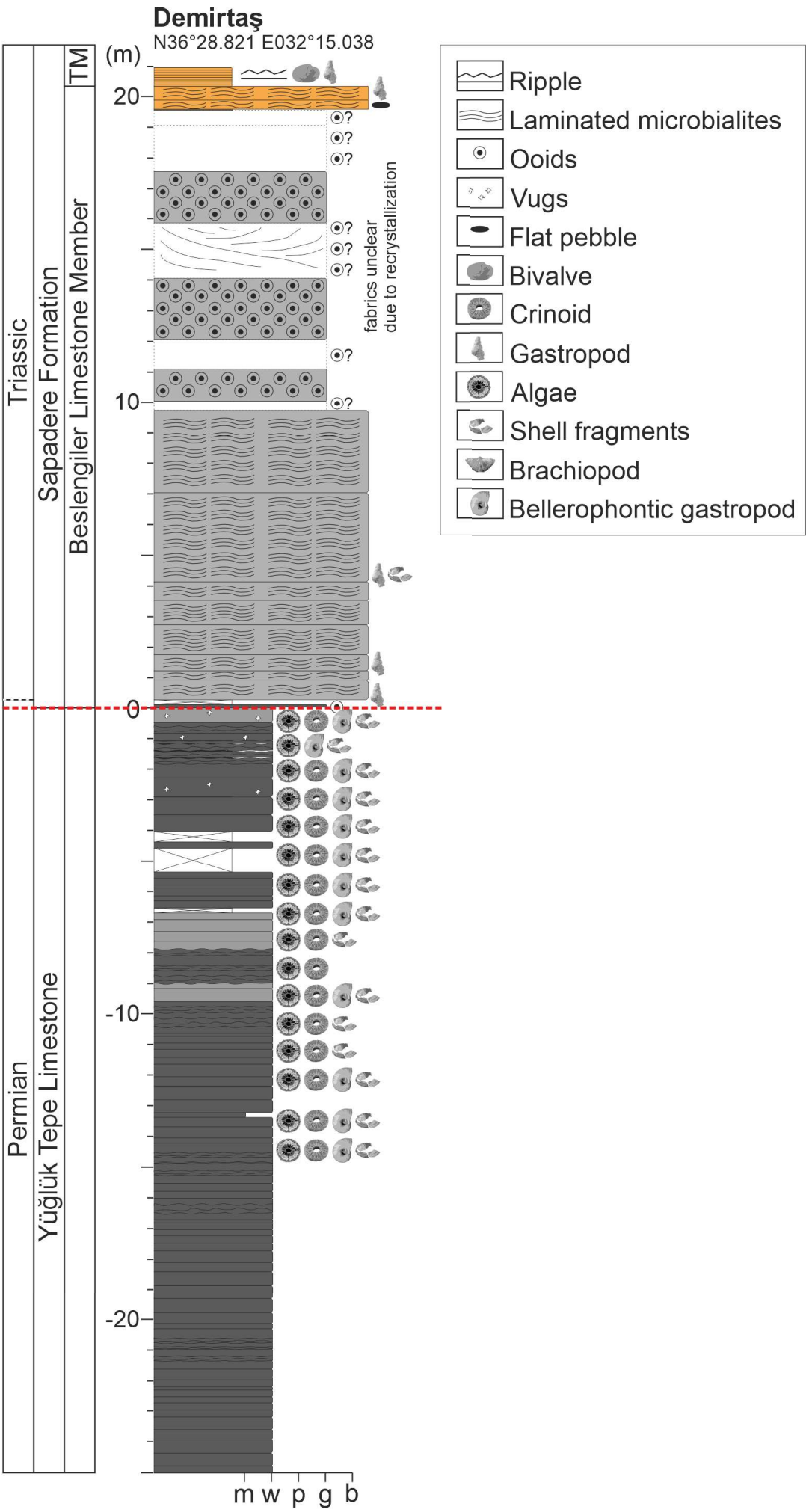

Figure_12_Demirtas_log

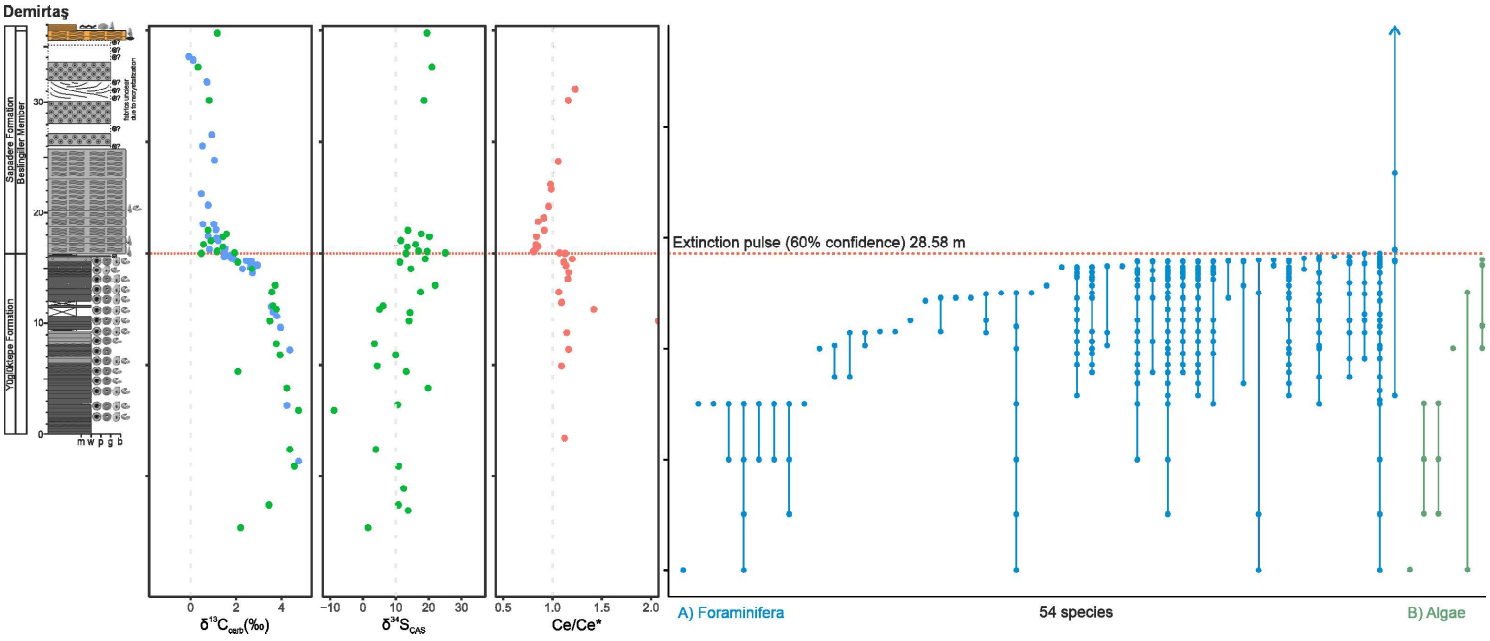

Figure_13_Demirtas_extinction_pulse

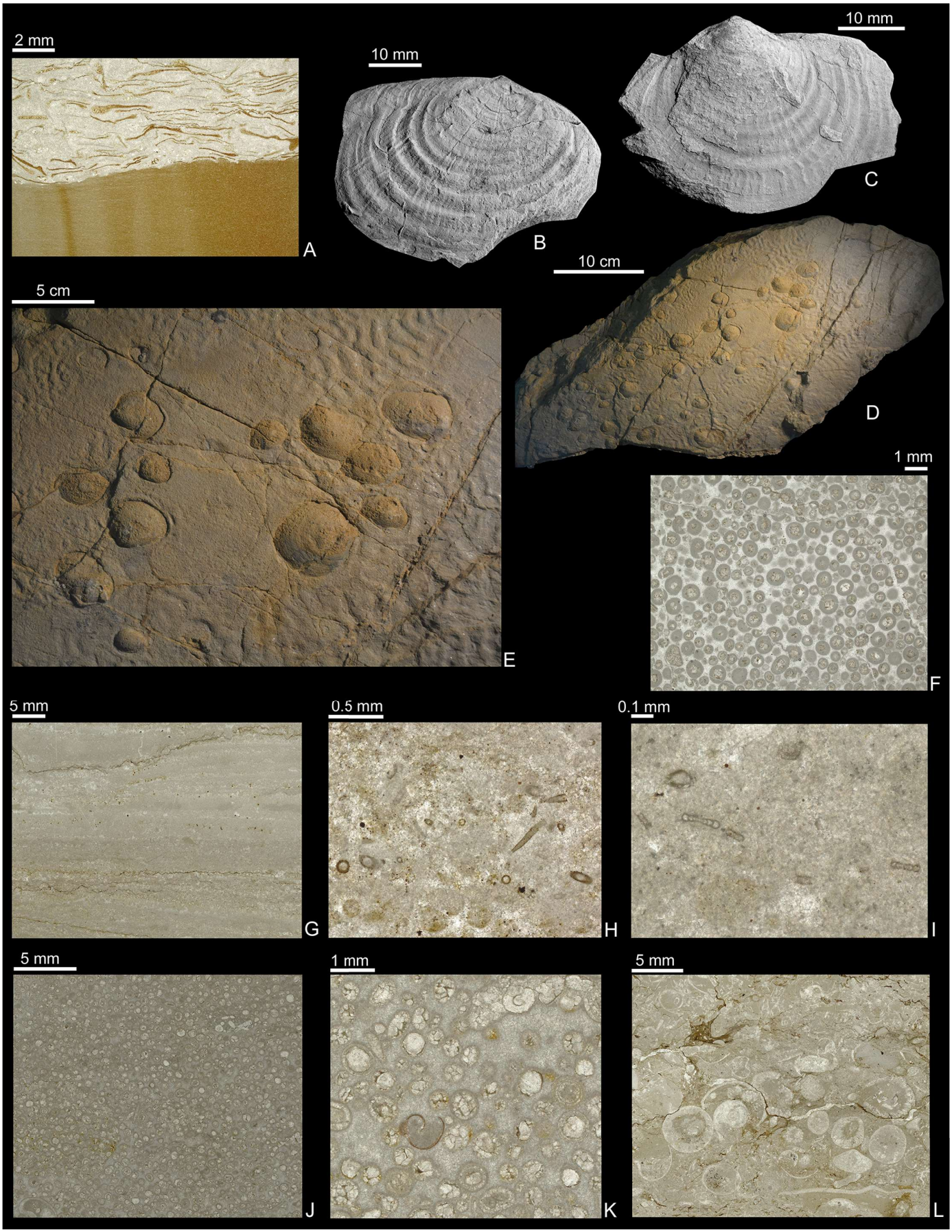

Demirtas.tif

Figure_14_Demirtas

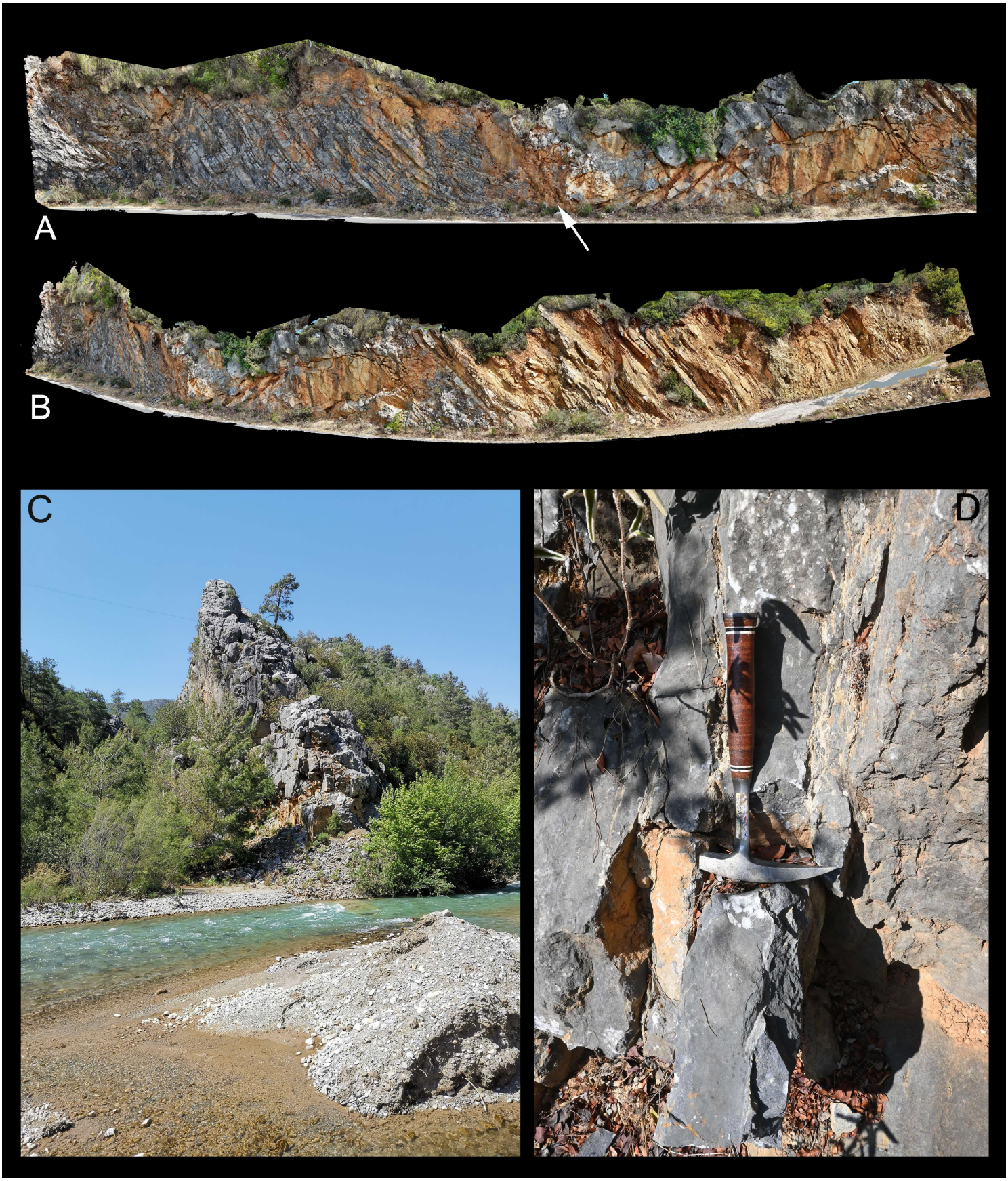

Figure_15_Oznurtepe

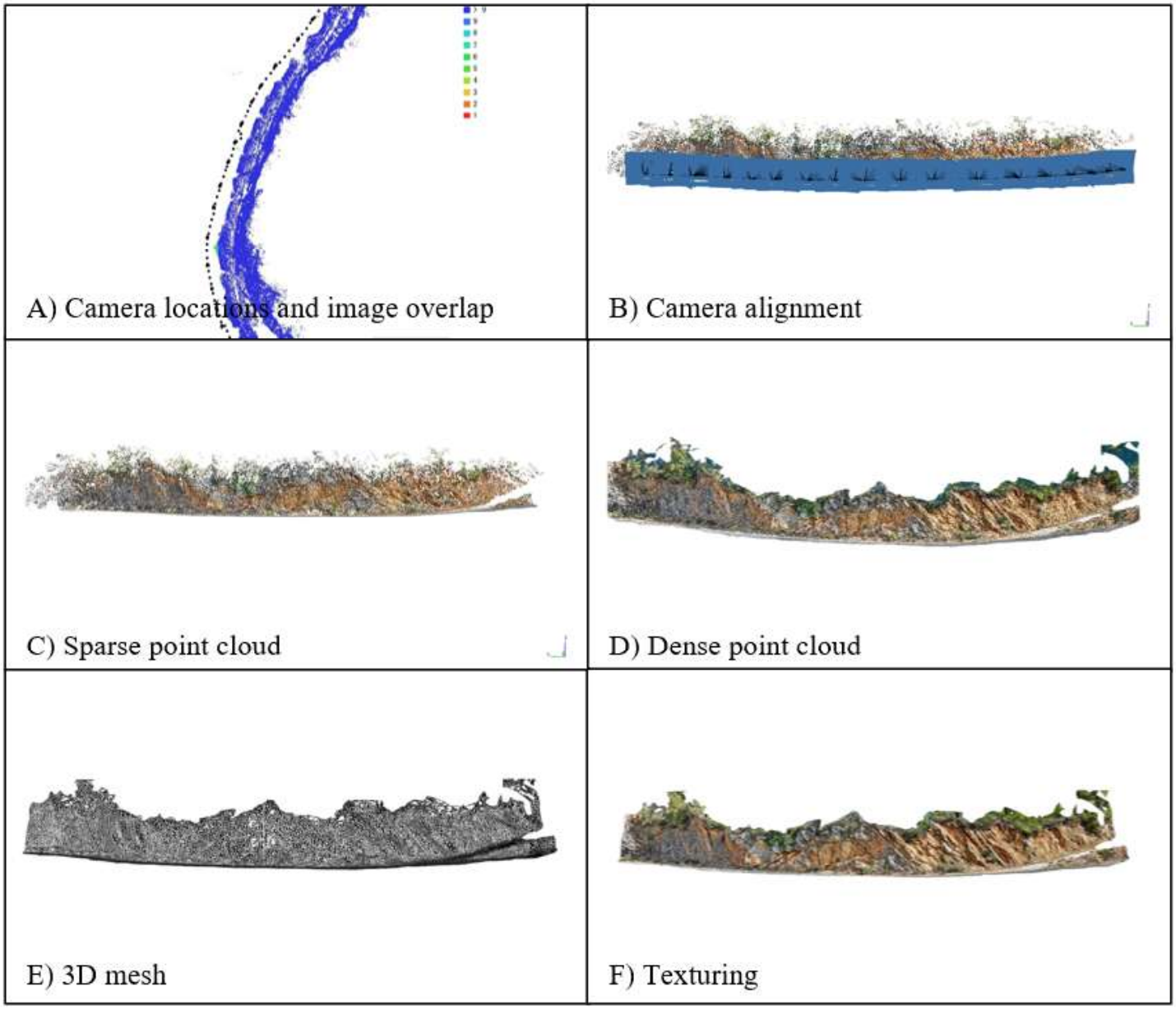

Figure_16_Oznurtepe_Road

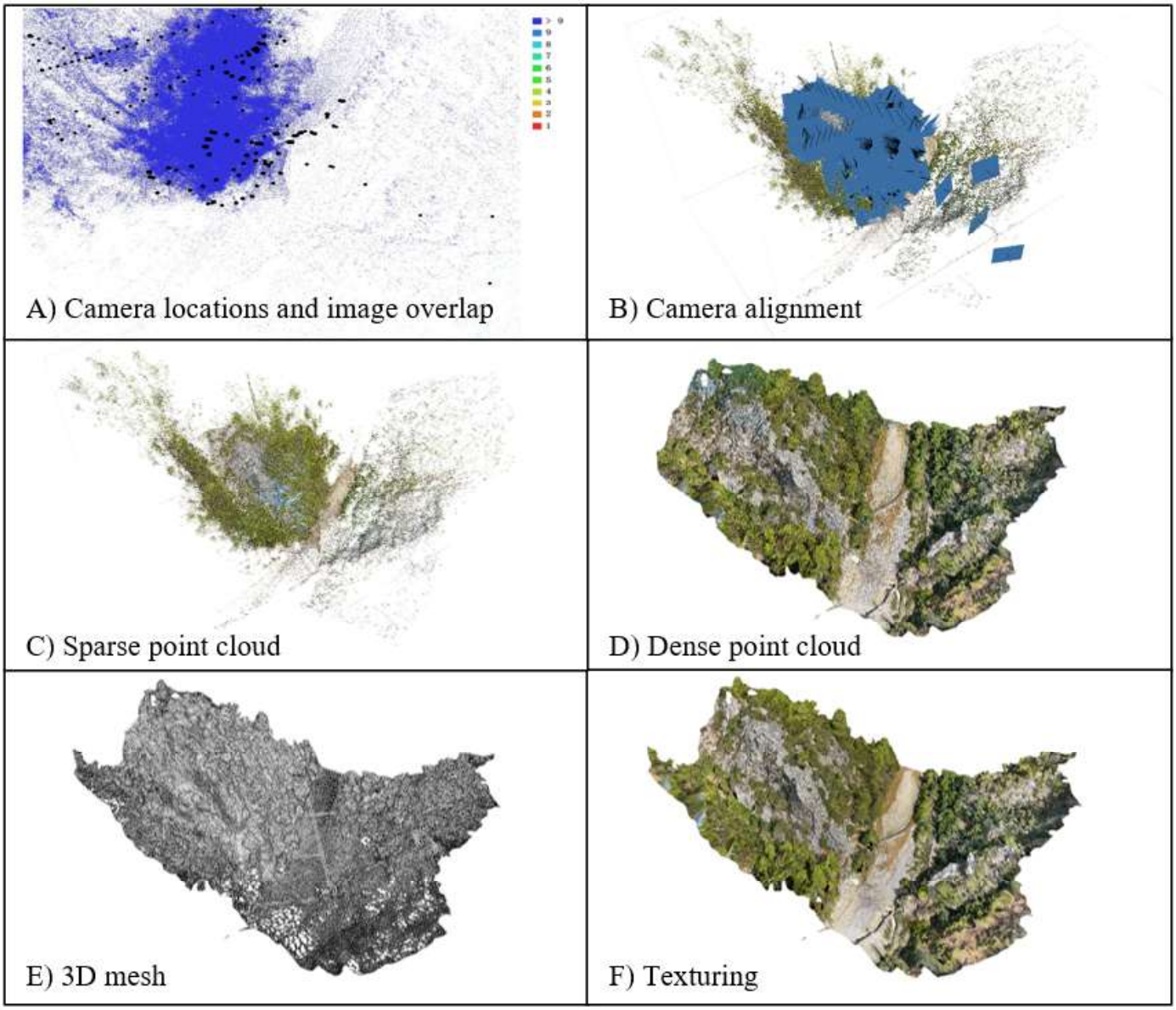

Figure_17_Oznurtepe_River

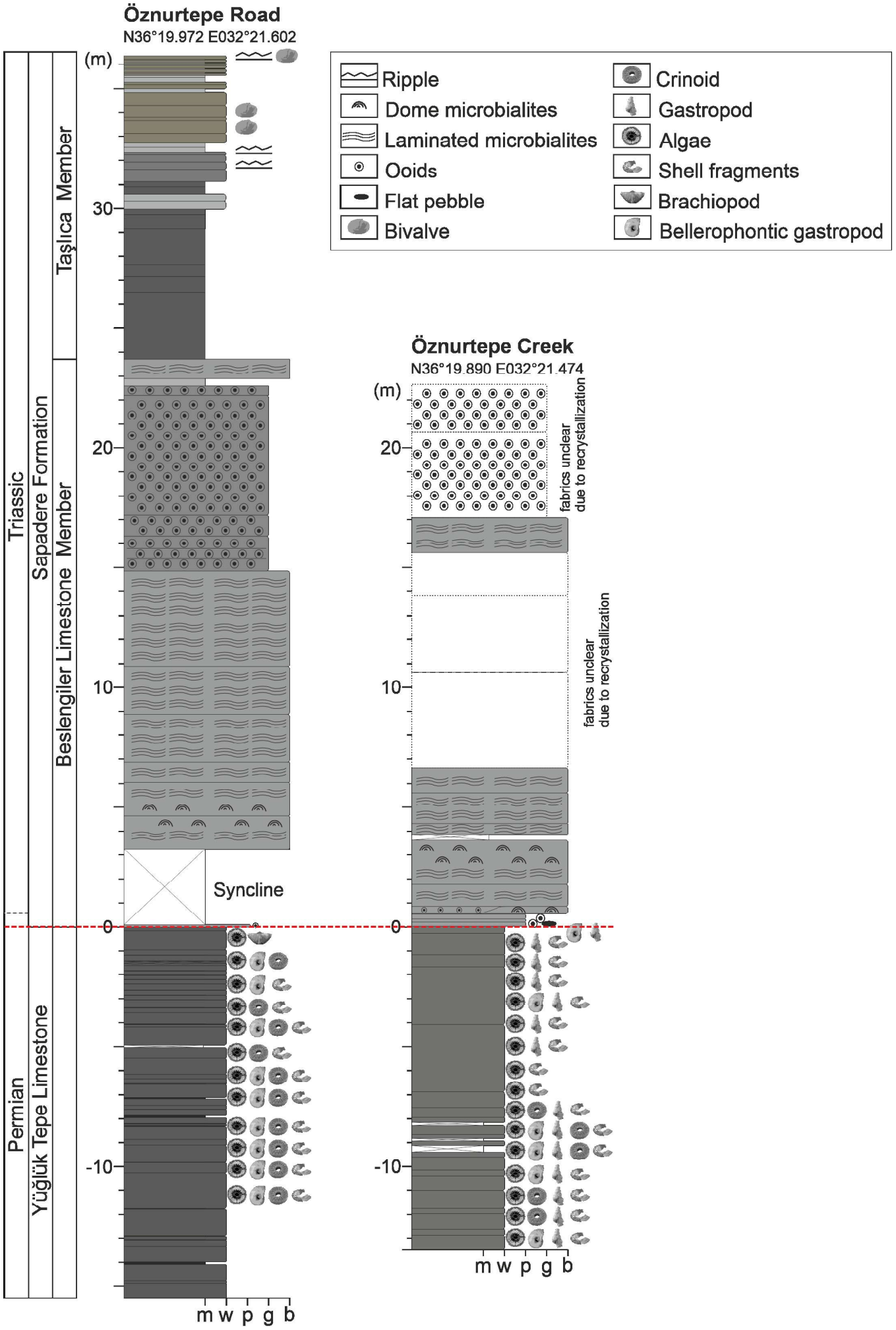

Figure_18_Oznurtepe_log

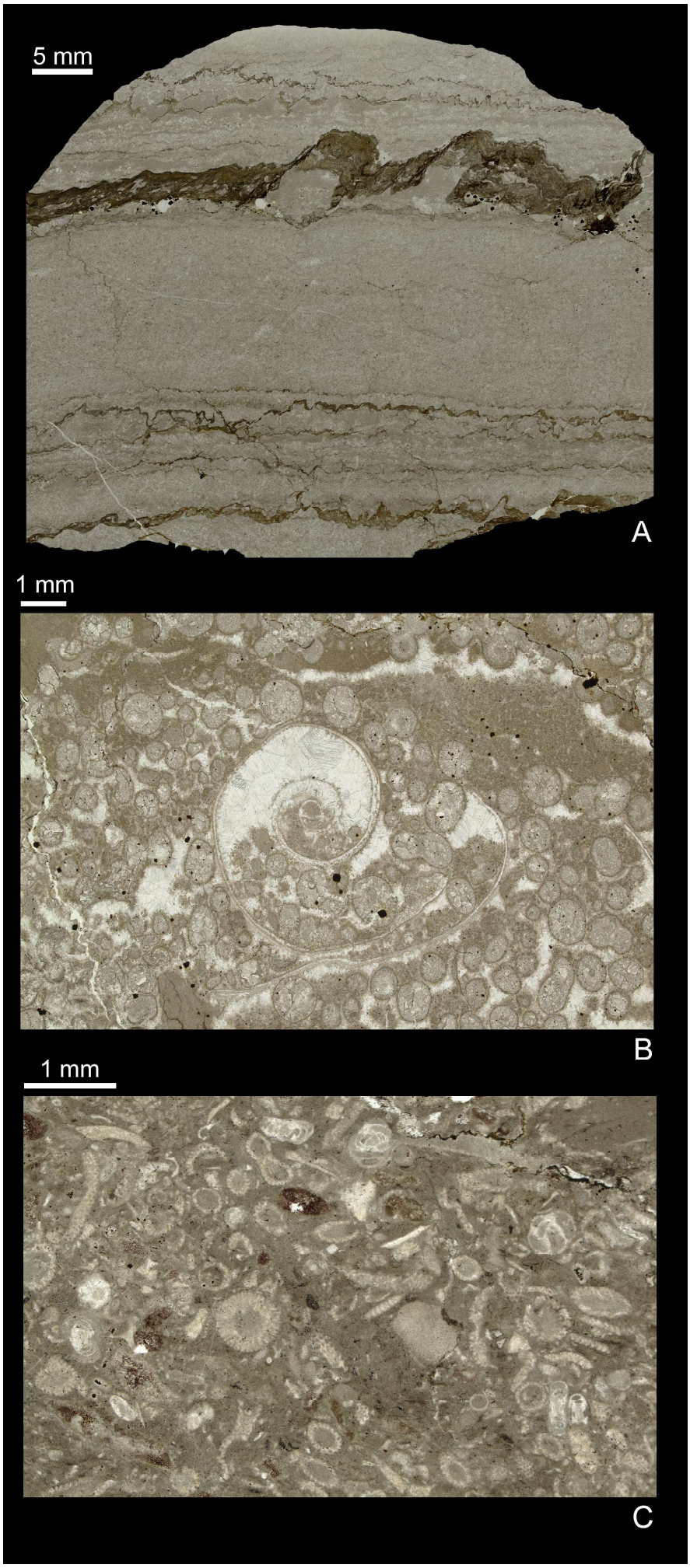

Figure_19_Oznurtepe

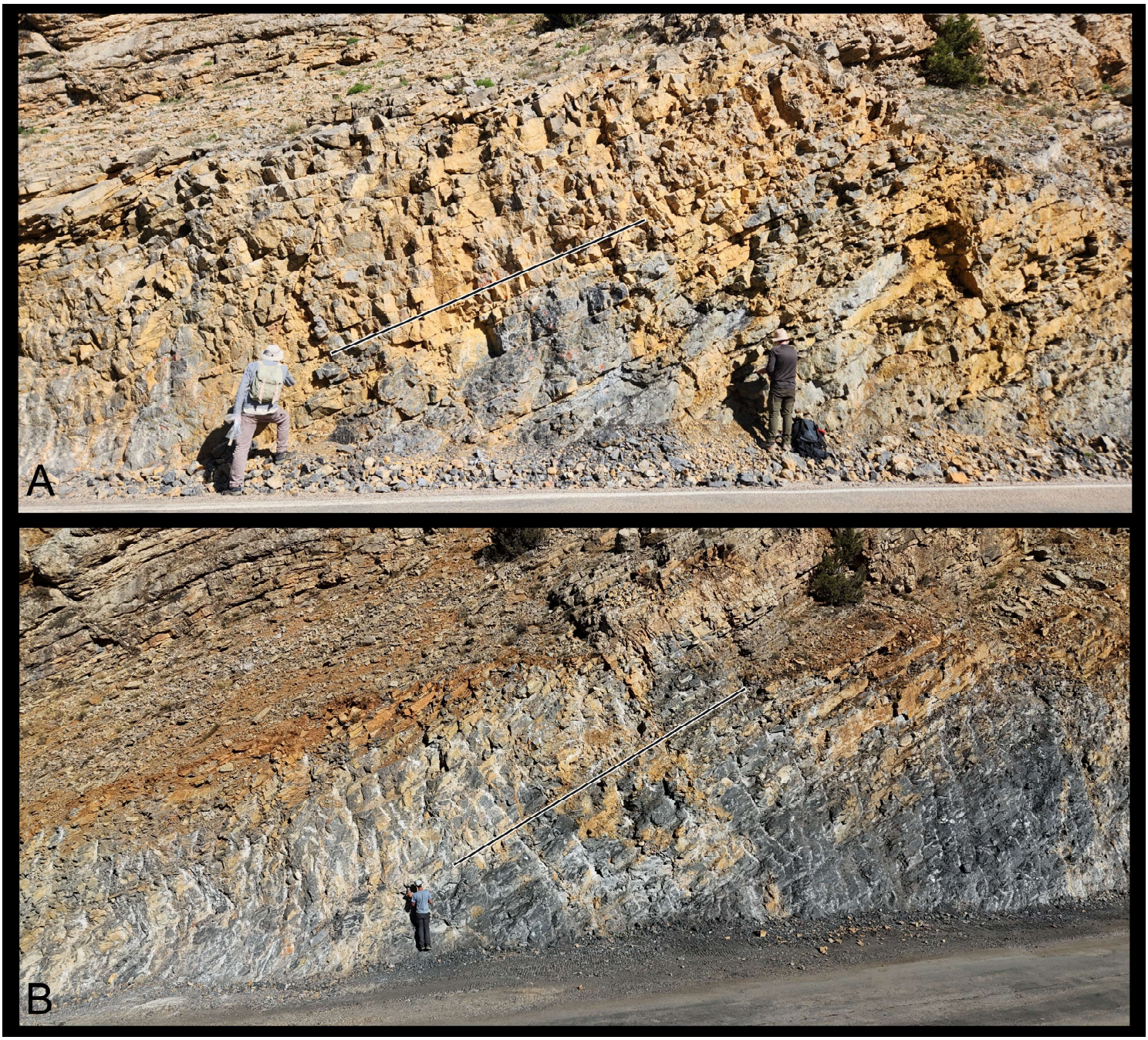

Figure_20_Taskent_Yolu

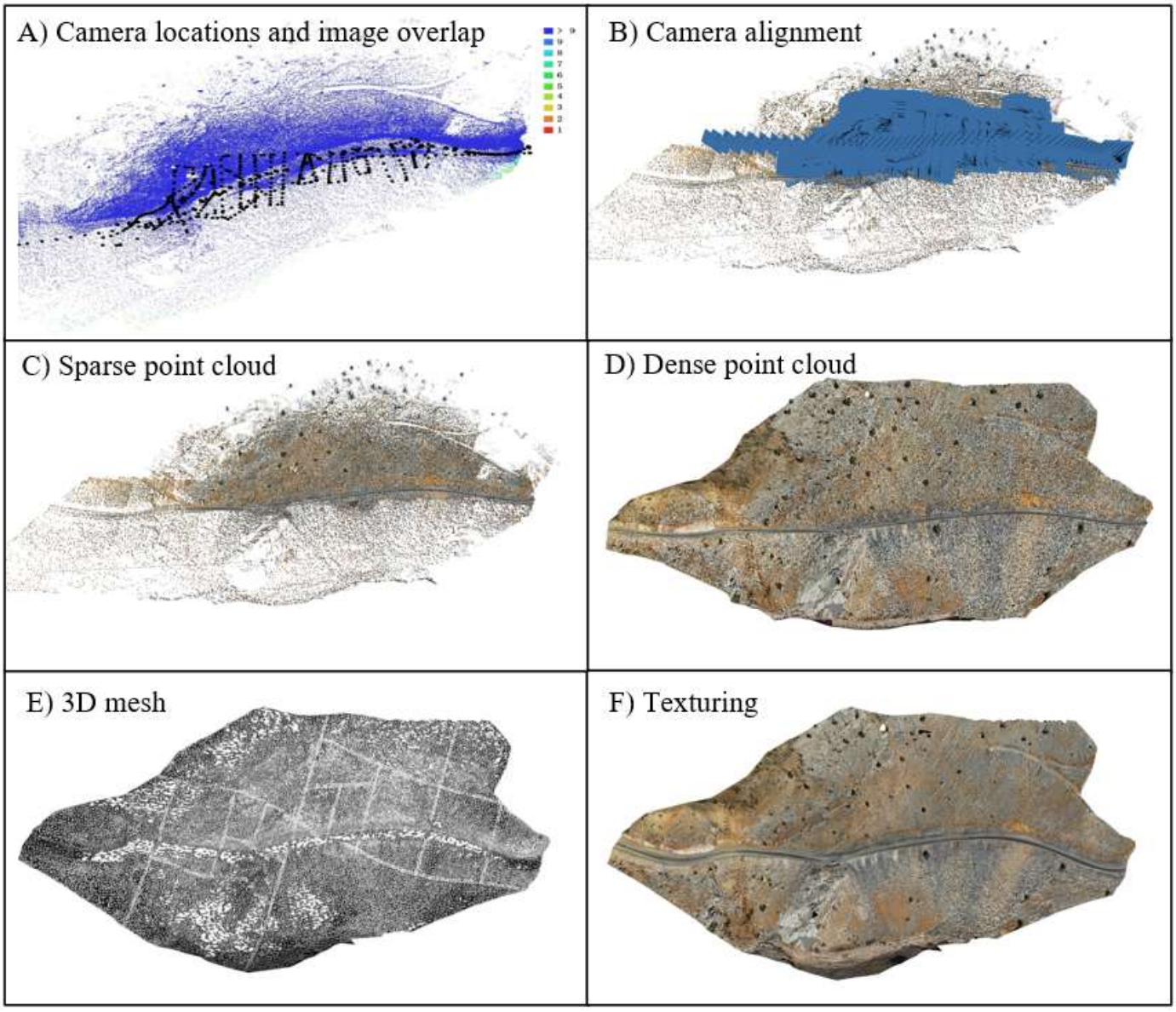

Figure_21_Taskent_Yolu

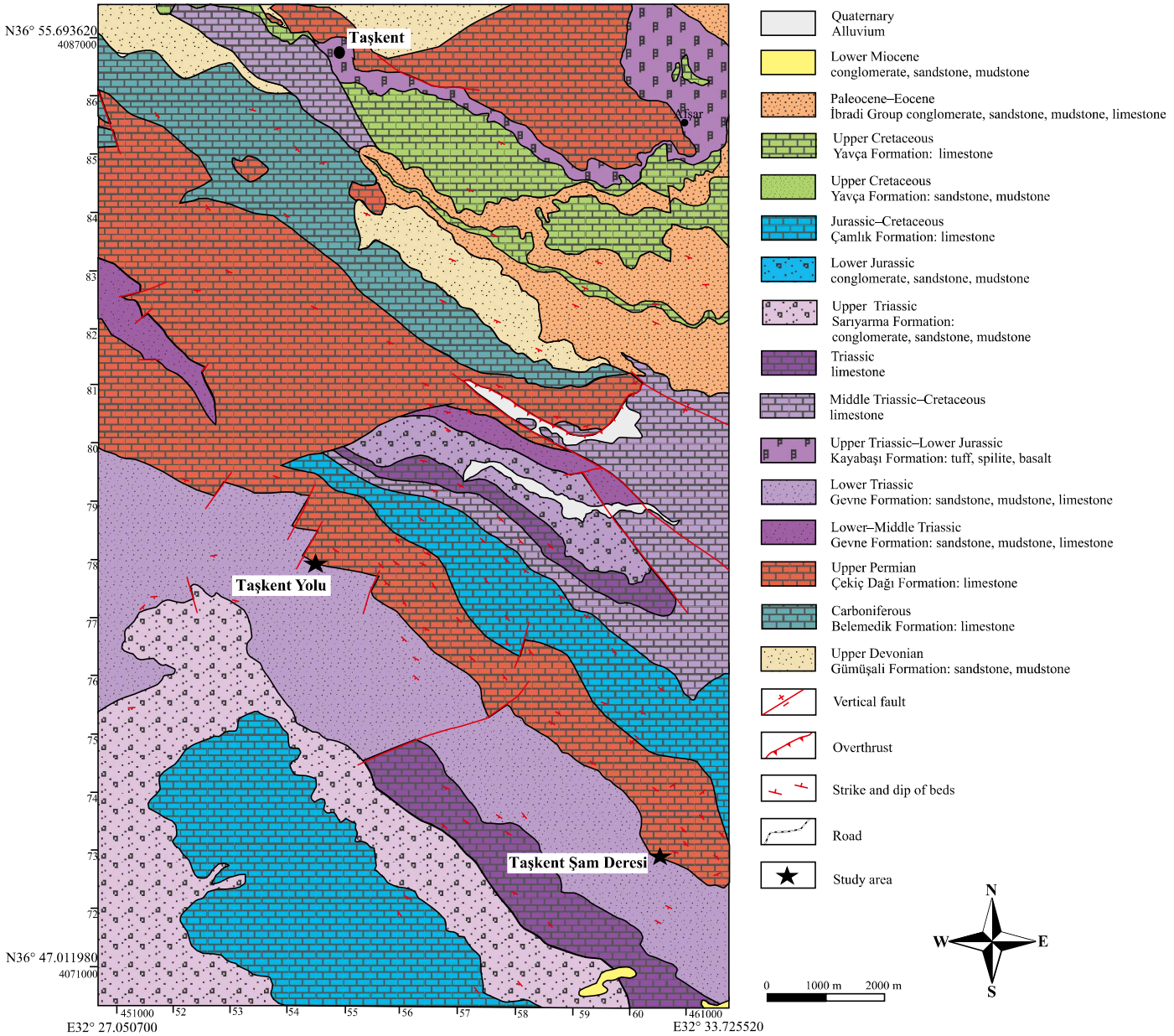

Figure_22_O 28 b2 b3 - O 29 a1 a4

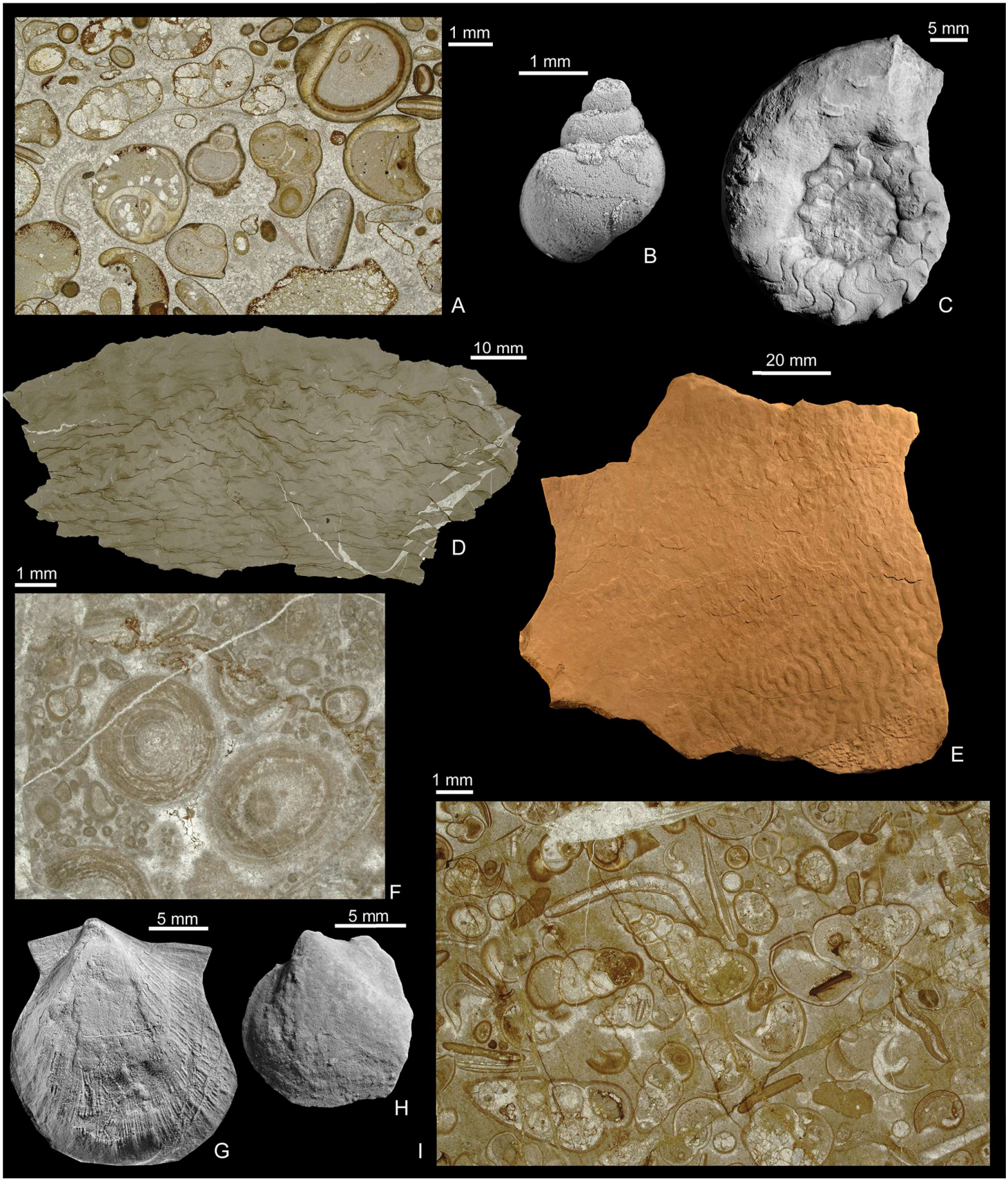

Taskent_Yolu.tif

Figure_23_Taskent_Yolu

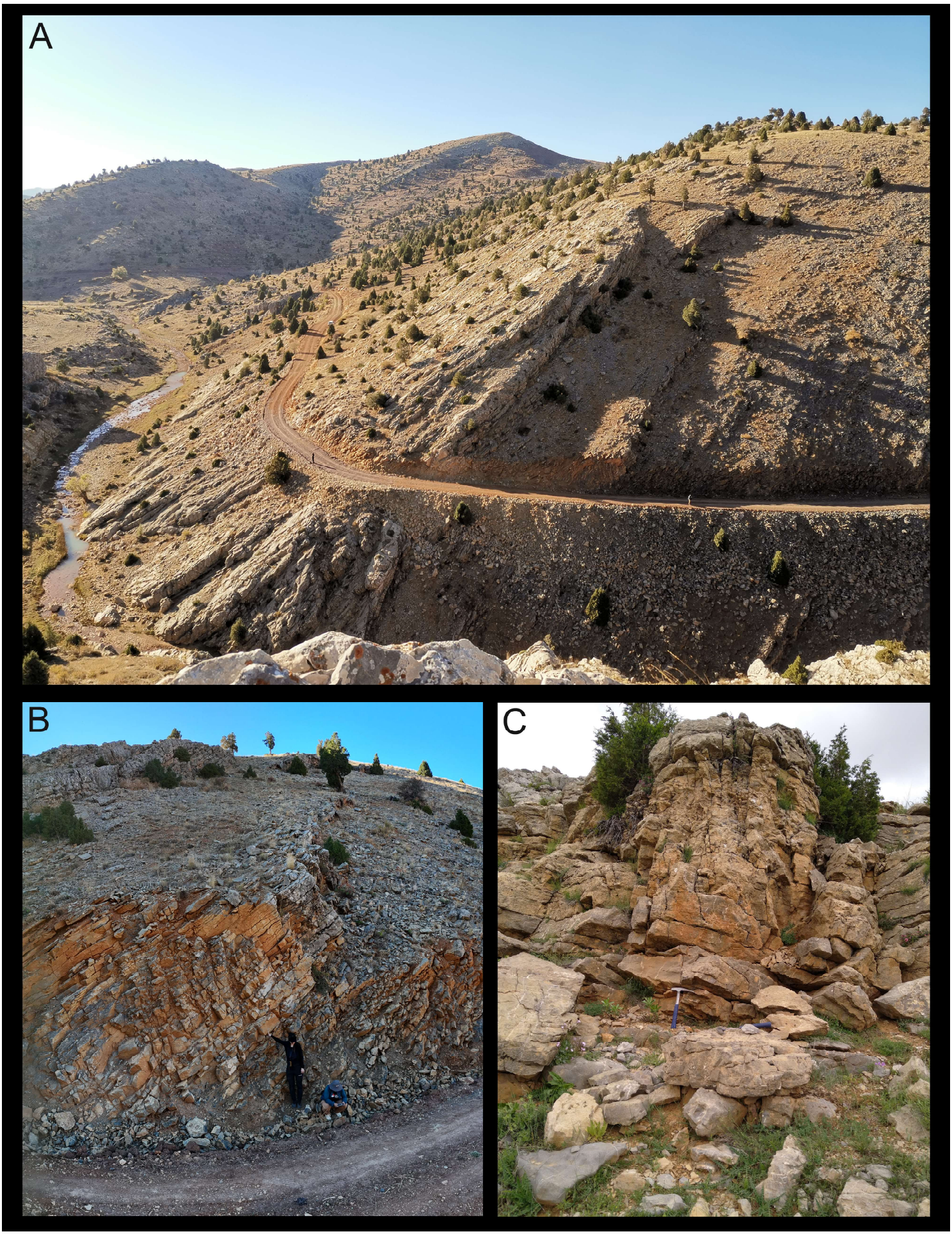

Figure_24_Taskent_Sam_Deresi

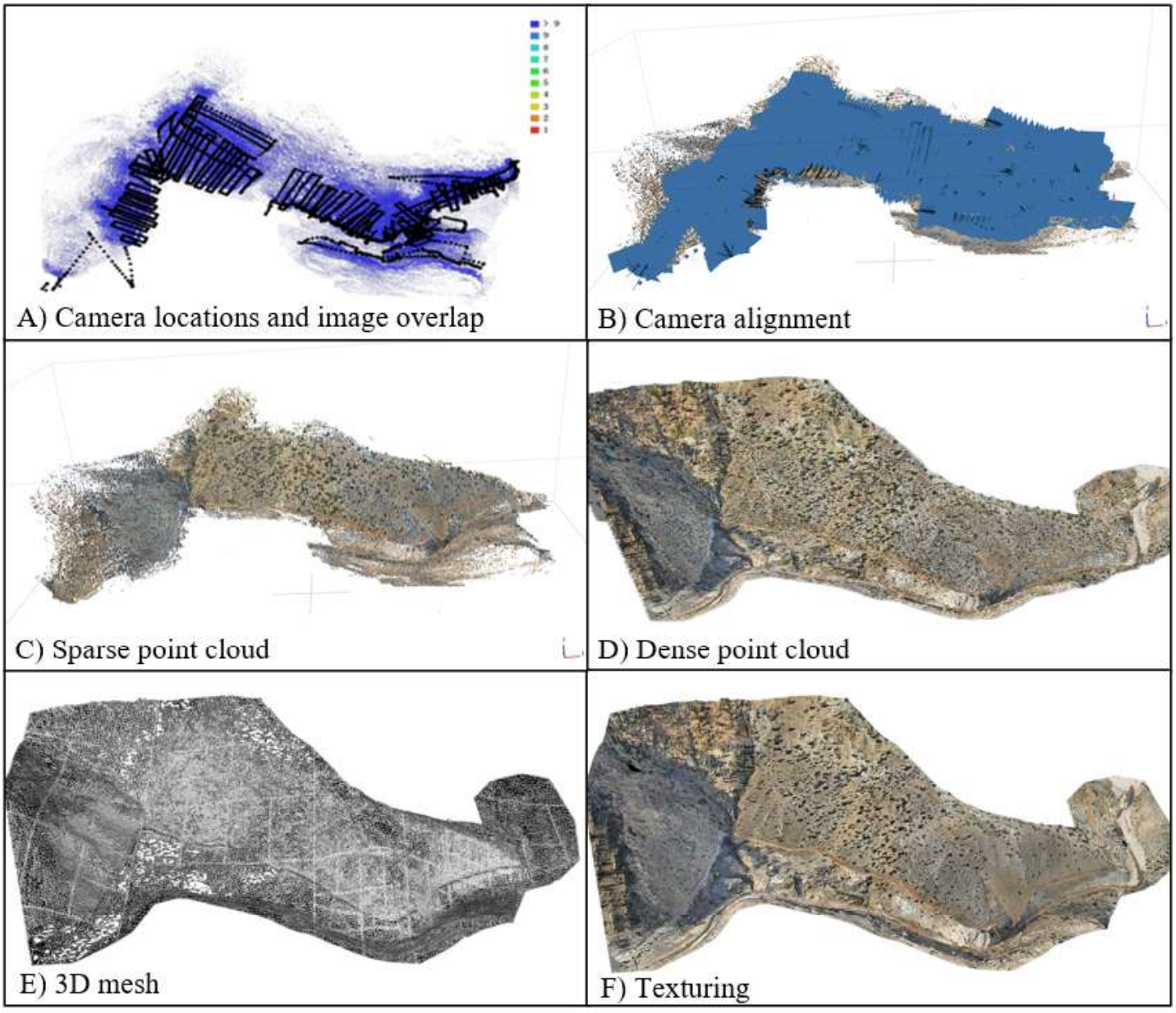

Figure_25_Taskent_Sam_Deresi_model

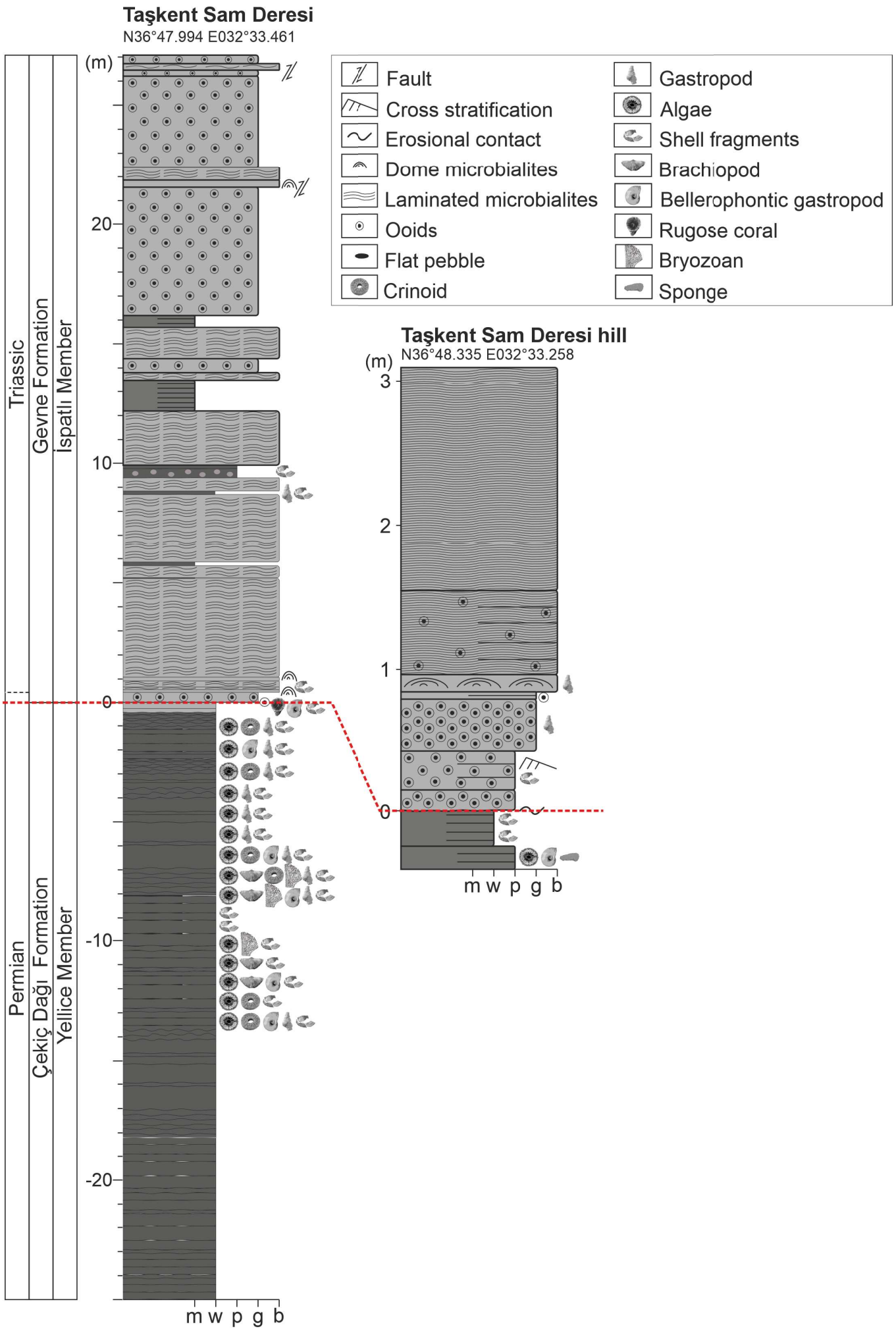

Figure_26_Taskent_log

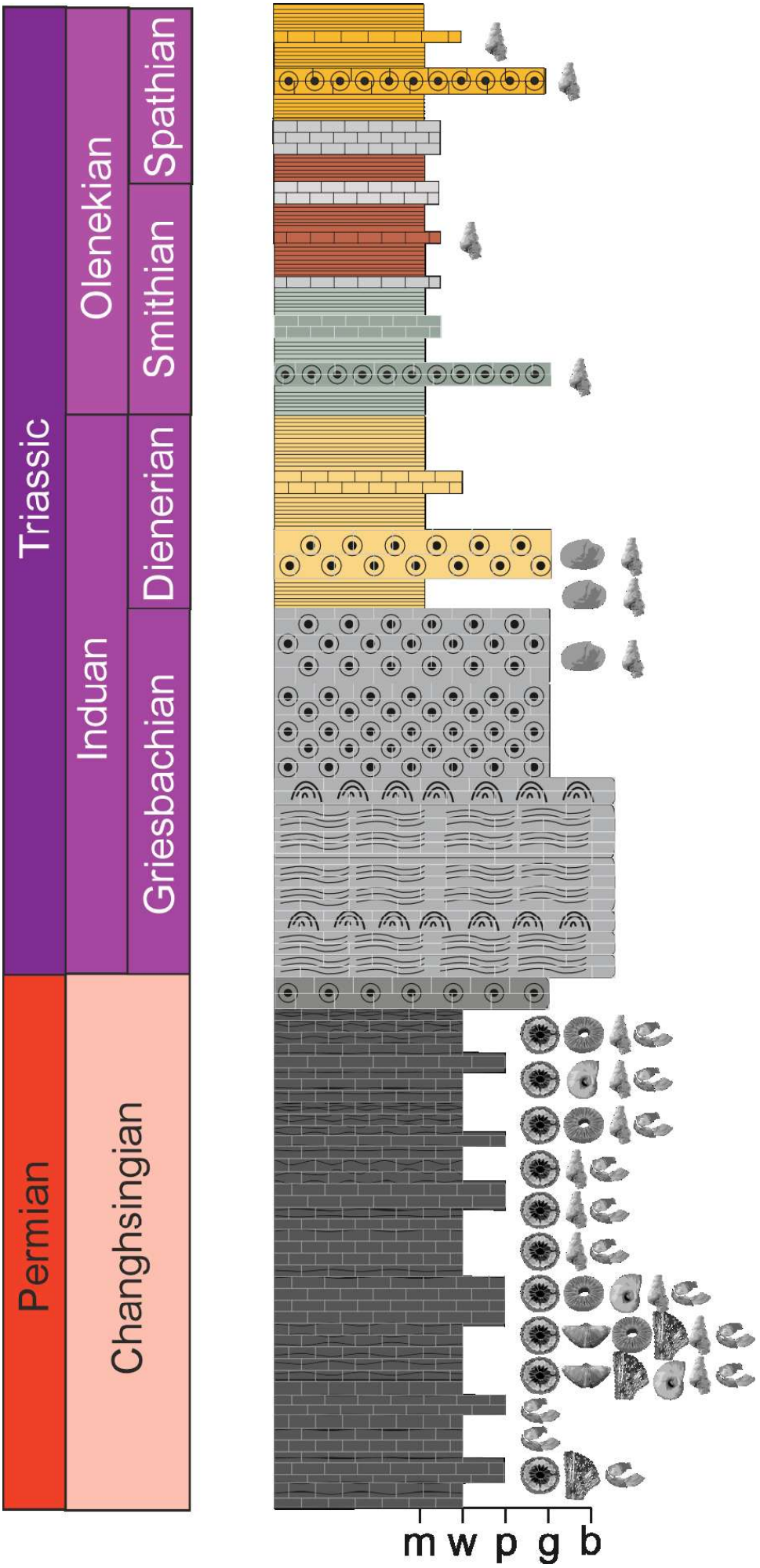

Figure_27_Taskent_generalized_log

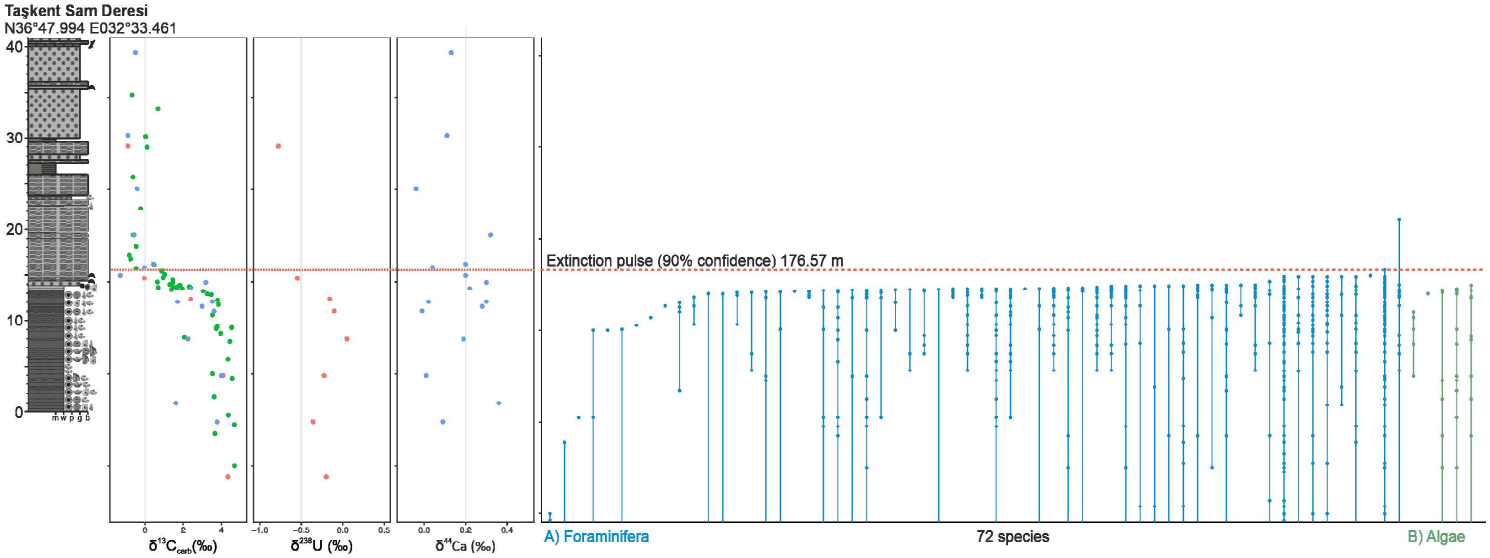

Figure_28_Taskent_extinction_pulse

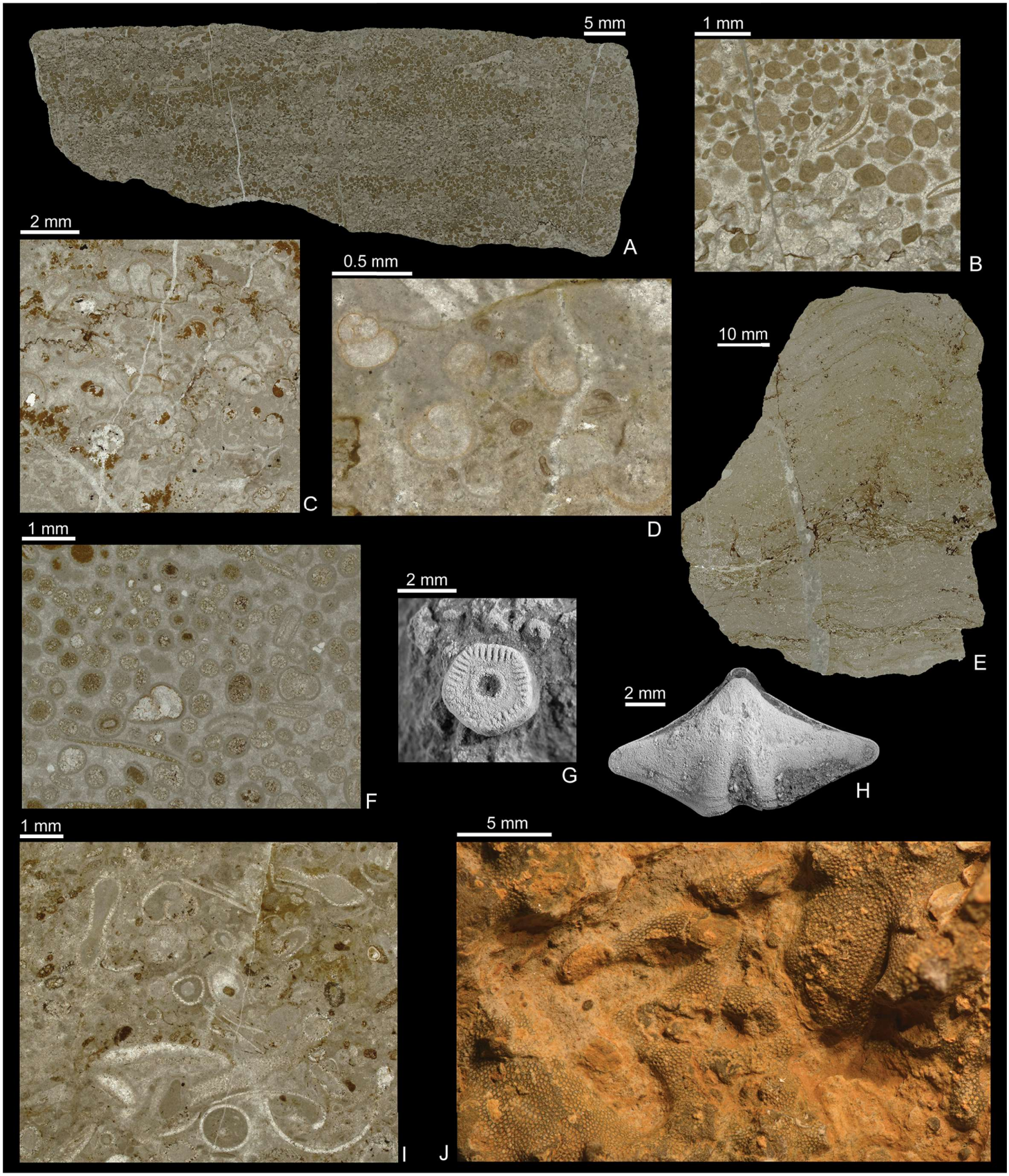

Taskent_Sam_Deresi_1.tif

Figure_29_Taskent_Sam_Deresi_1

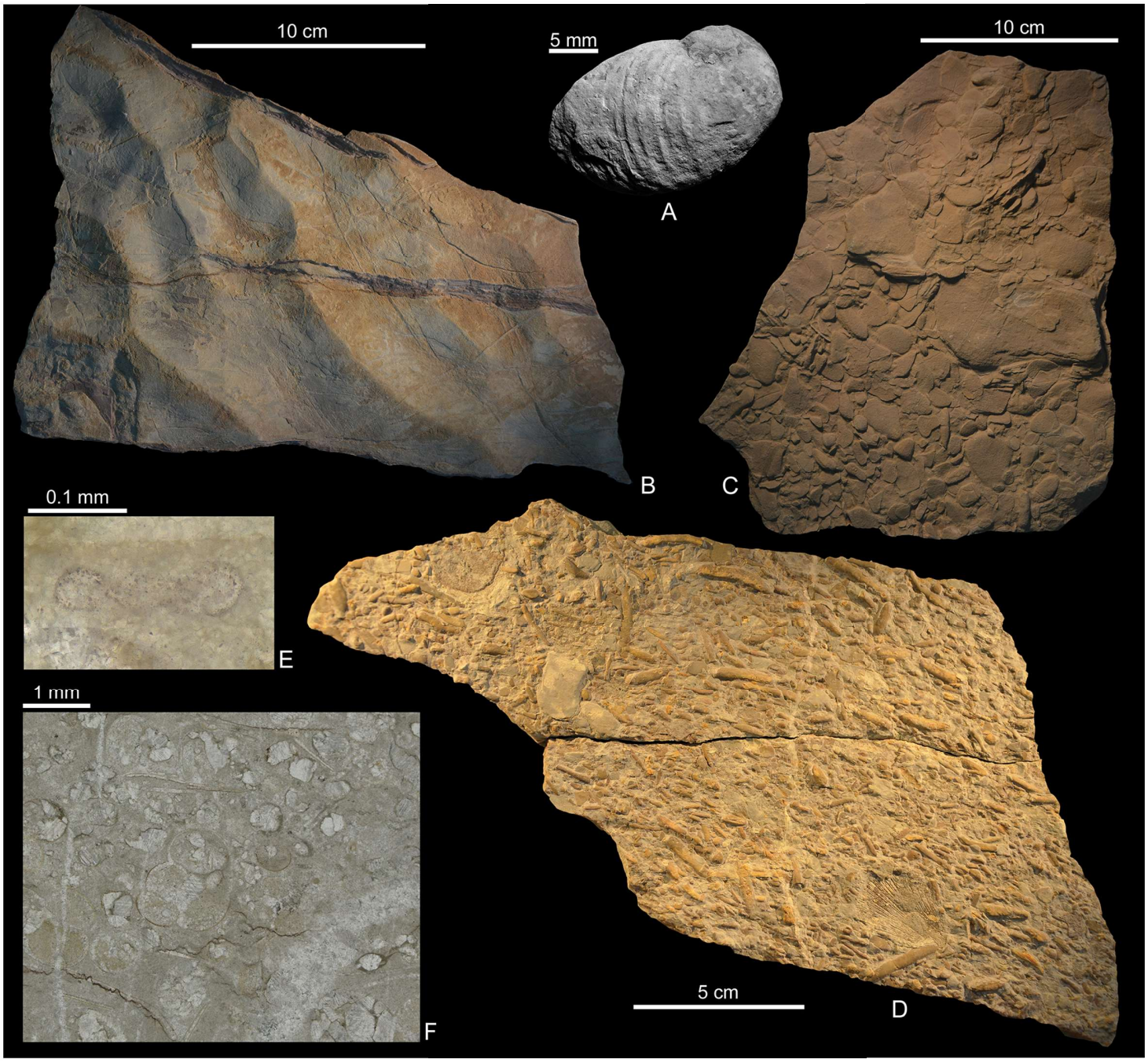

Taskent_Sam_Deresi_2.tif

Figure_30_Taskent_Sam_Deresi_2

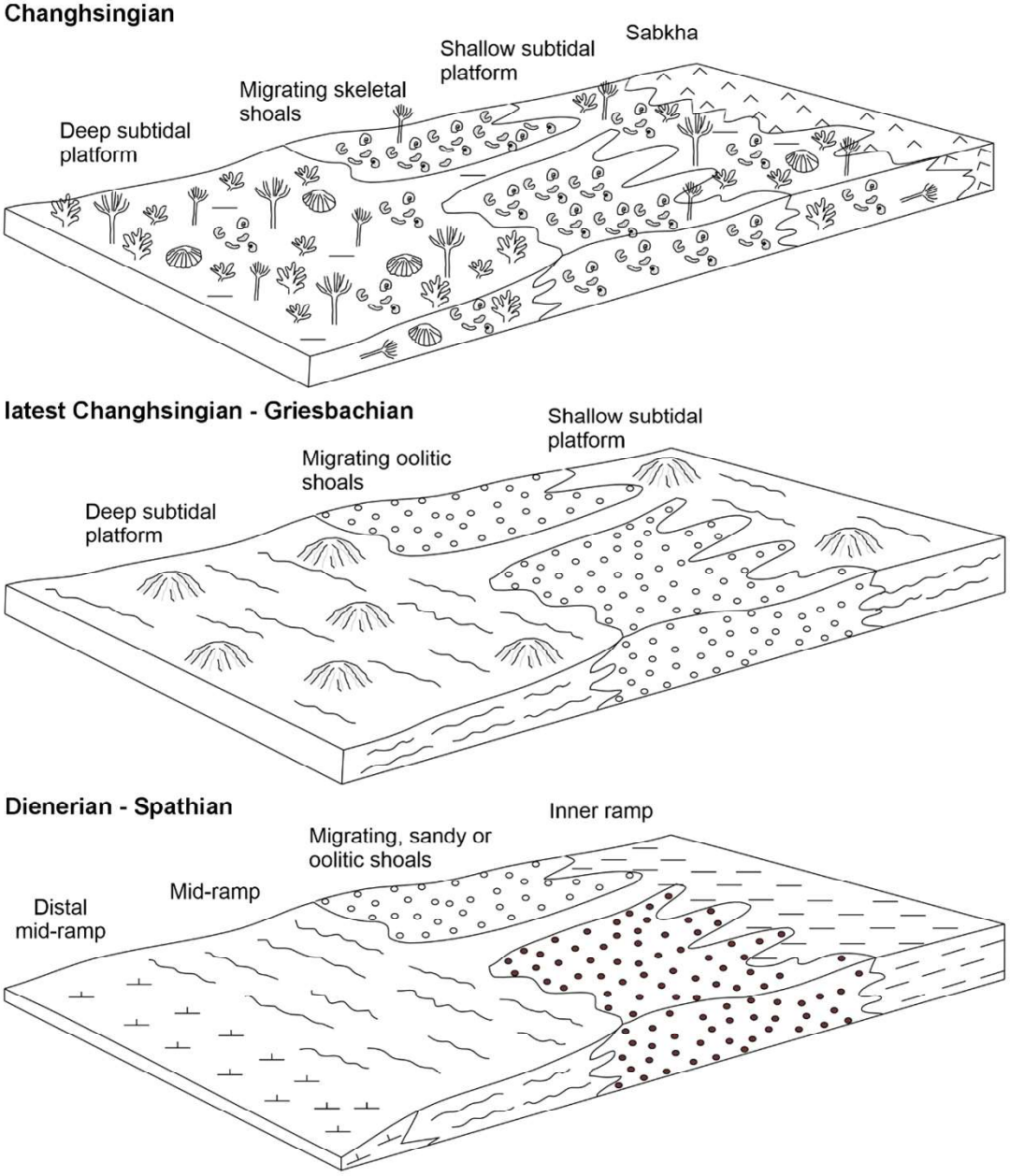

Figure 31_Environmental_evolution